UNCLASSIFIED

SECURITY CLASSIFICATION OF THIS PAGE (When Data Entered)



# REPORT DOCUMENTATION PAGE

READ INSTRUCTIONS BEFORE COMPLETING FORM

1. REPORT NUMBER: AFIT/CI/NR 88- 29
2. GOVT ACCESSION NO.:
3. RECIPIENT'S CATALOG NUMBER:
4. TITLE (and Subtitle): ACTIVE MODES OF THE PACIFIC INTERTROPICAL CONVERGENCE ZONE.
5. TYPE OF REPORT & PERIOD COVERED: MS THESIS
6. PERFORMING ORG. REPORT NUMBER:
7. AUTHOR(s): PATRICK MICHAEL HAYES
8. CONTRACT OR GRANT NUMBER(s):
9. PERFORMING ORGANIZATION NAME AND ADDRESS: AFIT STUDENT AT: UNIVERSITY OF WISCONSON -GREEN BAY
10. PROGRAM ELEMENT, PROJECT, TASK AREA & WORK UNIT NUMBERS:
11. CONTROLLING OFFICE NAME AND ADDRESS:
12. REPORT DATE: 1988
13. NUMBER OF PAGES: 90
14. MONITORING AGENCY NAME & ADDRESS (if different from Controlling Office): AFIT/NR Wright-Patterson AFB OH 45433-6583
15. SECURITY CLASS. (of this report): UNCLASSIFIED
15a. DECLASSIFICATION/DOWNGRADING SCHEDULE:
16. DISTRIBUTION STATEMENT (of this Report): DISTRIBUTED UNLIMITED: APPROVED FOR PUBLIC RELEASE



17. DISTRIBUTION STATEMENT (of the abstract entered in Block 20, if different from Report): SAME AS REPORT
18. SUPPLEMENTARY NOTES: Approved for Public Release: IAW AFR 190-1
LYNN E. WOLAVER 18 July 88
Dean for Research and Professional Development
Air Force Institute of Technology
Wright-Patterson AFB OH 45433-6583
19. KEY WORDS (Continue on reverse side if necessary and identify by block number):
20. ABSTRACT (Continue on reverse side if necessary and identify by block number): ATTACHED

DD FORM 1 JAN 73 1473 EDITION OF 1 NOV 65 IS OBSOLETE

UNCLASSIFIED

SECURITY CLASSIFICATION OF THIS PAGE (When Data Entered)

The eastern Pacific active modes (near 160°W) occurred approximately 10 times during each (non–ENSO) season, for an average period of 18 days. Active modes based on zonally–averaged intensities occurred less frequently, with a temporal scale between 22 and 28 days. Active convection in the eastern Pacific was not strongly related to active modes in the rest of the domain; strong east and west Pacific convection occurred simultaneously only four times during the normal seasons, for an average period between 30 and 60 days.

The intensity index was modified to estimate the latitudinal and longitudinal positions of active convection along the ITCZ. Time series of the zonal–average position and intensity showed that the ITCZ moved south as it intensifies.

Convective organization was described using composites of daily OLR from active days. Composites based on different active convection regions yielded different patterns: the zonally–averaged active days produced three zonally oriented cells of intense convection in the ITCZ region; requiring active convection at 160°W and in the zonal mean produced only two cells; this pattern also extended southeastward into the Southern Hemisphere.

# ABSTRACT

**Active Modes of the Pacific ITCZ.** (May 1988)

Patrick Michael Hayes, B.S., University of Wisconsin-Green Bay

Co–Chairmen of Advisory Committee: Dr. James P. McGuirk
Dr. Aylmer H.Thompson

Satellite–observed outgoing longwave radiation (OLR) data from eight six–month cool seasons were examined to find periods of active convection within the Pacific intertropical convergence zone (ITCZ). Descriptive statistics were used to define and describe the time–mean behavior of the Pacific ITCZ. Two seasons (76–77 and 82–83) showed distinctive El Nino–Southern Oscillation (ENSO) signatures in mean, standard deviation, and frequency distribution of OLR. Four other seasons (74–75, 75–76, 79–80, and 80–81) had "normal" OLR statistics. The remaining seasons preceded and followed the major 82–83 event and had intermediate seasonal–mean OLR fields.

Time series of an index measuring convective intensity in the ITCZ were analyzed to find active convection periods. Time–longitude diagrams of the intensity estimates showed how active modes develop, spread, and propagate across the Pacific. Three types of variability of the active modes were identified. The first type had small spatial scales (< 4000 km), short temporal scales (10–20 day durations), and occurred mostly in the eastern Pacific. The second type had longer spatial scales (5000–10,000 km), short temporal scales, and was found throughout the domain. The second type of variability also showed evidence of propagation. The third type had large temporal scales (greater than 30 days), medium spatial scales (2000–6000 km), and was a fixed feature. The third type of variability may be a result of combinations of two or more active periods of the first two types.

# ACTIVE MODES OF THE PACIFIC ITCZ

A Thesis

by

PATRICK MICHAEL HAYES

Submitted to the Graduate College of
Texas A&M University
in partial fulfillment of the requirement for the degree of

MASTER OF SCIENCE

May 1988

Major Subject: Meteorology

# ACTIVE MODES OF THE PACIFIC ITCZ

A Thesis

by

PATRICK MICHAEL HAYES

Approved as to style and content by:

James P. McGuirk
(Co-Chairman of Committee)

Aylmer H. Thompson
(Co-Chairman of Committee)

John M. Klinck
(Member)

James R. Scoggins
(Head of Department)

May 1988

# ABSTRACT

**Active Modes of the Pacific ITCZ.** (May 1988)

Patrick Michael Hayes, B.S., University of Wisconsin-Green Bay

Co-Chairmen of Advisory Committee: Dr. James P. McGuirk
Dr. Aylmer H.Thompson

Satellite-observed outgoing longwave radiation (OLR) data from eight six-month cool seasons were examined to find periods of active convection within the Pacific intertropical convergence zone (ITCZ). Descriptive statistics were used to define and describe the time-mean behavior of the Pacific ITCZ. Two seasons (76–77 and 82–83) showed distinctive El Nino-Southern Oscillation (ENSO) signatures in mean, standard deviation, and frequency distribution of OLR. Four other seasons (74–75, 75–76, 79–80, and 80–81) had "normal" OLR statistics. The remaining seasons preceded and followed the major 82–83 event and had intermediate seasonal-mean OLR fields.

Time series of an index measuring convective intensity in the ITCZ were analyzed to find active convection periods. Time-longitude diagrams of the intensity estimates showed how active modes develop, spread, and propagate across the Pacific. Three types of variability of the active modes were identified. The first type had small spatial scales (< 4000 km), short temporal scales (10–20 day durations), and occurred mostly in the eastern Pacific. The second type had longer spatial scales (5000–10,000 km), short temporal scales, and was found throughout the domain. The second type of variability also showed evidence of propagation. The third type had large temporal scales (greater than 30 days), medium spatial scales (2000–6000 km), and was a fixed feature. The third type of variability may be a result of combinations of two or more active periods of the first two types.

The eastern Pacific active modes (near 160°W) occurred approximately 10 times during each (non–ENSO) season, for an average period of 18 days. Active modes based on zonally–averaged intensities occurred less frequently, with a temporal scale between 22 and 28 days. Active convection in the eastern Pacific was not strongly related to active modes in the rest of the domain; strong east and west Pacific convection occurred simultaneously only four times during the normal seasons, for an average period between 30 and 60 days.

The intensity index was modified to estimate the latitudinal and longitudinal positions of active convection along the ITCZ. Time series of the zonal–average position and intensity showed that the ITCZ moved south as it intensifies.

Convective organization was described using composites of daily OLR from active days. Composites based on different active convection regions yielded different patterns: the zonally–averaged active days produced three zonally oriented cells of intense convection in the ITCZ region; requiring active convection at 160°W and in the zonal mean produced only two cells; this pattern also extended southeastward into the Southern Hemisphere.

## DEDICATION

To my wife, Dawn-Marie, and my parents, John and Millie.

. . . for Solomon the king saith so: ***The glory of God is to conceal a thing, but the glory of the king is to find it out***; as if, according to the innocent play of children, the Divine Majesty took delight to hide his works, to the end to have them found out; as if kings could obtain no greater honour than to be God's play–fellows in that game.

–FRANCIS BACON, *The Advancement of Learning (1605)*

## ACKNOWLEDGMENTS

I acknowledge the general support offered by my committee, particularly the stimulating encouragement provided by Dr. James P. McGuirk.

I thank the United States Air Force for the opportunity to return to Texas A&M University. I will cherish the experience that is being an Aggie for the rest of my life.

This research was sponsored, in part, by the Marshall Space Flight Center, National Aeronautics and Space Administration. Additional research funding was provided by the TAMU Computing Services Center, through the kind assistance of Mary Anne Kornegay.

An oceanographer wrote, *"Science is both an individual and a social activity."* I thank Cecilia Askue for sharing her office with me, and for countless enlightening discussions, some of which were about meteorology. Chuck LeMay, besides being a close friend of my family, conspired with Celia to help get me through several tough programming and dynamics classes. Completion of this research is a direct consequence of the great company and academic pointers provided by Capts. Askue and Lemay.

My final acknowledgment is for the unfaltering support of my wife, Dawn-Marie. This document is a testament to her efforts to preserve **our** sanity throughout our 21-month stay. Raising our two daughters and giving birth to our son, practically on her own, were the least of her trials while I was away at school. She proofed the numerous drafts of this text, and improved upon my efforts more times than I'd like to admit. I hope to continue study, some day, toward a Ph.D., and, with her by my side, I'm sure we'll succeed.

# TABLE OF CONTENTS

## TABLE OF CONTENTS (Continued)

# LIST OF TABLES

# LIST OF FIGURES

## LIST OF FIGURES (Continued)

## LIST OF FIGURES (Continued)

# I. INTRODUCTION

One of the most striking features of the planet's long-time average cloudiness is the zonal band of concentrated convection lying near the equator. The spatial and temporal variability of this intertropical convergence zone (ITCZ) on large (planetary and seasonal/annual/interannual) scales has been well-documented in studies of monsoon behavior (Krishnamurti and Subrahmanyan, 1982) and low-frequency oscillations of tropical circulation (Madden and Julian, 1971; Liebmann and Hartmann, 1982).

Smaller-scale temporal and spatial variability is difficult to study over the tropical oceans for several reasons. First, conventional surface and upper air data are virtually non-existent in some tropical regions. Except for special field programs such as the Global Atmospheric Research Program's (GARP) First GARP Global Experiment (FGGE), the GARP Atlantic Tropical Experiment (GATE), and the Line Islands Experiment (LIE), observations come mainly from widely scattered island stations and infrequent ship reports. Even in the long records of some tropical stations, the diurnal and annual signals overwhelm fluctuations on other time scales. Finally, analyses of variables such as geopotential (Lin and Mock, 1986) and moisture (Thompson *et al.*, 1984; and McGuirk *et al.*, 1986) generally are less reliable in the tropics. These problems make the use of satellite data an attractive alternative and the preferred means to study variability of tropical weather systems.

In this study, outgoing longwave radiation (OLR) data are examined to determine the time-mean behavior of convection over the tropical Pacific during several six-month cool seasons. Appropriately-filtered OLR were analyzed to find preferred times and places for intense convection. A number of active episodes were identified

---

Format is similar to that of the *Journal of the Atmospheric Sciences*.

using indices of ITCZ intensity. Convective organization during active modes was described using time–longitude sections and composites of daily OLR.

A survey of previous work on the variability of tropical convection in general, and on the ITCZ in particular, is presented in Section II. In Section III, the problem is defined, research objectives are listed, and research methodology is outlined. The OLR data set is described in Section IV along with the assumptions about, and limitations of, these data. Data processing procedures are also discussed in Section IV. Section V contains a description of the procedures used to identify active modes, and Section VI discusses techniques used to describe convective organization during active modes. A summary and discussion of the results is presented in Section VII.

# II. PREVIOUS WORK

Considerable research has been devoted to spatial and temporal variability of tropical circulation and convection. The scales of interest range from long-period, global phenomenon such as the El Nino-Southern Oscillation (ENSO) events, to synoptic and smaller-scale features, as in the GARP Atlantic Tropical Experiment (GATE) experiment. In later years, the availability of satellite observations greatly advanced the understanding of tropical meteorology. Previous work bearing on this study falls into three categories: the general investigation of variability of tropical convection; the more specific research on the variability of the intertropical convergence zone (ITCZ); and, work done with the NOAA outgoing longwave radiation (OLR) data.

## Variability of Tropical Convection

The variability of tropical convection on long-time scales has been well-documented in studies of the ENSO phenomenon. During "warming" or intense ENSO events, tropical convection rapidly intensifies and expands eastward in conjunction with a warming equatorial eastern Pacific Ocean. Liebmann and Hartmann (1982) showed that warm SST anomalies during ENSO were accompanied by an increase in the amount of high cloud. This increase in high cloud amount during warming events in 1976-77 and 1982-83 is reflected in satellite infrared radiation (IR) observations as exceptionally cool IR emissions over the southeastern tropical Pacific.

Heddinghaus and Krueger (1981) investigated annual and interannual variability of tropical convection using empirical orthogonal function (EOF) analysis of monthly mean OLR data. They found that the first eigenvector (the solar-forced annual cycle

of convection) contributed 66% of the total OLR variance. The second eigenvector (the spring–fall semiannual cycle) contributed 6% of the variance and showed that the Northern Hemisphere ITCZ is best developed during the northern autumn at around 10°N in the Pacific.

Intraseasonal variability (ISV) of tropical circulation in the Pacific was described by Madden and Julian (1972). They used spectral analysis of 5–10 years of daily radiosonde and station pressure data from tropical islands. Results showed that disturbances originated over the maritime continent, spread eastward across the tropical Pacific, and then repeated, with a period of 40–50 days. Patterns of cloudiness near the equator have the same strong, low–frequency, 20–60 day period and also appear to propagate eastward. In results from EOF analysis of low–pass filtered OLR data, Murakami (1980) noted that subtropical OLR anomalies poleward of 10°N move west–northwestward, while equatorial anomalies propagate eastward.

Lau and Chan (1985, 1986) reported more complex changes of a 40–50 day oscillation of tropical convection over the Indian and western Pacific Oceans. They used complex EOF analysis of low–pass filtered OLR to study propagation characteristics of the 40–50 day tropical oscillation. Time series of area–averaged OLR over the western and central Pacific showed an east–west oriented dipole pattern of convection anomalies. This cloudy/clear pattern had three propagation modes: 1) eastward from the Indian Ocean to the central Pacific; 2) northward from the Indian Ocean to the Indian subcontinent; and 3) northwestward from the equatorial western Pacific to the South China Sea. Lau and Chan noted that this 40–50 day signal "substantially diminishes over the equatorial eastern Pacific." Little or no ISV signal has been found east of the dateline in the eastern North Pacific. Most studies of ISV of tropical convection focus on the East Asian monsoon region and nearby western Pacific

Ocean.

Weickmann *et al.* (1985) statistically related OLR data and 250 mb streamfunction fields to study oscillations of tropical disturbances. After constructing time series of OLR means and variances, they noted several characteristic convection regimes. Relatively high mean OLR and low variance were found in the semi-permanent subtropical high pressure systems. Conversely, low mean OLR and high variance were prevalent over the intertropical and Southern Pacific convergence zones. Where persistent deep convection occurs over tropical land masses such as Africa and South America, both the mean and the variance were anomalously low.

The relationship between ISV and short-period variability of tropical convection was investigated by Murakami *et al.* (1986). Time series of temporally filtered OLR showed that the *amplitude* of short-period fluctuations (periods shorter than 24 days) and the ISV signal oscillated with the same period and were *negatively* correlated. The domain was the tropical western Pacific, where transient disturbances tend to be most active during the wet (negative) half-cycle of the ISV (24–91 day periods). Nakazawa (1986) confirmed this relationship, noting that most of the synoptic-scale Pacific Ocean typhoons developed during the wet half-cycle of the 30–60 day OLR perturbations at 10°N.

**Intertropical Convergence Zone**

One of the most interesting aspects of tropical meteorology is the distinctive, yet elusive, ITCZ. Various authors describe the ITCZ differently in terms of its characteristic features. Early observations of mean fields of cloudiness, precipitation, and surface wind confluence showed a near-equatorial zone of maxima of these elements. Later observational and theoretical studies revealed surface pressure, upward vertical motion, and sea surface temperature (SST) extrema near this zone.

Recent research shows that the convergence–cloudiness–rainfall axis does not coincide with the zone of maximum SST and minimum surface pressure (Hastenrath, 1985). The instantaneous location and intensity of these circulation and convection features fluctuate on all time scales. Analysis of aircraft–measured data gathered during the North Pacific Experiment (NORPAX) from November 1977 to January 1978 led Ramage *et al.* (1981) to conclude that the ITCZ was a "well–defined, highly variable, unpredictable phenomenon of daunting complexity."

For the purpose of this research, the ITCZ is defined in terms of the OLR data used to study it. The ITCZ over the Pacific Ocean is defined as the ensemble of **all** convective activity occurring across the Pacific in the zonal band between the equator and 15°N. Included in this definition are the long–time mean cloudiness, interannual variations such as the ENSO events (even though they tend to wander outside of the stated boundary), tropical cyclones, typhoons, and cloud clusters. Excluded from this definition (and outside the scope of this study) are the Southern Pacific convergence zone (SPCZ) and features restricted to the far western Pacific such as monsoonal cold surges. Convection associated with mid–latitude frontal systems occasionally extends into, and interacts with, the ITCZ; such phenomena *are* of interest to this study. This definition is applicable both locally in time and space, as well as in the zonal and long–time average.

The ITCZ lies just north of the equator in the annual mean, and follows the seasonal march of the sun, swinging further poleward over continents than over oceans. Gruber (1972) analyzed brightness values from ESSA–series satellites to determine the position of the maximum brightness in the ITCZ region. He found that the ITCZ remained north of the equator over both oceans year–round. In the northeastern Pacific, the position varied between 15°N (during late summer) and

5°N (during late winter).

Hartmann and Recker (1986) examined nine years of OLR data with 12–hour temporal resolution, noting maximum ITCZ convection during June–July–August (JJA). Between–season variability has a spatial dependence, with the largest fluctuation occurring over the tropical land masses. Locations distant from the influence of continents, as in the central Pacific, have a weaker seasonal cycle of ITCZ intensity and position.

One manifestation of synoptic–scale ITCZ disturbances is the tropical plume or tropical intrusion. McGuirk and Thompson (1984) presented strong evidence linking explosive development of localized ITCZ convection with an upper–level trough extending equatorward from the mid–latitudes. This enhanced convection, or tropical plume, appears to last for about three days and then subsides as the upper trough progresses eastward past the quasi–stationary tropical plume origin point (Smith *et al.*, 1985). In his climatology of over 150 plume events during three northern winters, Smith (1986) found that plume activity is most vigorous in the eastern North Pacific and during the November–April cool season when the zonal–mean ITCZ is weak.

Two techniques used in studies of the Atlantic ITCZ were used in this research. Murakami (1979) computed area–averaged infrared radiation (IR) brightness values and displayed results in time series and time–longitude diagrams. He related the variation of IR to fluctuations in convective intensity in the Atlantic ITCZ. Frank (1983) used full–disc IR imagery to estimate subjectively the latitude/longitude position of the Atlantic ITCZ. He presented time series of the 3–hourly estimates and a frequency diagram of the central Atlantic (23°W) latitudinal position (see his Figs. 3 and 4). He found a bimodal distribution of ITCZ position, with peaks near 6°N and 8°N latitude.

Both of these studies were conducted using data gathered during GATE.

**OLR Data Analysis**

Perhaps the most important assumption in this study is that satellite-sensed OLR over tropical regions is a good analog for convective activity. In the tropics, OLR amplitude is modulated mostly by cold clouds within the sensor's field of view. In particular, it varies with cloud top temperature. Cold, high tops near the tropopause emit low radiation on the order of 220 $W/m^2$ or less, while trade wind cumulus and clear oceanic regions appear warmer and emit OLR at 260 $W/m^2$ or more. Several researchers have used this relationship to study fluctuations of tropical convection on several temporal and spatial scales.

Lau and Chan (1983) examined short-term climate variability using seven years of OLR. They noted two basic modes of fluctuation in the OLR data and, from these, concluded that there are strong teleconnections, both within the tropics and between the tropics and middle latitudes (see their Figs. 9 and 10). Meehl (1987) used monthly mean OLR over eight years to describe the annual cycle and interannual variability of tropical convection. From the above studies and numerous other examples (Murakami, 1980; Liebmann and Hartmann, 1982; Lau and Chan, 1986), it appears that the assumption that OLR is analogous to tropical convection is well-founded. There are, however, important limitations to be considered when using OLR data. These are outlined in Section IV.

In summary, much research has been conducted to describe the large-scale variability of tropical convection. Satellite data, particularly digitized and gridded outgoing longwave radiation, is a preferred means to study convection and circulation over data-sparse tropical oceans. The predominant signals of low-frequency variability are the annual and semiannual cycles and the 30-60 day oscillation. Vari-

ability of ITCZ convection has been examined in the Atlantic and western Pacific regions. The annual cycle of solar heating affects both the intensity and position of the Pacific ITCZ, and short–period fluctuations appear to be correlated with phases of intraseasonal variability. ITCZ variation on temporal scales smaller than that of the 30–60 day fluctuation have not received much attention.

## III. RESEARCH OBJECTIVES

There were two primary objectives of this study. The first was to find periods of time and locations in space where the Pacific Intertropical Convergence Zone (ITCZ) had unusually intense convective activity during several six-month cool seasons. The second objective was to describe convective organization during these active modes. To attain these two objectives, several tasks were accomplished.

The behavior of the Pacific ITCZ was described quantitatively using outgoing longwave radiation (OLR) satellite data. Descriptive statistics were used to define both the seasonal mean OLR fields and the associated OLR standard deviation fields. Regions with relatively low mean OLR, in conjunction with high OLR standard deviation, identified the average location of the ITCZ. The combination of these OLR parameters adequately defined the temporal mean position and extent of the Pacific ITCZ.

Indices measuring area-averaged OLR in the ITCZ region were defined using the position information obtained from the seasonal mean ITCZ behavior. These indexes were based upon a fundamental assumption that cool OLR anomalies over the tropical oceans implied widespread, or intense (or both) deep convection. One index estimated the intensity of ITCZ convection; the other estimated the latitudinal position of the most intense convection. Both indices used daily OLR that was low-pass filtered to remove high-frequency variability. Both indexes provided estimates at 24 h and 2.5° longitude resolution throughout the domain.

Time series of the the intensity estimates were used to find extreme departures from the seasonal mean behavior. Periods and places having area-averaged OLR values significantly *less than* the mean over a long period of time were identified as "active" regions. Time-longitude sections of the intensity estimates were used to

show: 1) how active modes developed through time and space; and, 2) how ITCZ convection in different parts of the domain varied. Time series of the intensity and position estimates were compared to determine how changes in ITCZ intensity were related to variability of ITCZ position.

To describe convective organization during the active modes, composites of daily OLR were constructed. Days were selected as "active" using three methods, and the composites obtained using days from the three methods were compared. A test was devised to analyze the convective patterns in the composites for statistical significance.

# IV. DATA

Fluctuations in amount of high clouds (with tops in the upper tropical troposphere) modulate infrared radiation (IR) emission observed to space over the tropics. Scanning radiometer measurements taken by sun-synchronous NOAA polar-orbiting satellites have produced outgoing longwave radiation (OLR) data since June 1974. Digitized OLR has been the preferred data in many investigations of tropical climate variability, and are the data used in this study of ITCZ variability.

Discussion of the data and preliminary processing is presented in two parts. The first outlines how NOAA derives OLR from window radiance measurements. The relationship between window radiance and equivalent cloudtop temperature is also discussed. The second part describes procedures used to process further the OLR data for this study. Treatment of missing data, removal of seasonal trends, and temporal filtering are addressed.

## NOAA OLR Data

Twice-daily observations of upwelling 10.5–12.5 $\mu$m window-channel infrared radiation (IR) are taken around the globe, with morning and evening equator crossing times varying from 0230 to 0900 LST (southbound) and 1430 to 2100 LST (northbound). Original 8 km resolution data are spatially-averaged, digitized, and archived on square grids of 2.5° latitude-longitude resolution. The IR measurements taken over the equator are therefore effectively smoothed to approximately 280 km spatial resolution. Gruber and Winston (1978) and Gruber and Krueger (1984) describe the data in detail. This study uses an 8-year subset of the NOAA data; the time period spans 21 October 1974 to 10 May 1984 (with some missing portions).

These data were adjusted at NOAA for bias due to changes in satellites and

window–channel radiometers, and were standardized with respect to equatorial crossing times. In the corrected data, scene–to–scene variation is on the order of 10 to 100 times larger than the 1 $W/m^2$ instrument uncertainty (Short and Cahalan, 1983). The only substantial period of missing data stretches from March through December 1978. Other missing portions are confined mostly to narrow north–south bands on individual satellite passes.

A fundamental assumption used in this study is that low, or cold, OLR anomalies over the tropical oceans imply intense and/or widespread deep convection. This assumption is substantiated when considering how OLR is derived from satellite–observed window radiance. NOAA uses a three–step procedure. Window radiance ($R_o$) is converted to radiance equivalent brightness temperature ($T_{rb}$) through Planck's Law:

$$T_{rb} = \frac{c_2 \cdot \nu_o}{\ln[c_1 \cdot \nu_o^3/(R_o + 1)]} , \qquad (1)$$

where $R_o$ is the window radiance observed at the central wave number, $\nu_o$. The constants $c_1$ and $c_2$ are

$$c_1 = 1.191 \times 10^{-5} \text{ erg cm}^2 \text{ sec}^{-1} , \text{ and}$$

$$c_2 = 1.439 \text{ cm } ^\circ\text{K}.$$

Next, flux equivalent brightness temperature ($T_{fb}$) is obtained using an empirical regression formula:

$$T_{fb} = ( a - b \cdot T_{rb} ) \cdot T_{rb} \qquad (2)$$

(from Ohring *et al.*, 1984), where, for example, for the NOAA 7 observations, a = 1.2149, b = 0.001055 $K^{-1}$. Similar expressions were used for the other IR sensors onboard the NOAA SR series, TIROS N, and NOAA 6 satellites. Finally, OLR flux emittance, $F_{olr}$, is derived using the Stefan–Boltzmann Law:

$$F_{olr} = \sigma \cdot T_{fb}^4. \tag{3}$$

The approximate relationship between equivalent cloudtop temperature ($T_c$) and OLR emittance (OLR) is:

$$\frac{\Delta OLR}{\Delta T_c} \approx 2 \frac{W}{m^2 \circ K} \tag{4}$$

with respect to a reference point of: OLR $\approx$ 250 W/$m^2$ at $T_c$ = 273°K (from Cahalan *et al.*, 1982). This correlation between satellite–observed window radiance and equivalent cloudtop temperature is the basis of the fundamental assumption used in this study.

One disadvantage of these data is the imprecise physical link between OLR and *three–dimensional* convective structure. The OLR information provides only a one–dimensional plan view of small regions of middle and upper tropospheric clouds. Low, or cold, anomalies of OLR over the tropical oceans indicate either more than usual cloudiness in the upper troposphere, in the vicinity of the gridpoint, or more deep convection than is usual, or both. Circulation and vertical structure cannot be inferred using only OLR analyses. The close correlation between areas with relatively cool OLR values and regions of deep convection in the tropics makes these data appropriate for the purpose of this study.

## OLR Pre-Processing for This Study

The NOAA OLR data were processed to facilitate analysis of the Pacific ITCZ during Northern Hemisphere cool seasons. Missing data at gridpoints were filled by temporally averaging to 24 h resolution. This averaging reduced the amount of missing data by approximately half. The remaining missing gridpoint values were filled by interpolation over adjacent space and time gridpoints.

### *Selection of OLR Domain*

The spatial domain of this study is the Pacific Ocean, from 120°E to 90°W, and from 40°N to 10°S (Fig. 1). With data points spaced every 2.5°, this domain results in daily grids of 61 (zonal) by 21 (meridional) points. This spatial domain contains the temporal mean position of the Pacific ITCZ, as well as extreme departures in position from that mean location. Equatorial and subtropical convection that is related to the ITCZ is also captured in this domain.

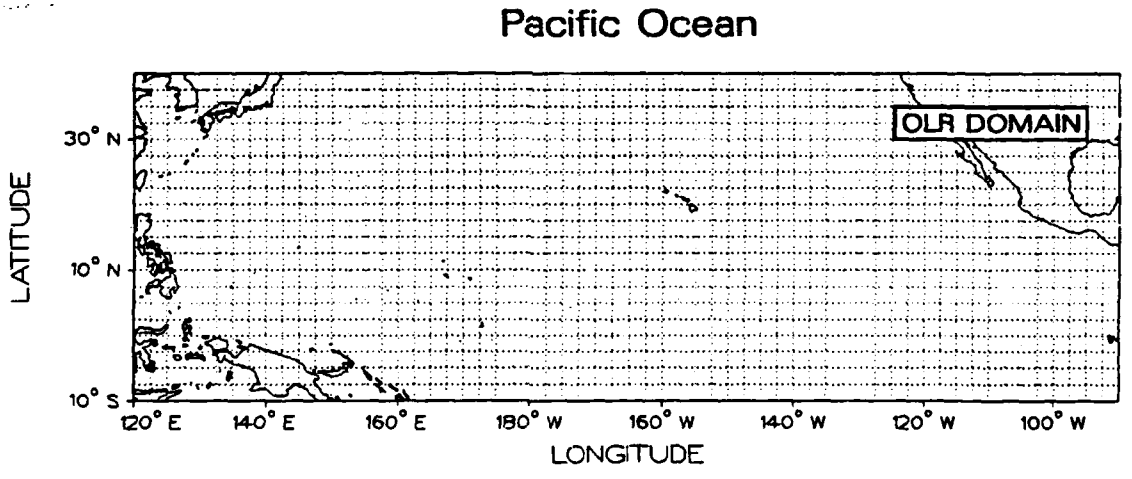


Fig. 1. Spatial domain of this study. Grid represents 2.5° spacing of OLR.

An appropriate temporal domain was selected to allow study of wintertime ITCZ activity. Previous studies indicate that during the Northern Hemisphere winter the seasonal mean ITCZ is weak, and unique disturbances within the ITCZ develop (see, for example, McGuirk, 1987). OLR from 1 November to 30 April during eight winter seasons (1974–75, 75–76, 76–77, 79–80, 80–81, 81–82, 82–83, and 83–84) were retained for further analysis. In addition, to account for boundary effects of temporal filtering, 10–day buffers on each end of all six–month seasons were added. Each of the 8 "six–month" seasons contained OLR from 21 October to 10 May.

*Average OLR Fields*

Researchers have used OLR to determine estimates of monthly, seasonal, and annual mean fields of cloudiness (e.g., Gruber *et al.*, 1986). Figure 2 shows maps of the 8–season mean OLR and the associated standard deviation. Obvious features are the regions of warm mean OLR with low standard deviations that mark the average location of the Pacific subtropical high and the equatorial dry zone. The Pacific ITCZ appears as the zonal band of low mean OLR with correspondingly high standard deviation, centered near 8°N latitude.

These 8–season mean fields are the gridpoint averages of the eight individual seasonal–average maps. OLR anomalies (the difference between the season–average and the 8–season grand average) were computed for each season to show interannual variability of the mean fields (Fig. 3). Seasonal standard deviation (temporal variation) maps associated with the season–average OLR are shown in Fig. 4.

The anomaly maps illustrate both the similarities and the interannual variation between temporal mean convection in the eight cool seasons. As an example, during the 1982–83 ENSO event, widespread intense convection, indicated by very large negative OLR anomalies, over the entire equatorial Eastern Pacific is obviously

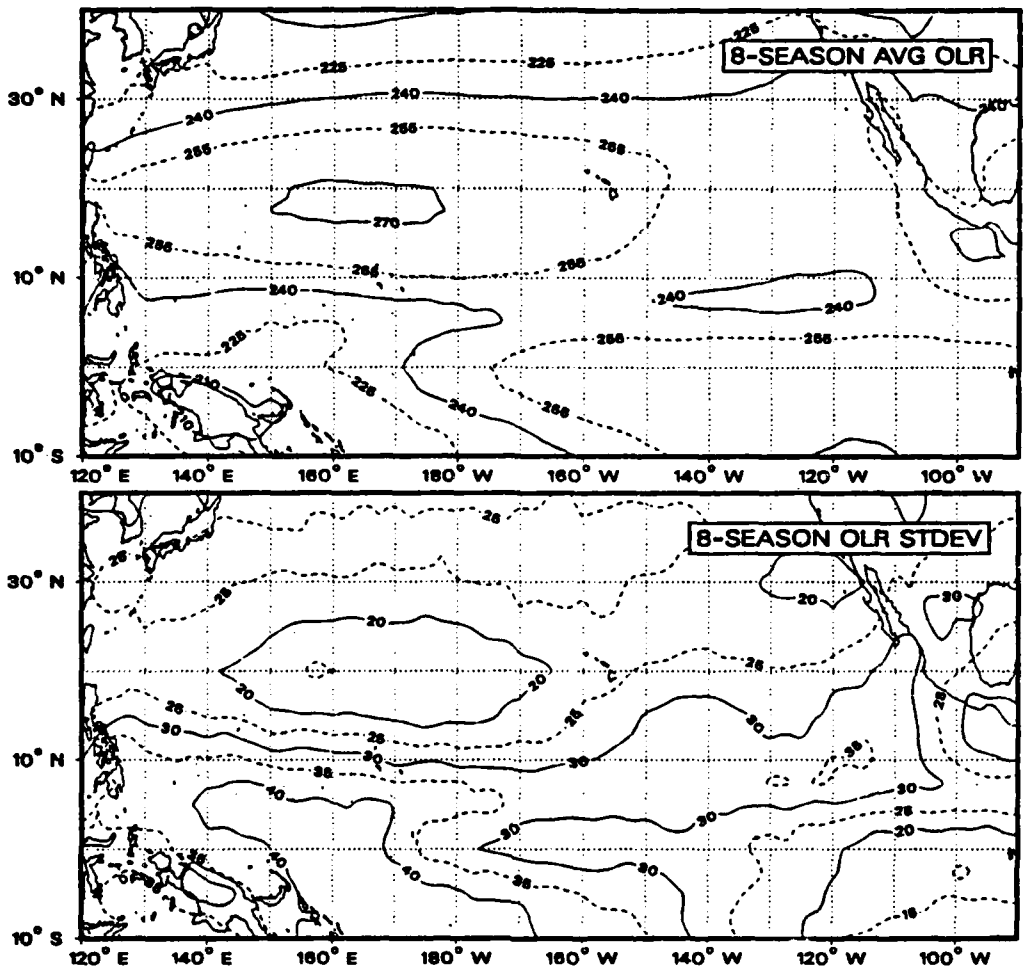


Fig. 2. 8–season average OLR (top) and average standard deviation (bottom). *Units are* $W/m^2$, *averaged across 8 six–month cool seasons.*

different from any other seasonal mean condition. In contrast to the 82–83 season, the 76–77, 80–81, and 81–82 seasons have weak OLR anomalies, indicating season–average convection patterns similar to the long–time mean. An interesting feature common to both the 74–75 and 75–76 seasons are warm/cool dipole–like anomalies located near 165°W/5°S and 150°W/15°N, respectively. Another feature of the anomaly maps is that the negative (or cloudy) anomalies are oriented primarily west–east, often with slight tilts to the ENE (see, for example, Fig. 4a, the 74–75, 75–76,

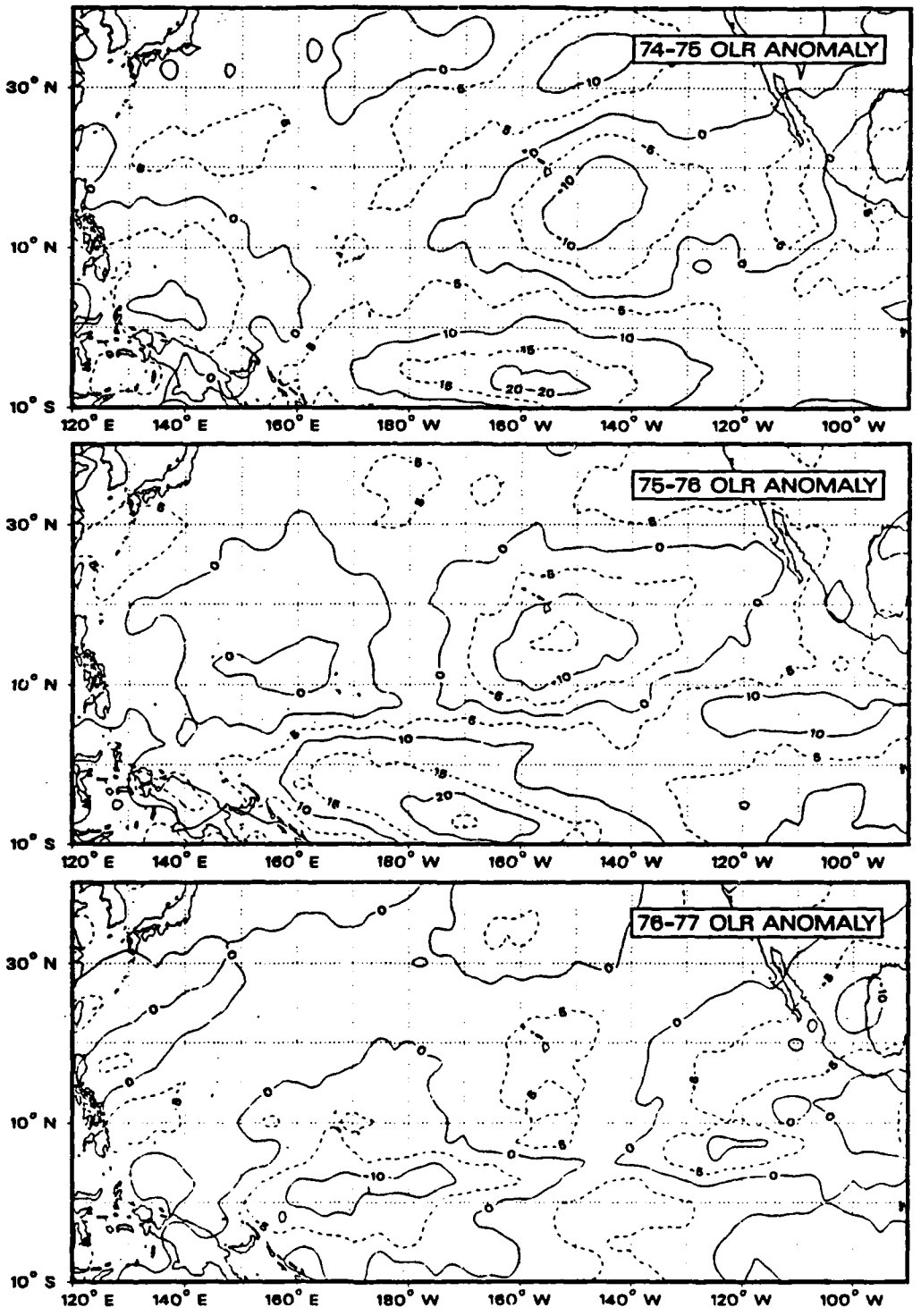


Fig. 3a. Seasonal OLR anomaly fields for 6-month cool seasons. Nov 74–May 75 (top), 75/76 (middle), and 76/77 (bottom).

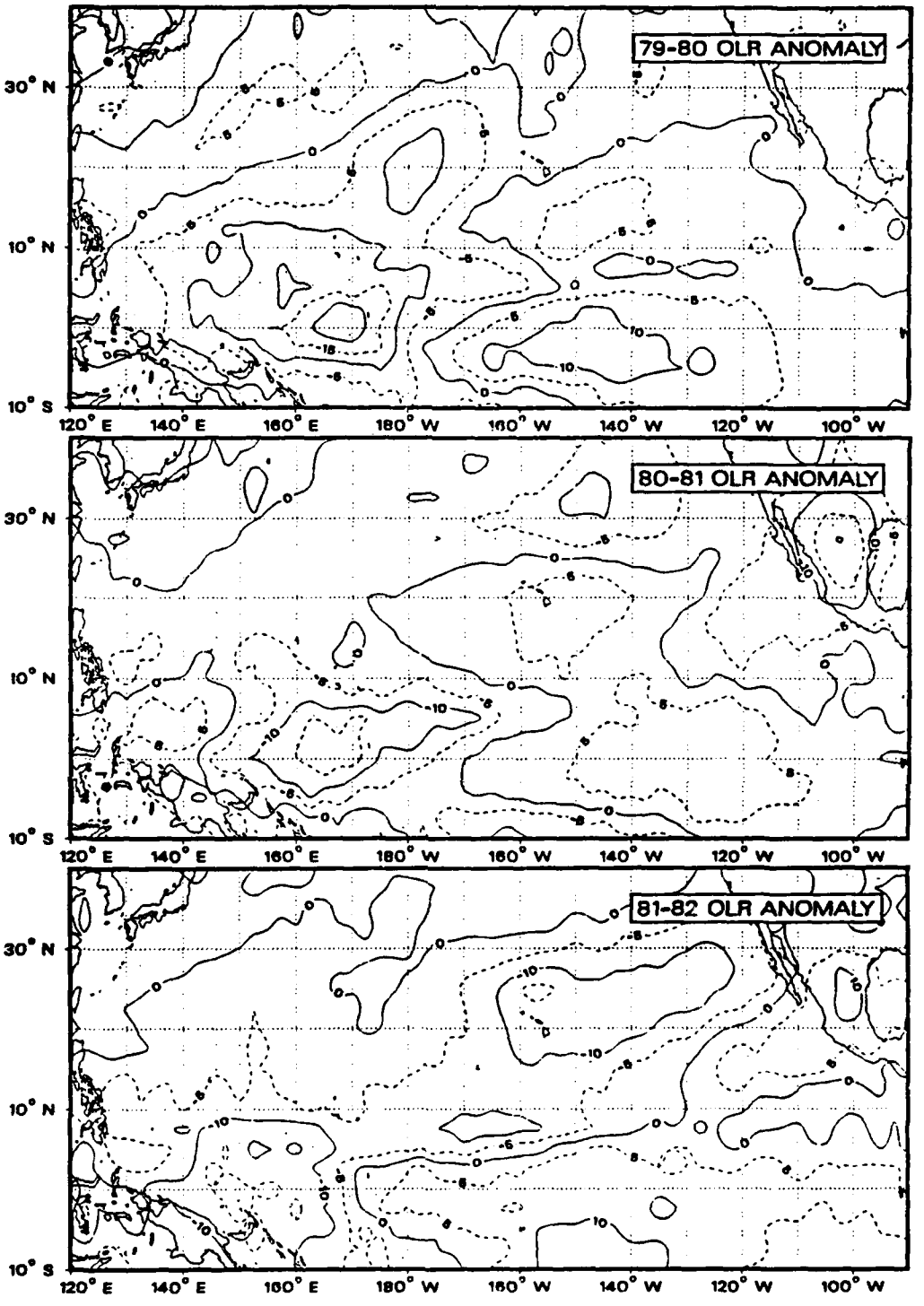


Fig. 3b. Same as Fig. 3a, except 79/80 (top), 80/81 (middle), and 81/82 (bottom).

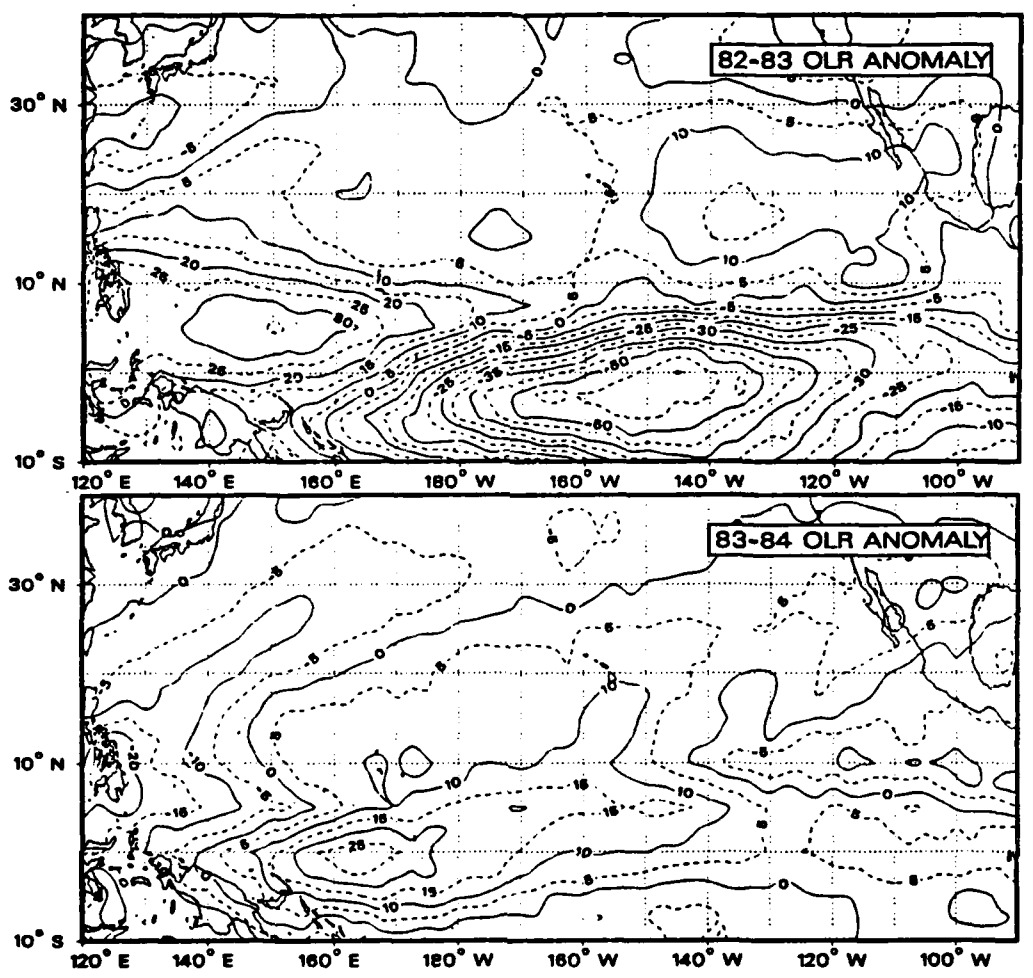


Fig. 3c. Same as Fig. 3a, except 82/83 (top), and 83/84 (bottom).

and 76–77 seasonal anomalies).

The standard deviation (variability through time) fields show three zones of high variance along the ITCZ. A western zone, stretching southeastward from the Phillipine Islands, is associated with the Southern Pacific convergence Zone (SPCZ). The other zones are located near 160°W/8°N and between 90°W and 120°W at 15°N. The seasonal fields of standard deviation are well-correlated (negatively) with their respective OLR anomaly fields. Warm OLR in the subtropical high and equatorial

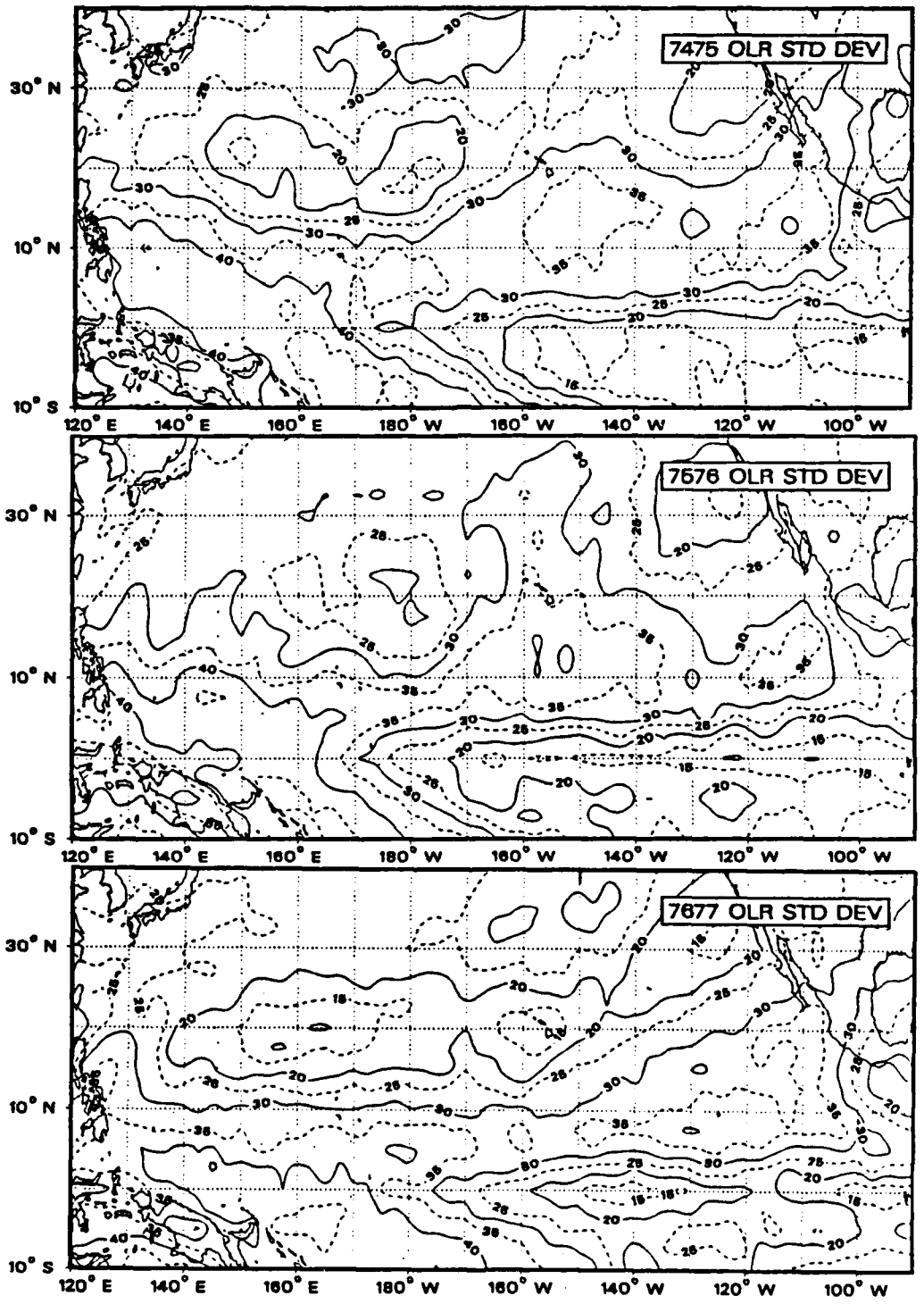


Fig. 4a. Seasonal OLR standard deviation fields for 6-month cool seasons. Nov 74–May 75 (top), 75/76 (middle), and 76/77 (bottom).

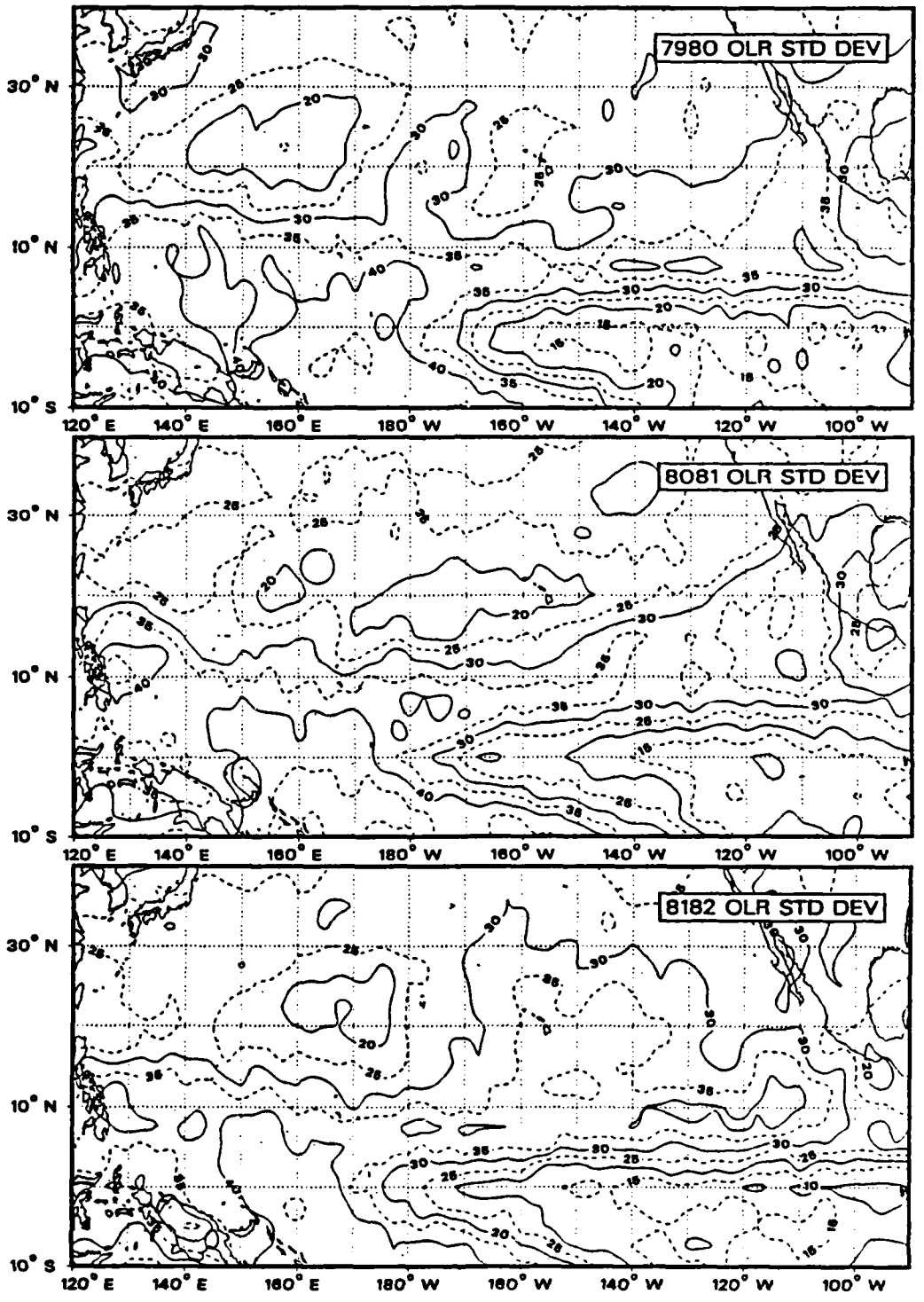


Fig. 4b. Same as Fig. 4a, except 79/80 (top), 80/81 (middle), and 81/82 (bottom).

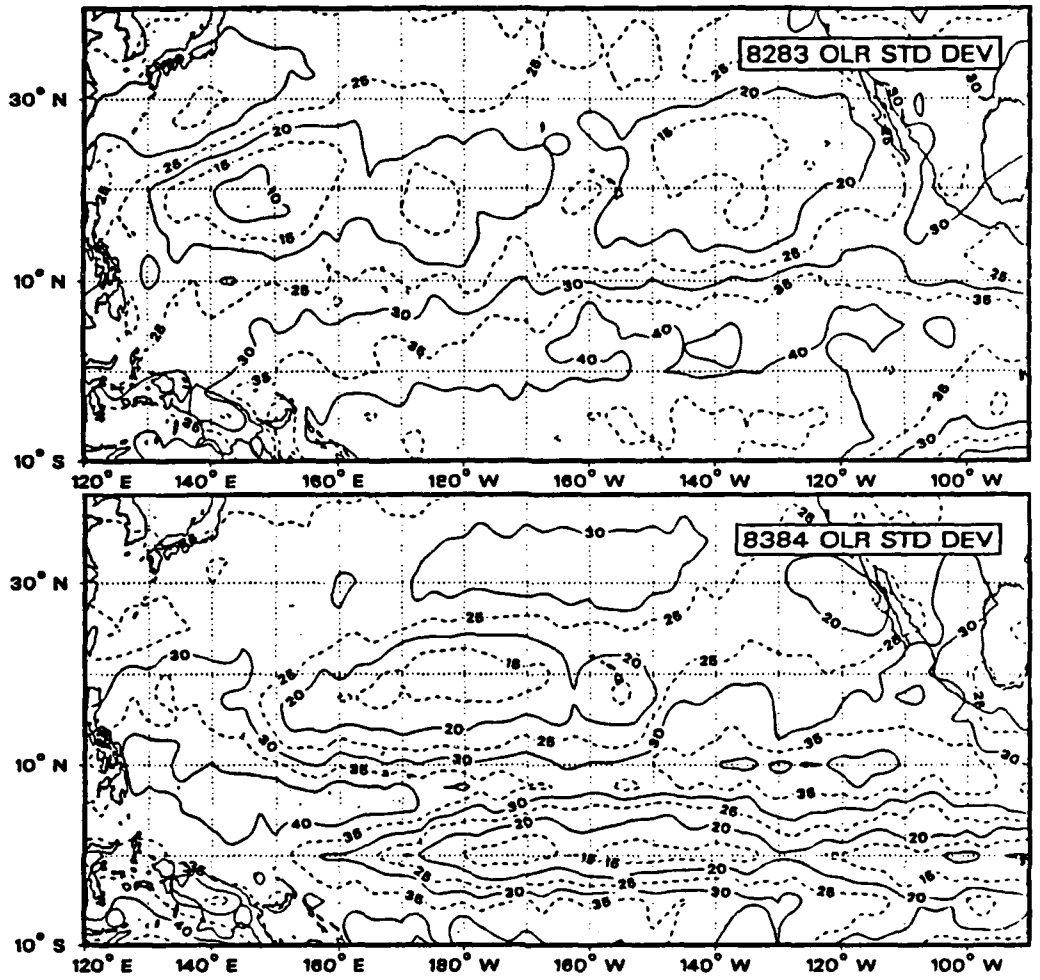


Fig. 4c. Same as Fig. 4a, except 82/83 (top), and 83/84 (bottom).

dry zone is persistent, while cool OLR in the ITCZ and SPCZ is highly–variable. There are regions in some seasons that are exceptions to this general behavior. For example, over the maritime continent (primarily Indonesia), there is strong, persistent convection year–round, resulting in *low* seasonal–mean OLR and *low* standard deviation.

These seasonal and grand mean OLR and standard deviation maps describe the average position of the ITCZ as well as interannual departures from average. This

position information about the temporal mean ITCZ was used to develop the ITCZ indices described in Section V.

*Seasonal Component of ITCZ Variability*

A time series of daily OLR at any single gridpoint shows that a large portion of the variation in time is due to the annual and semiannual cycles of solar insolation (Fig. 5). In order to study variability on shorter time scales (periods of less than 6 months), the temporal mean and the annual and semiannual components were calculated for each season, and were then subtracted from the daily data.

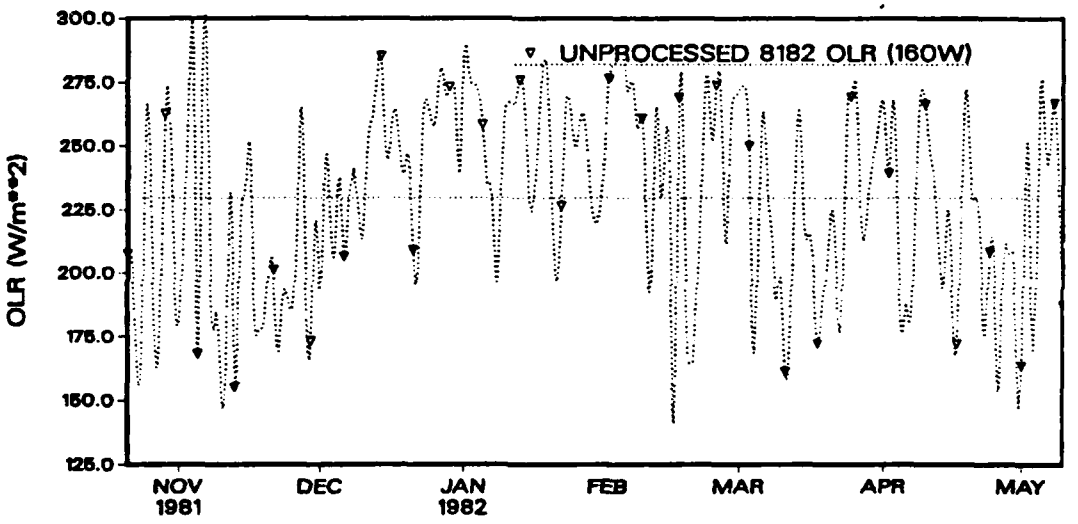


Fig. 5. Daily OLR at 160°W/7.5°N during the 81–82 cool season. Symbols appear every 7 days, horizontal line is the seasonal mean, units are W/m$^2$.

Over a given cool season, a time series of daily OLR can be represented as a sum of three components;

$$\mathbf{olr}_{(i,j,t)} = \overline{\mathbf{OLR}}_{(i,j)} + \widetilde{\mathbf{OLR}}_{(i,j,t)} + \mathbf{OLR}'_{(i,j,t)}. \qquad (5)$$

$\mathbf{olr}_{(i,j,t)}$ are the daily OLR values; $\overline{\mathbf{OLR}}_{(i,j,t)}$ are the seasonal mean values at each

gridpoint, averaged across 185 days at each gridpoint, for each season. $\widetilde{\mathbf{OLR}}_{(i,j,t)}$ is the slowly–varying (periods longer than $\approx$ 90 days) component; and the residual, $\mathbf{OLR}'_{(i,j,t)}$, contains short temporal scale variability (periods less than 90 days). Indices used are $i$ = 1 to 61 for zonal gridpoints; $j$ = 1 to 21 for meridional gridpoints; and $t$ = 1 to 185 for days in the given record.

Figure 6 is a plot of the time series of these components observed at a representative gridpoint during the 81–82 cool season. Curve A is the series of $\mathbf{olr}_{(i,j,t)}$; Curve B represents the sum of the seasonal mean and long–period component ( $\overline{\mathbf{OLR}}_{(i,j)} + \widetilde{\mathbf{OLR}}_{(i,j,t)}$ ); and Curve C (on the lower horizontal axis) is the series of the residual, $\mathbf{OLR}'_{(i,j,t)}$.

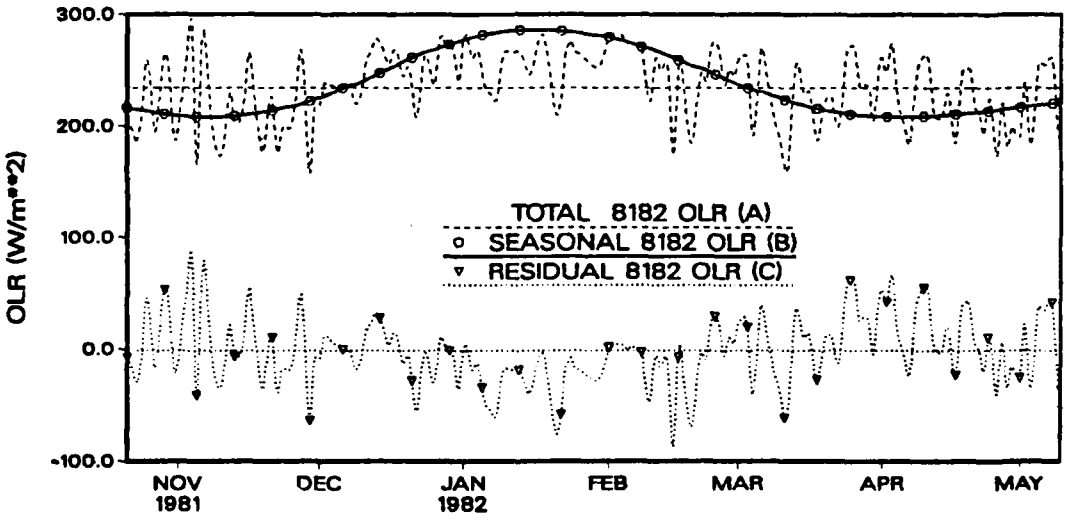


Fig. 6. Time series of three OLR components at 160°W/7.5°N during 81–82 cool season. Units are W/m$^2$, and the three curves are described in the text.

The long–period component ($\widetilde{\mathbf{OLR}}_{(i,j,t)}$) was obtained by fitting a least squares curve to the OLR time series (185 days) at each gridpoint. The relative strength of the seasonal cycle was captured by solving for the first two terms in a tempo. al Fourier decomposition of the original OLR series. For example, in a given cool season and at

a given gridpoint location (fixed $i$ and $j$), the residual–plus–long–period component was expressed as the Fourier series of the original daily series minus the seasonal mean (from (5));

$$\mathbf{olr}_{(t)} - \overline{\mathbf{OLR}} = \widetilde{\mathbf{OLR}}_{(t)} + \mathbf{OLR}'_{(t)} = \sum_{n=1}^{\infty} \left[ a_n \cos n\omega t - b_n \sin n\omega t \right] \quad (6)$$

where the index $t$ counts through the 185–day cool season, and the fundamental frequency, $\omega$, was defined in terms of the annual cycle:

$$\omega = \frac{2\pi}{365} .$$

The infinite Fourier series in (6) was truncated using only the first two terms (the annual and semiannual cycle; $n$ = 1,2) to estimate the Fourier coefficients $a_1$, $a_2$, $b_1$, and $b_2$. These coefficients were computed for each gridpoint location in every cool season. An index was defined to estimate the amplitude of the annual and semiannual cycle as:

$$\mathbf{season}_{(i,j)} = \sqrt{(a_1^2 + a_2^2 + b_1^2 + b_2^2)_{(i,j)}} , \quad (7)$$

where the a's and b's are from (6). Plots of these estimates for each season appear in Fig. 7. Notice the large amplitude of the seasonal cycle in the ITCZ region compared to that in the subtropical high region. In general, regions of large amplitude of the annual/semiannual cycle in Fig. 7 correspond closely to the areas of large standard deviation in Fig. 4. The truncated Fourier series made up the long–period component, $\widetilde{\mathbf{OLR}}_{(i,j,t)}$, appearing in (5) and (6). After subtracting the long–period component and the time–mean ($\overline{\mathbf{OLR}}_{(i,j)}$) from the original data, further processing

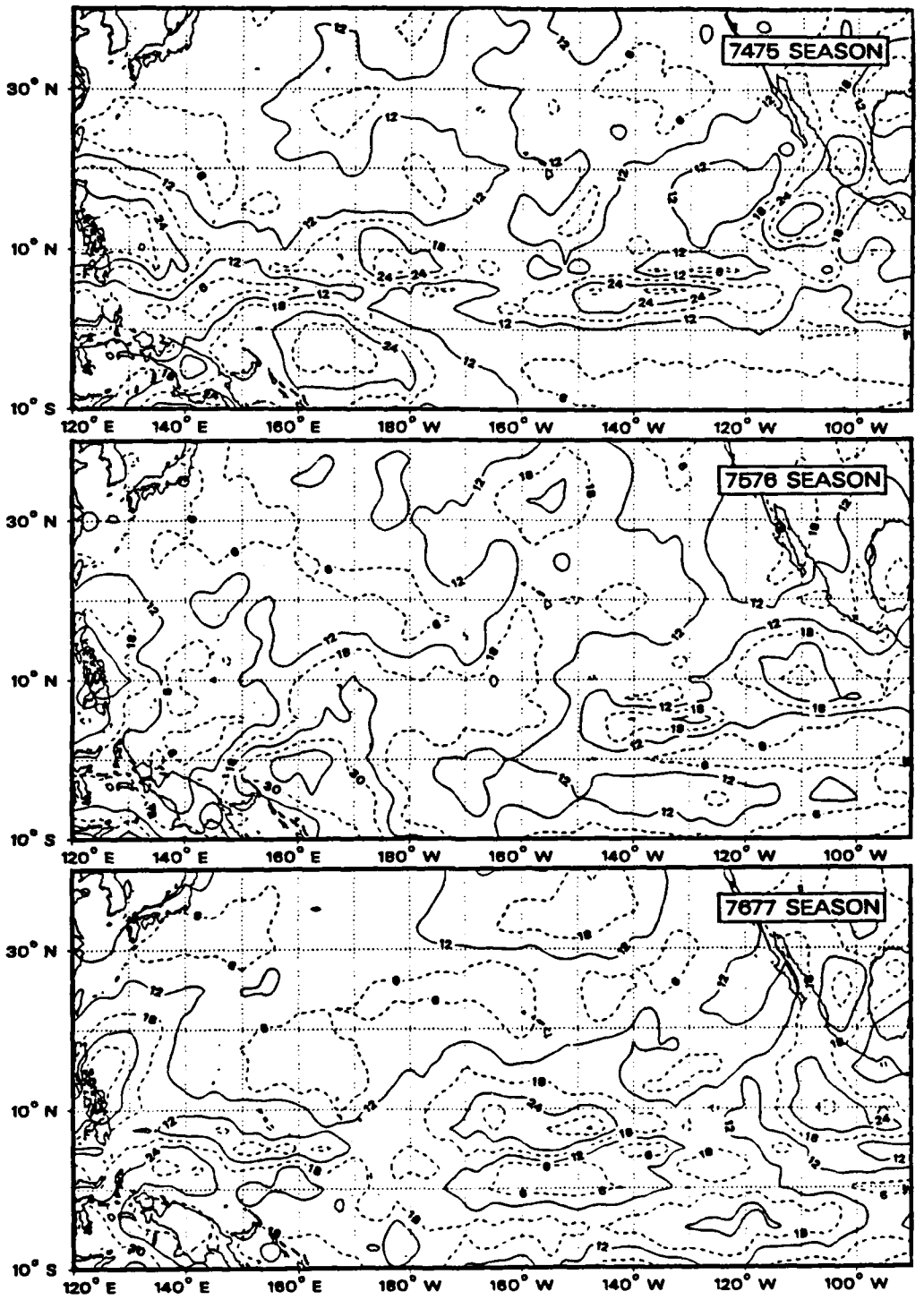


Fig. 7a. Relative strength of the seasonal cycle of convection calculated from cool-season OLR data. Nov 74–May 75 (top), 75/76 (middle), and 76/77 (bottom).

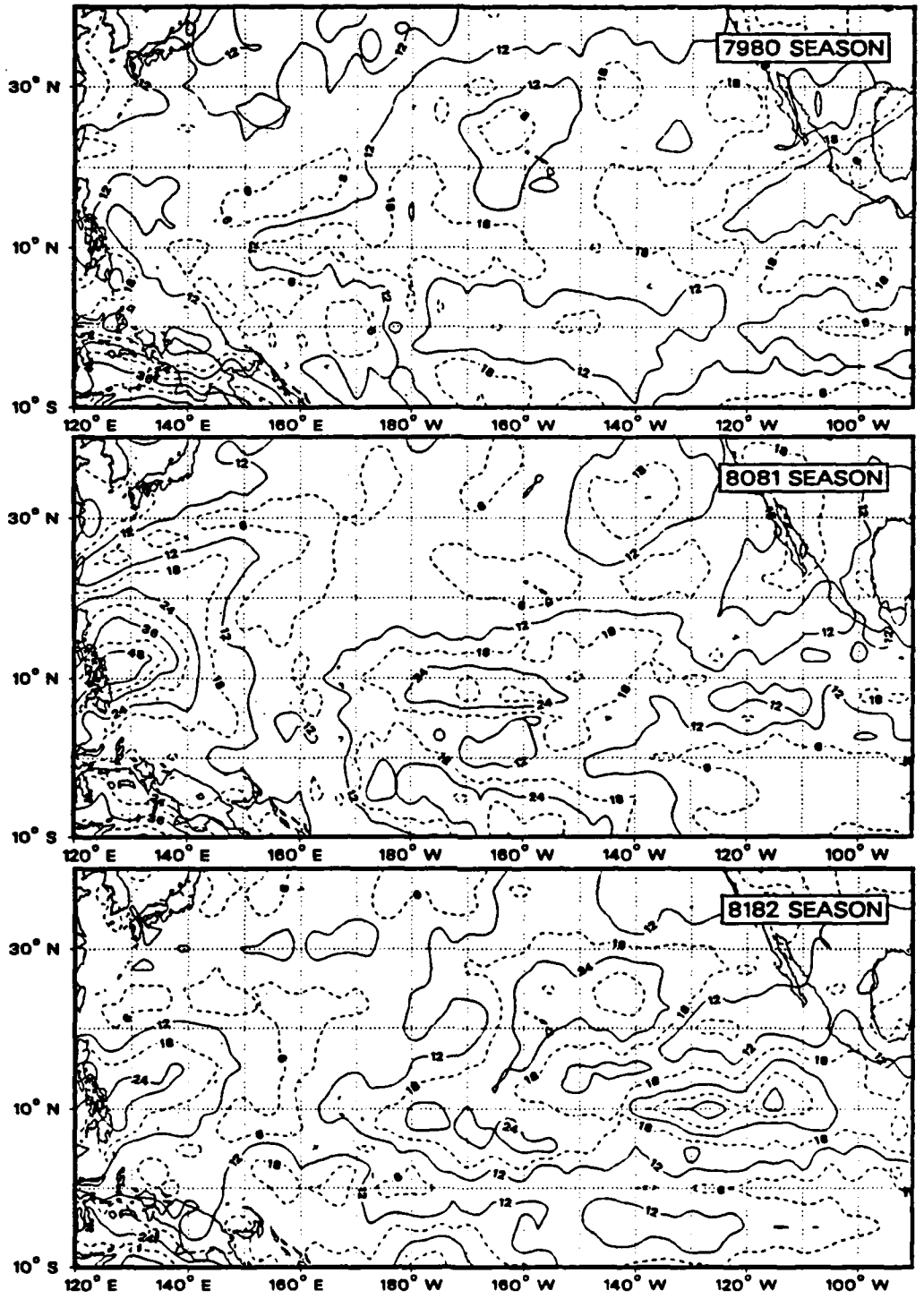


Fig. 7b. Same as Fig. 7a, except 79/80 (top), 80/81 (middle), and 81/82 (bottom).

continued with the residual, or short-period component, $\mathbf{OLR}'_{(i,j,t)}$:

$$\mathbf{olr}_{(i,j,t)} - \overline{\mathbf{OLR}}_{(i,j)} - \widetilde{\mathbf{OLR}}_{(i,j,t)} = \mathbf{OLR}'_{(i,j,t)}. \quad (8)$$

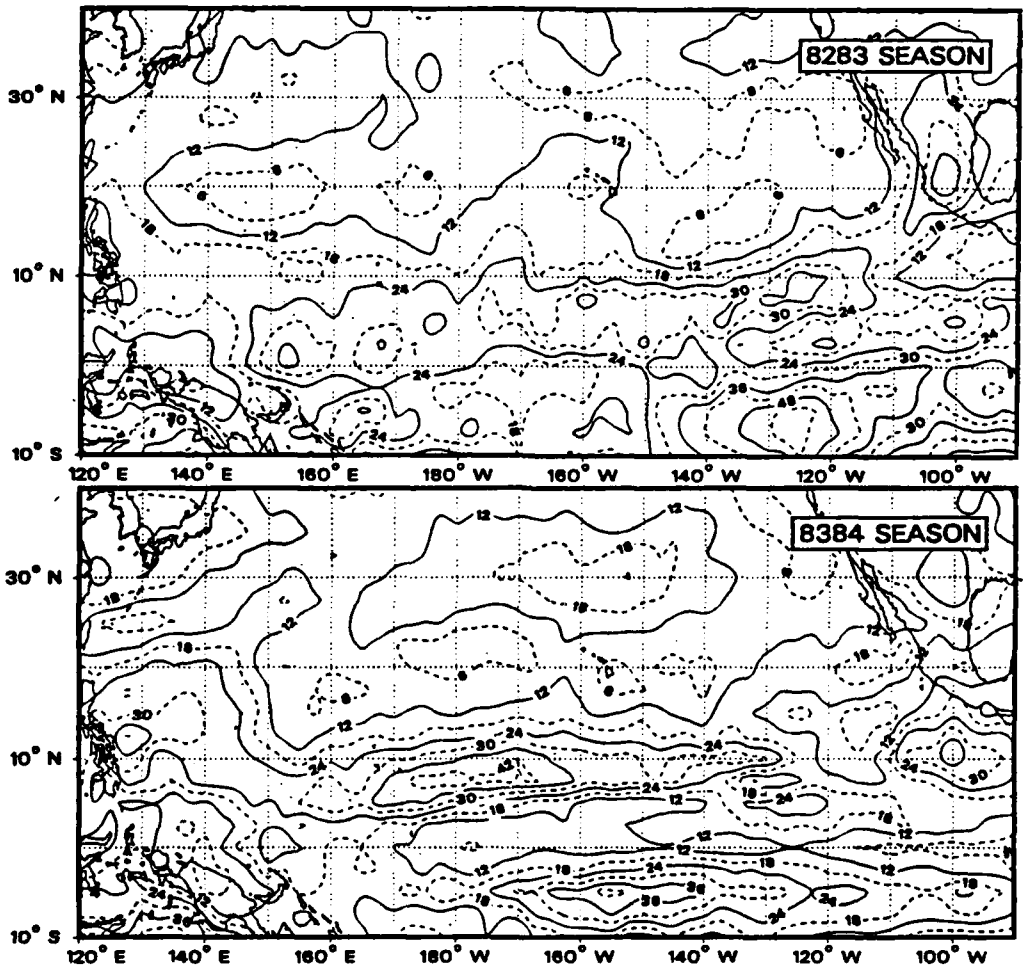


Fig. 7c. Same as Fig. 7a, except 82/83 (top), and 83/84 (bottom).

The results were nearly-stationary time series at each gridpoint throughout each cool season. Figure 8 is a plot of the series of the daily OLR ($\mathbf{OLR}'_{(i,j,t)}$) from (8)) at 160°W/7.5°N during the 81-82 cool season. The time series is only

"nearly–stationary" because, as is apparent in Fig. 8, there still remains some long–period trend. However, the long–period variability remaining in the $\mathbf{OLR}'_{(i,j,t)}$, is not forced by the annual/semiannual solar cycle. This unforced long–period or low–frequency variability is due probably to global–scale fluctuations in the Earth's general atmospheric circulation, and is of some interest in this study.

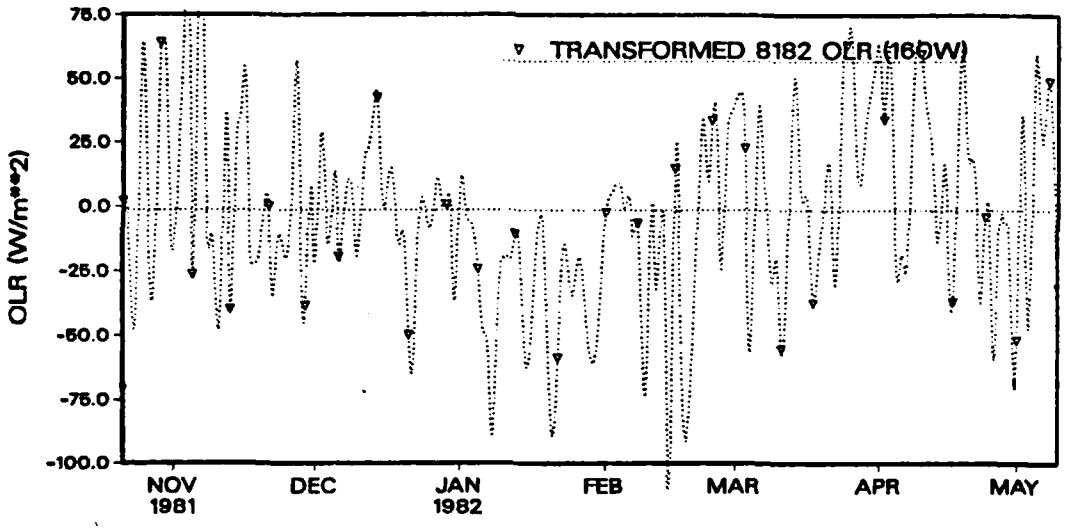


Fig. 8. Time series of transformed OLR at 160°W/7.5°N. Units are W/m$^2$, horizontal line is seasonal mean. Symbols spaced every seven days.

As part of the descriptive statistical analysis, frequency distributions of the data in appropriate locations are presented. If the OLR data are not approximately normally distributed, tests for significance of means or confidence intervals will be invalid. The range of data shown in Fig. 8 was divided into ten class intervals, each of width 25 W/m$^2$, from −125 to +125 W/m$^2$. Sampling was conducted in the three main convective regimes of interest in this study. The subtropical anticyclone was sampled at 20°N, between 170°W to 150°W, or at nine gridpoints in the seasonal average center of the warm OLR anomaly. The ITCZ and the equatorial dry zone were sampled at 7.5°N and 5°S, respectively, over the same zonal strip (170°W to

150°W). The occurrences of transformed OLR ($\mathbf{OLR}'_{(i,j,t)}$ from (8)) in the intervals noted, in these three regions, and in each season, were totaled and are presented in Fig. 9.

The distribution of transformed OLR in the subtropical anticyclone (dashed curves in Fig. 9) is nearly Gaussian, except for negative tails in some seasons. This region has the narrowest range (small $\sigma$) of OLR, with expanded spreads of OLR during the two ENSO seasons, 76–77 and 82–83. The mode is positive (relatively cloud–free) in all seasons except the strong ENSO (82–83) season.

OLR in the ITCZ region (solid curves) is broadly distributed (high $\sigma$) with the largest negative tail (most negative anomalies, or cloudiness). Three seasons (76–77, 79–80, and 80–81) show a bimodal tendency with a second (minor) positve maxima. This may be indicative of periods when the ITCZ was inactive, or active at a position different from 7.5°N latitude. The primary mode is negative (relatively cloudy) in five of eight seasons.

The equatorial zone (dotted curves) has variable OLR distributions. During half of the seasons (74–75, 75–76, 79–80, and 81–82), the equatorial and subtropical distributions are similar, while during the others (ENSO seasons 76–77 and 82–83, and 80–81 and 83–84), the equatorial distribution appears similar to that of the ITCZ. This behavior is probably linked to interannual variations in the average position of the ITCZ. When the seasonal average position of the ITCZ is south of the long–time mean, the equatorial zone has more cloudiness (with OLR distributed similar to the ITCZ); and when north of the long–time mean, the equator is more cloud–free, like the subtropical anticyclone.

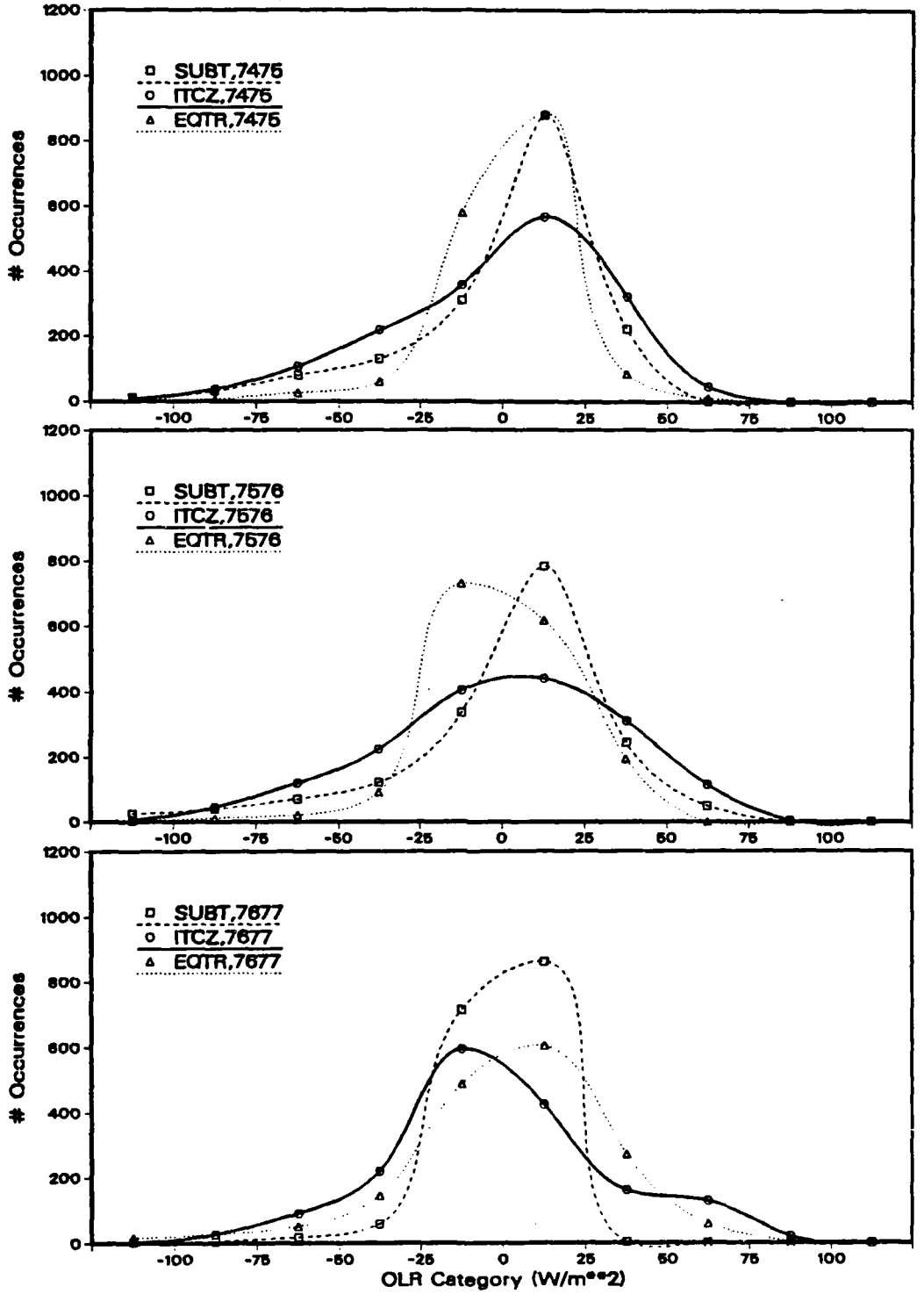


Fig. 9a. Frequency of occurrence of transformed OLR in three zonal bands; at 20°N, 7.5°N, and 5°S. Nov 74–May 75 (top), 75/76 (middle), and 76/77 (bottom).

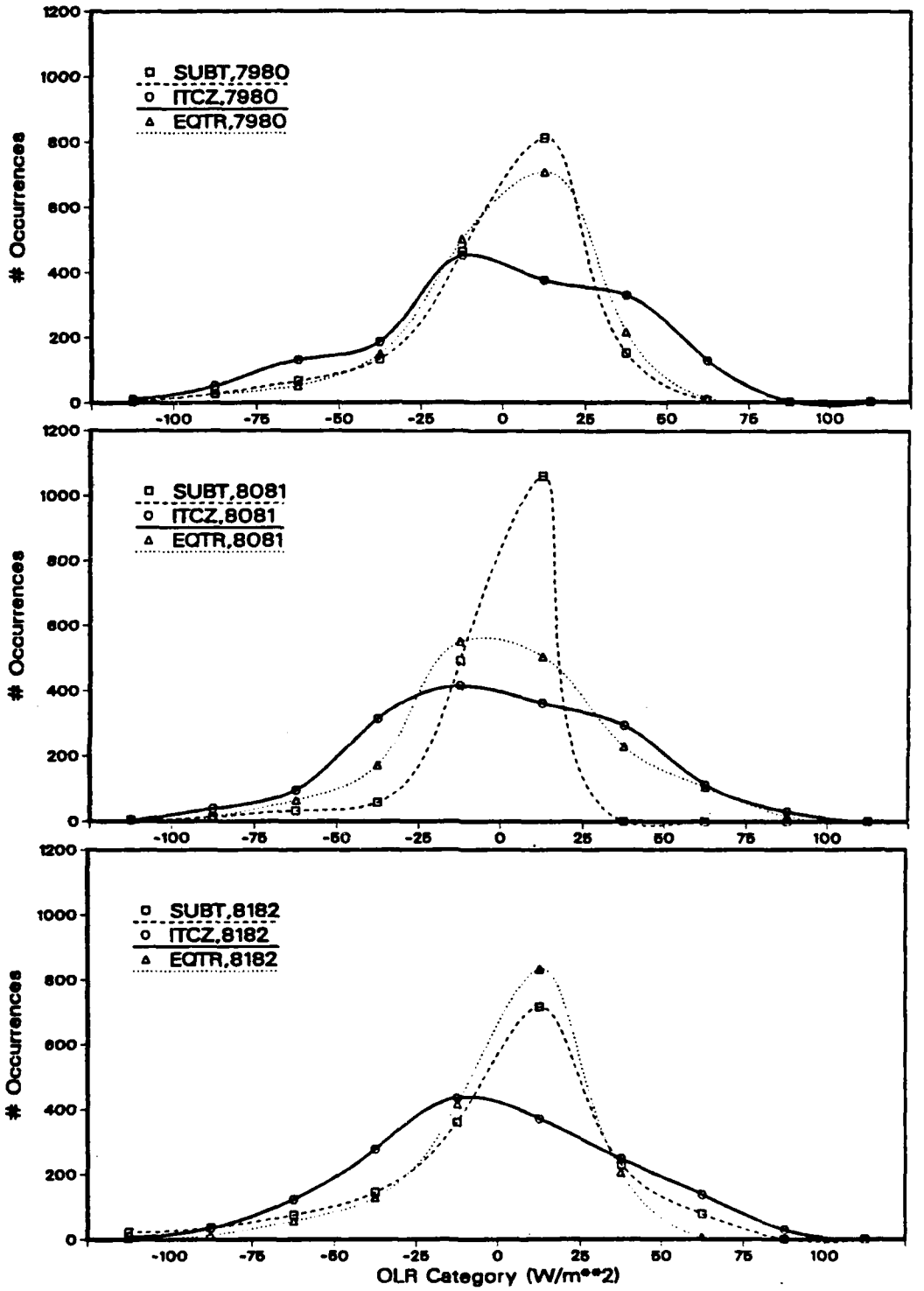


Fig. 9b. Same as Fig. 9a, except 79/80 (top), 80/81 (middle), and 81/82 (bottom).

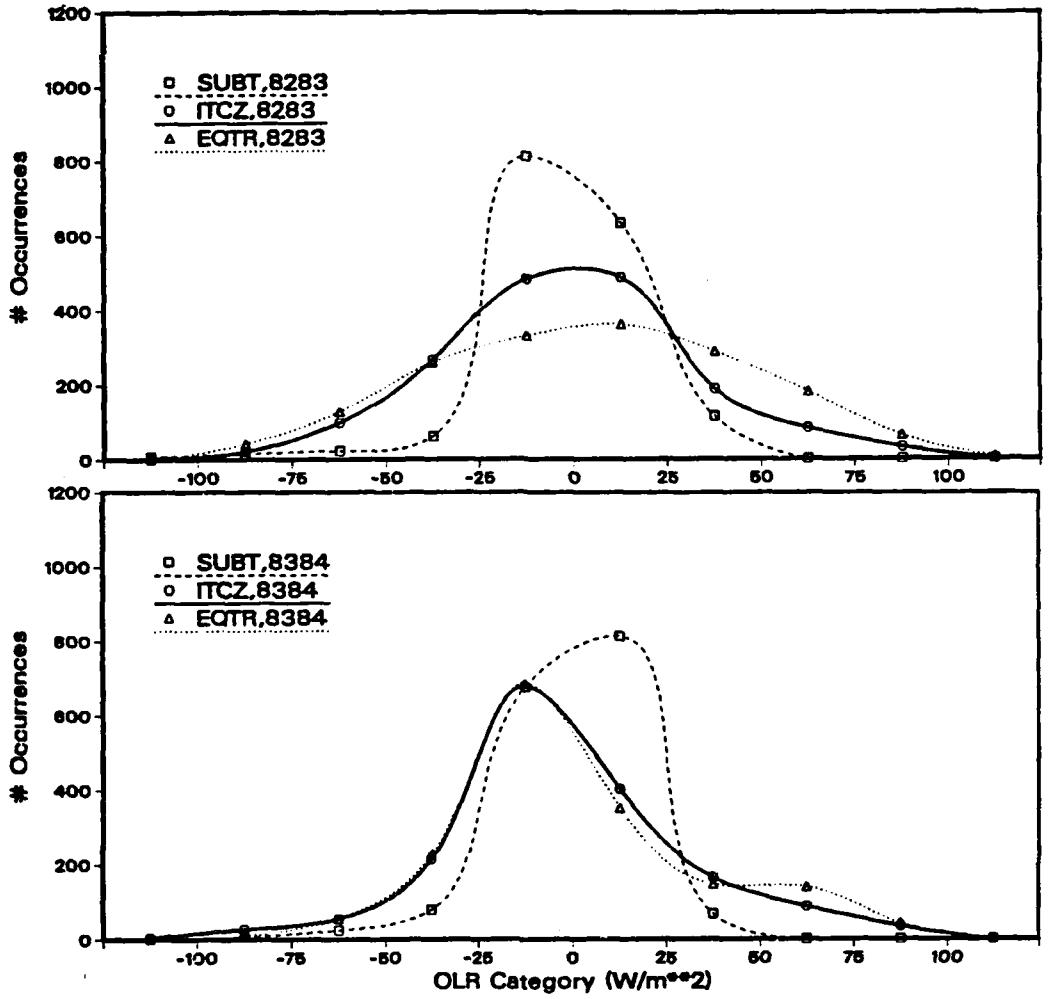


Fig. 9c. Same as Fig. 9a, except 82/83 (top), and 83/84 (bottom).

*Temporal Filtering*

Low–pass filtered, or low–frequency, OLR were used to develop indices measuring intensity and position of convection in the ITCZ. Desired results from these indices guided the design of the time filter.

One concern in the design of the filter was selection of a cut–off frequency, the period of fluctuations at which at least half of the original amplitude is retained. Cut–off frequency affected three characteristics of the ITCZ indices: the number

of episodes observable during each 185–day season; the amplitude of the intensity estimates; and the minimum duration of each convective episode. First, for *higher* cut–off frequencies (or *shorter* periods, in days), more episodes could be captured during the 185–day seasons. Next, since the filtering technique used successive averaging to remove increasingly longer short period variation, as the cut–off frequency *decreases* (period *increasing*), so also the amplitude of the signal is reduced. Finally, the lower limit of the duration of a given episode is determined by the cut–off frequency. If the cut–off frequency is set too *low* (period too *long*), significant intense convection lasting for short periods may not be resolved by the index.

In a compromise of the considerations listed above, *two* low–pass filters were used, one with a cut–off period of 10 days, and the second with a 20–day cut–off. The 10–day data containing more short–period variability were used for the intensity index. These data proved too "noisy" for display in a time–longitude format and for the position index. The 20–day data, with less short–period variability, were used for these applications.

Temporal filtering was accomplished by using multiple applications of a simple 1–2–1 averaging operator on the daily OLR (from (8)). The desired cut–off periods were obtained by selecting the appropriate number of applications of the operator. The number of iterations required was determined by examining the amplitude response function of the 1–2–1 operator.

This response function, for the operator applied one time, is:

$$R(P) = 1 - 2w_2 \sin^2\left(\frac{\pi \Delta t}{P}\right) \tag{9}$$

(after eqn (4) by Bettge and Baumhefner, 1980; hereafter termed BB) where R is the response amplitude, a function of P, the period in days, and of $\Delta t$, which is 1 day.

The weight, $w_2$, in (9), equals 0.5 in the 1–2–1 operator.

For $m = 7$ iterations, the response function is:

$$R_{m=7}(P) = \left[1 - \sin^2\left(\frac{\pi \Delta t}{P}\right)\right]^{m=7} \qquad (10)$$

Table 1 lists the response function [R in (10)] as a function of period (P) for $m = 7$ iterations (see the column labeled "10–day low–pass" ). Notice that for $m = 7$, this filter (10) completely eliminates disturbances ($R \approx 0$) with periods shorter than 4 days; and the filter retains signals ($R \geq 0.5$) with periods longer than the desired cut–off of 10 days. Also shown in Table 1 is the response function for $m = 28$ iterations (the column labeled "20–day low–pass" ); this filter retains activity with periods longer than the second cut–off of 20 days.

TABLE 1. Response function (R) of filters used in this study.

| Period (days) | Fraction of original amplitude retained. 10–day low–pass | 20–day low–pass |
|---|---|---|
| 360 | 1.00 | 1.00 |
| 240 | 1.00 | 0.99 |
| 180 | 1.00 | 0.99 |
| 150 | 1.00 | 0.99 |
| 120 | 1.00 | 0.98 |
| 90 | 0.99 | 0.97 |
| 60 | 0.98 | 0.92 |
| 40 | 0.96 | 0.85 |
| 30 | 0.93 | 0.73 |
| 20 | 0.84 | 0.51 |
| 15 | 0.74 | 0.29 |
| 12 | 0.62 | 0.14 |
| 10 | 0.50 | 0.06 |
| 8 | 0.33 | 0.01 |
| 6 | 0.13 | 0.00 |
| 4 | 0.01 | 0.00 |
| 2 | 0.00 | 0.00 |

The boundary days $t = 1$ (21 October) and $t = 185$ (10 May) were not filtered using the 1–2–1 time-averaging operator because there are no time-adjacent points before and after (respectively) these days. There are several ways to filter boundary values; all methods introduce contamination. BB compared four different boundary conditions (BC) (fold, constant, linear extrapolation, and cubic spline extrapolation) and concluded that one–dimensional filtering is not sensitive to the choice of BC, and that, for all four conditions, the interior domain remained unchanged with respect to all amplitudes and phase shifts. They found only small differences between the four BCs immediately adjacent to the boundaries. As the BC averaging operator used in this study (modified 1–2–1) is only one gridpoint in length, a "fold" boundary condition filter was used. Contamination due to this boundary approximation extends into the interior of the six–month cool–season data. For this reason, each record includes the 10–day "buffers" on either end to absorb this contamination.

Plots of the time series of the unfiltered OLR (Curve A), the 10–day low–pass filtered OLR (Curve B), and the 20–day low–pass filtered OLR (Curve C) are shown in Fig. 10. The 10–day series contains several local extrema missing from the 20–day series, although the 20–day OLR capture the general trend of convective activity at this location. As is discussed in the following section, the 10–day OLR were used to select *single days* having intense convection. The 20–day data were used to find broader *ranges of time and space* with active convection.

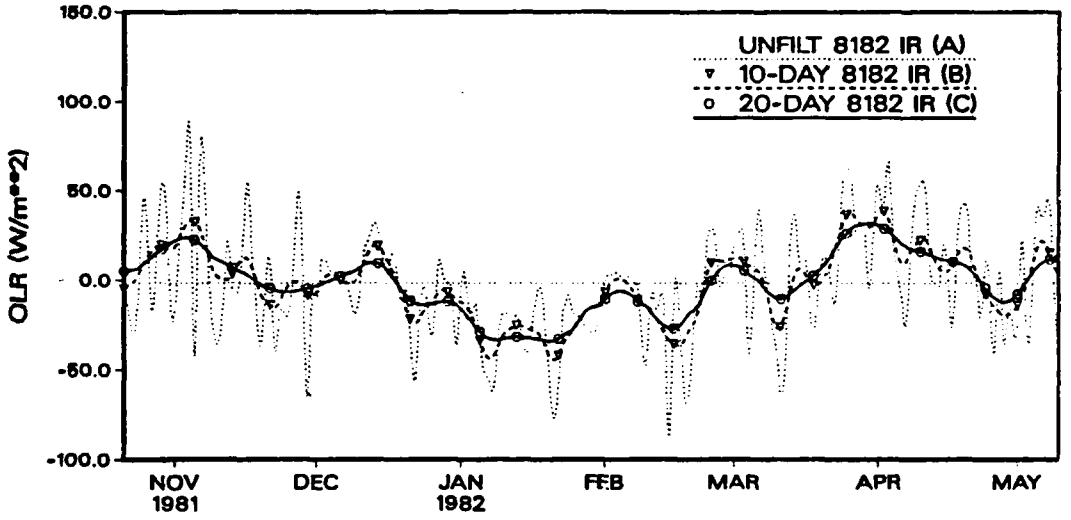


Fig. 10. Time series of OLR at gridpoint 160°W/7.5°N during 81–82 season. Curve A, unfiltered; Curve B, 10–day; and Curve C, 20–day.

# V. LOCATING ACTIVE CONVECTION IN THE ITCZ

The first objective of this research was to find preferred periods and regions of intense ITCZ convection. Toward this end, the first task was to construct an index that measured convective intensity in terms of the OLR data. Active regimes were identified using time series of the intensity estimates. Time–longitude sections of this index showed how active modes originated in the central Pacific and spread longitudinally with time. A second index, measuring the latitudinal position of maximum convection, was also developed.

## ITCZ Intensity Index

Murakami (1979) studied both the temporal mean and day–to–day behavior of the Atlantic Ocean ITCZ during GATE. He used satellite–observed IR brightness collected every 3 hours at 1° latitude/longitude resolution in the zonal band between 5°N and 10°N (see his Figs. 4 and 5). The intensity index developed in this study was patterned after that of Murakami.

The intensity index measured area–averaged OLR in the ITCZ region at meridians across the Pacific on every day of each season. The ITCZ region used for the index was selected based on the information obtained from the seasonal fields of average OLR and standard deviation. Figure 11 shows the region over which the daily OLR were area–averaged. Estimates of ITCZ intensity were computed at every 2.5° of longitude between 120°E and 90°W; that is, 61 positional estimates across the Pacific, each day of each cool season. Zonally–averaged intensities were computed for each day as well.

The longitudinal estimates of convective intensity were derived by averaging OLR at four points between 12.5°N and 5°N at the given meridian. The four

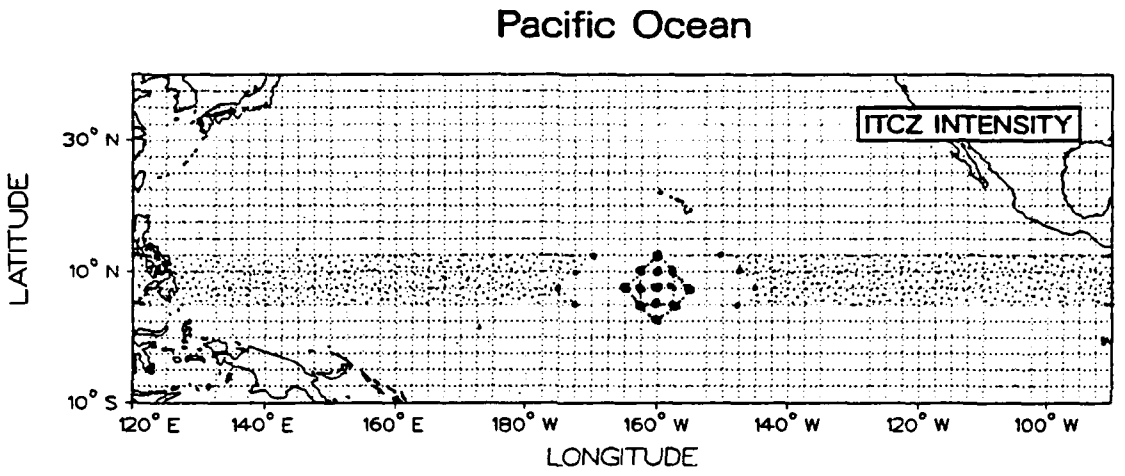


Fig. 11. ITCZ region used for longitudinal estimates of ITCZ intensity. OLR between 12.5°N and 5°N were averaged at every 2.5° longitude across the domain.

intensities were obtained (at 12.5°, 10.0°, 7.5°, and 5.0°N latitude) by applying a 13–point, weighted–averaging template at the given latitude/longitude gridpoint. Figure 11 illustrates the arrangement of the gridpoints in the template as it is applied at the 160°W/7.5°N location. The center point was weighted at $\frac{3}{8}$, the four corner points at $\frac{1}{32}$, and the other eight points were weighted $\frac{1}{16}$. The template spans an area of approximately 500,000 km$^2$, which is roughly equivalent to a small–sized synoptic event. This template was applied at the four latitude parallels listed, and the intensity estimate assigned to the given meridian was the average of these four.

One feature apparent in the mean behavior of the cool season ITCZ is that convective activity differs significantly between the western, central, and eastern Pacific (see Figs. 2 and 3). To minimize this bias, the seasonal mean intensity (averaged across 185 days) at each meridian was removed. The zonally–averaged intensity is thus less sensitive to the more–active western Pacific convection, and became more representative of convection across the entire domain.

The intensity index was constructed using both the 10– and 20–day filtered OLR. Figure 12 shows the time series of intensity estimates at 160°W longitude during the

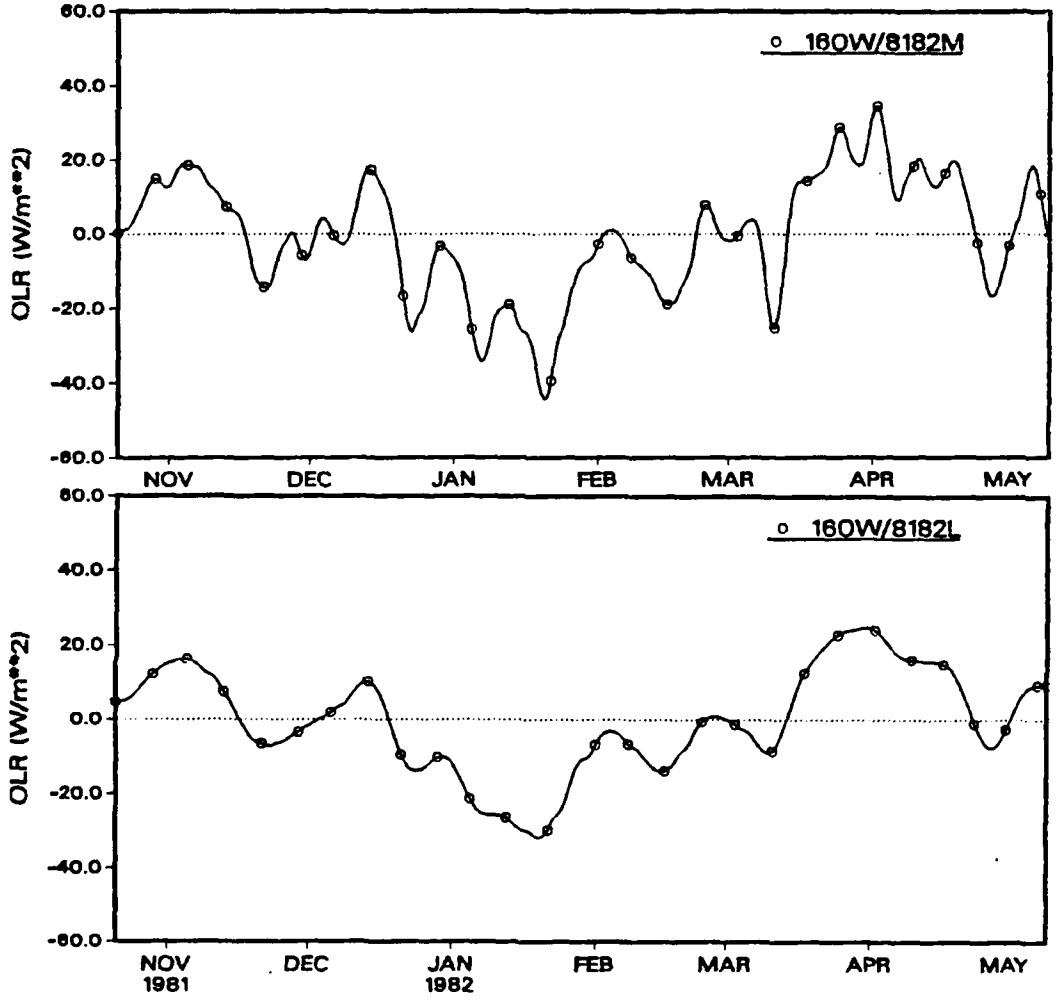


Fig. 12. ITCZ intensity estimates at 160°W during the 81–82 cool season. Ordinate units are $W/m^2$, relative to seasonal means; 10–day (top) and 20–day (bottom).

81–82 cool season. Figure 13 depicts the series of zonally–averaged intensity for the same season; 10–day filtered estimates are on top and 20–day estimates are on the bottom of both figures. Notice that the seasonal average (horizontal line) has been forced to zero in both the 10–day and the 20–day series. Time series of intensity at

160°W (solid) and the zonal-average intensity (dashed) during all eight cool seasons are shown in Fig. 14.

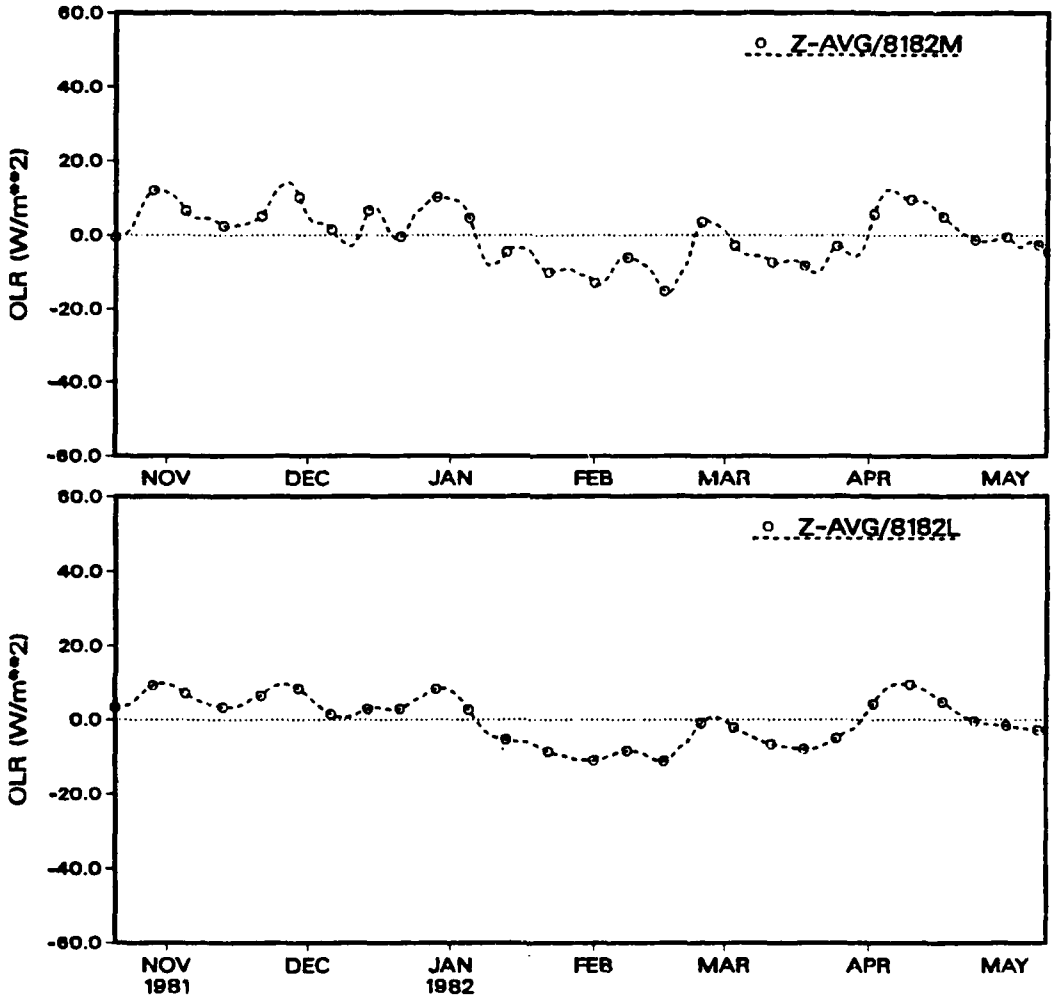


Fig. 13. Same as Fig. 12, except zonally-averaged intensity estimates.

### Identification of Active Regimes

The first objective was accomplished by finding regions in time and space during which the ITCZ intensity index indicated cool area-averaged OLR. These

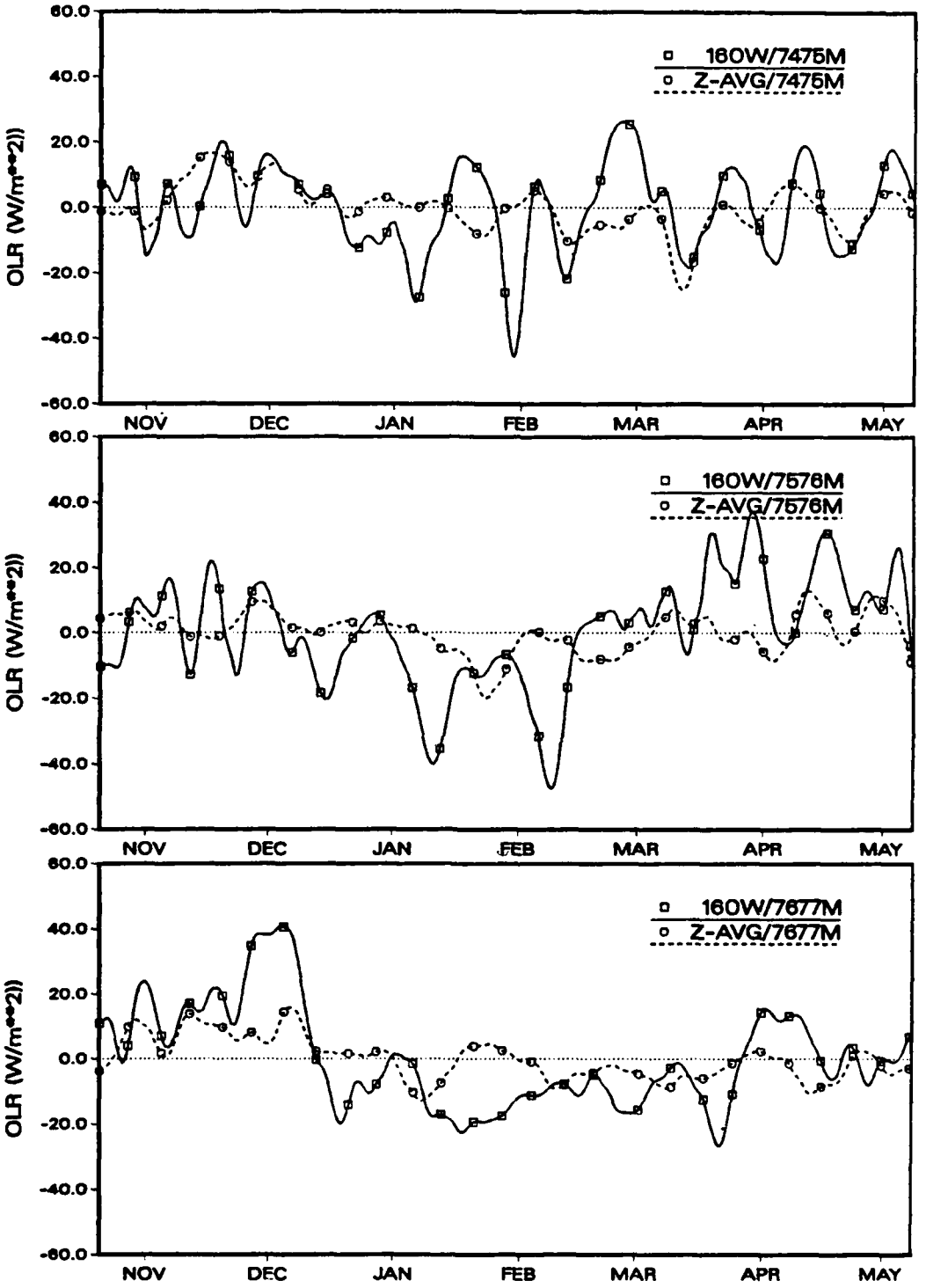


Fig. 14a. Combination of Figs. 12 and 13; gridpoint (solid) and zonally-averaged (dashed) estimates. Nov 74–May 75 (top), 75/76 (middle), and 76/77 (bottom).

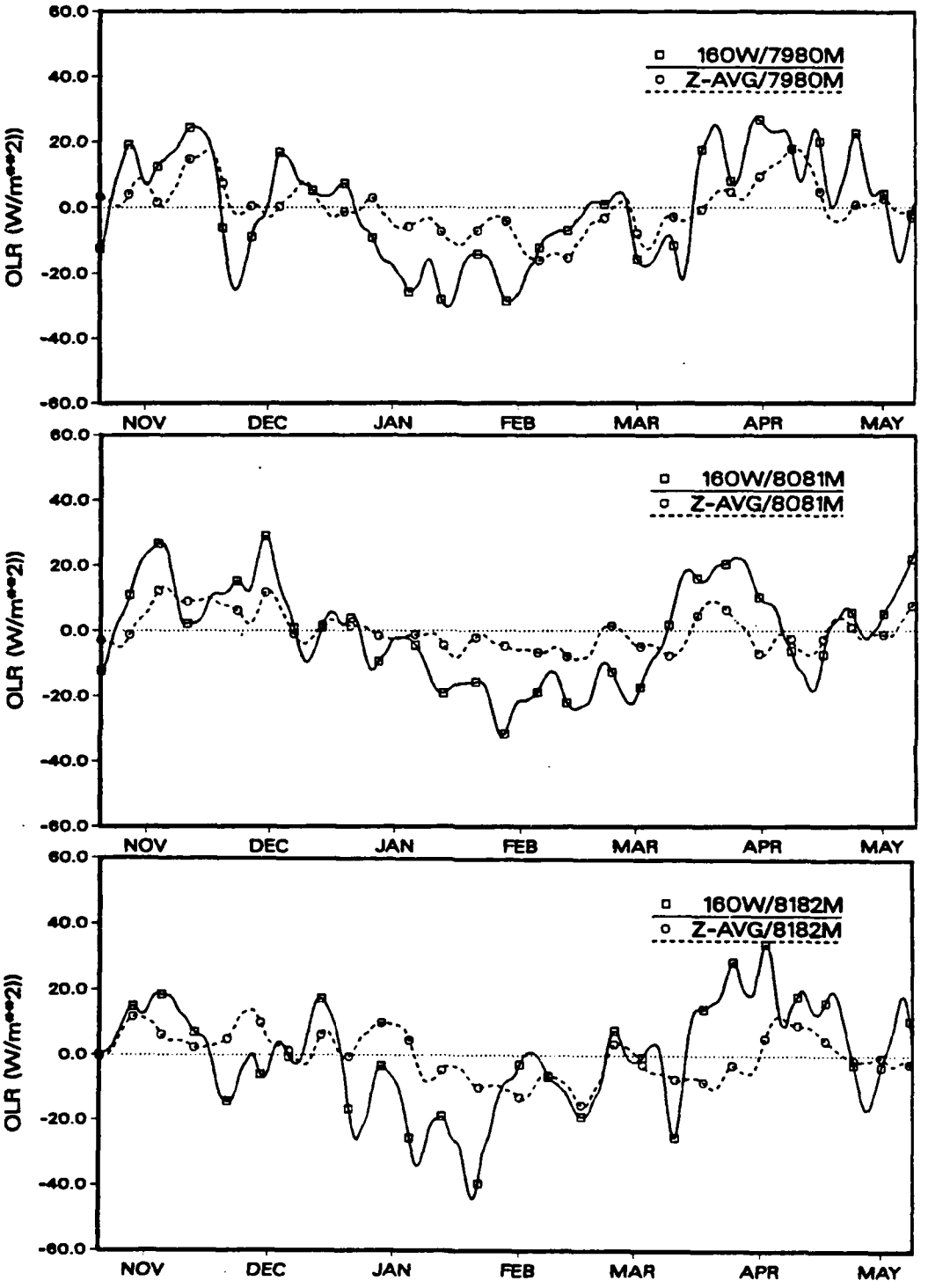


Fig. 14b. Same as Fig. 14a, except 79/80 (top), 80/81 (middle), and 81/82 (bottom).

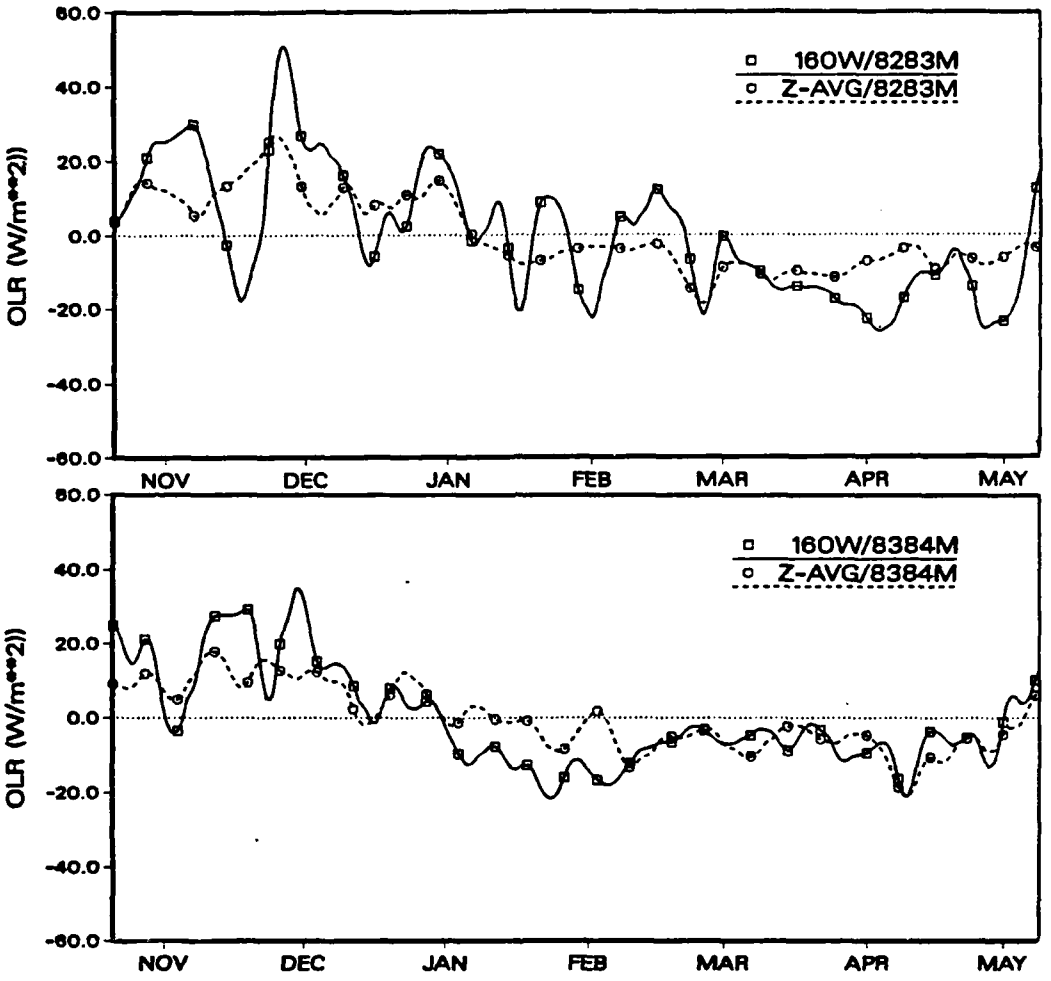


Fig. 14c. Same as Fig. 14a, except 82/83 (top) and 83/84 (bottom).

regions, particularly if they had exceptionally low (large negative) values over a long time, corresponded to regions within the Pacific ITCZ that had comparatively strong convective activity. The term "comparatively" must be used because the intensity index was scaled with respect to the mean behavior at each longitude within each season.

Three methods of identifying active modes were tested. These methods used local minima in time series of the intensity index to select days with "active"

of the intensity estimates. For reasons discussed previously, the 10–day filtered OLR were used to develop the time series, and the 20–day OLR were used to form the time–longitude sections.

For the first method, called the "gridpoint" method, the time series of intensity at 160°W were analyzed to find days during which the index was low (largely negative, below the seasonal mean). In Fig. 14, each seasonal series has several candidate "active" days. For example, there are ten local minima of the intensity index (neglecting minor minima) during the 74–75 season (top of Fig. 14a). Other seasons have similar numbers of active days, although the depth of the minima (and relative strength of the ITCZ convection at that day and location) may vary considerably. During the ENSO seasons, 76–77 and 82–83, the 160°W series lose their early–season large amplitudes near the end of the season. This indicates the more consistent, widespread cloudiness associated with these prolonged eastern Pacific convective events.

The second method, called the "zonal–average" method, used local minima in the zonally–averaged series of intensity. The dashed curves in Fig. 14 show that there are fewer candidate active days obtained using this method than with the gridpoint method. In the 74–75 zonally–averaged series (top of Fig. 14a), there are only seven active time periods. Numbers obtained from other seasons are similar (e.g., six from the 79–80 season, six from 81–82, and seven from 83–84).

The third method used days that had low index values on *both* the 160°W and zonally–averaged series. This gridpoint/zonal–average comparison corrected two problems observed in the first two methods. In the gridpoint method, the convective activity measured by the intensity time series often was localized, occurring in only a limited region of the ITCZ. Activity in the remainder of the ITCZ was usually

unrelated to activity observed at 160°W (see the time–longitude sections in Fig. 15). The zonal–average method often found days during which the zonal–mean OLR in the ITCZ region was relatively low due to widespread convection in only one half of the domain, usually in the Western Pacific. To correct these problems, the gridpoint/zonal–average method required minima in area–averaged OLR in both the zonal–average and 160°W time series. This method obtained an "Eastern Pacific–bias" in selecting days with active ITCZ convection.

**Time–Longitude Sections**

Time–longitude sections of ITCZ intensity estimates for eight cool seasons are shown in Fig. 15. The contour interval is 5 $W/m^2$ and regions with area–averaged OLR less than –5 $W/m^2$ are shaded. These shaded regions have above–average intensity of convection in the ITCZ (between 5°N and 12.5°N). The vertical lines represent the intensity estimates sampled by the 160°W time series of Figs. 12 and 14.

The interannual variability of ITCZ convection on subseasonal (periods between 20 and 180 days) time scales is apparent in Fig. 15, especially when considering the ENSO–related map of the 82–83 season (Fig. 15g). The entire western Pacific becomes relatively featureless after 15 January 1983. Recall from Figs. 3c and 4c that the ENSO signal (as it appears in this data set) is strongest just south of the ITCZ region used in the intensity index. Also, a major portion of the amplitude of the ENSO signal may have been removed along with the annual and semiannual cycle. For these reasons, the ENSO signal in Fig. 15g may appear weaker than would be expected.

In several instances (e.g., 23 Dec 81/160°W; 20 Feb 82/175°W; and 3 Mar 82/180°W, in Fig. 15f, are typical examples), shaded regions in non–ENSO seasons

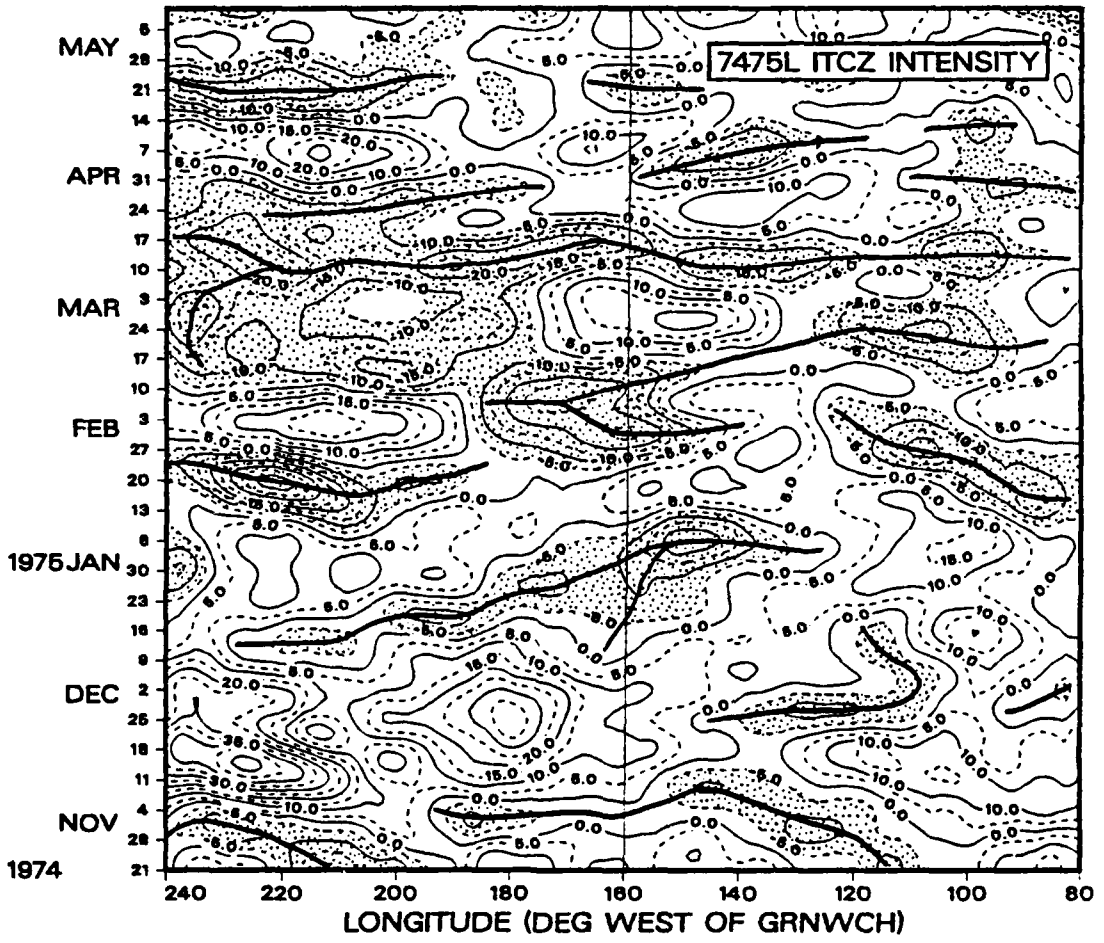


Fig. 15a. Time-longitude section of ITCZ intensity estimates during 74–75 cool season. Intervals are 5 W/m$^2$ with values < –5 W/m$^2$ shaded.

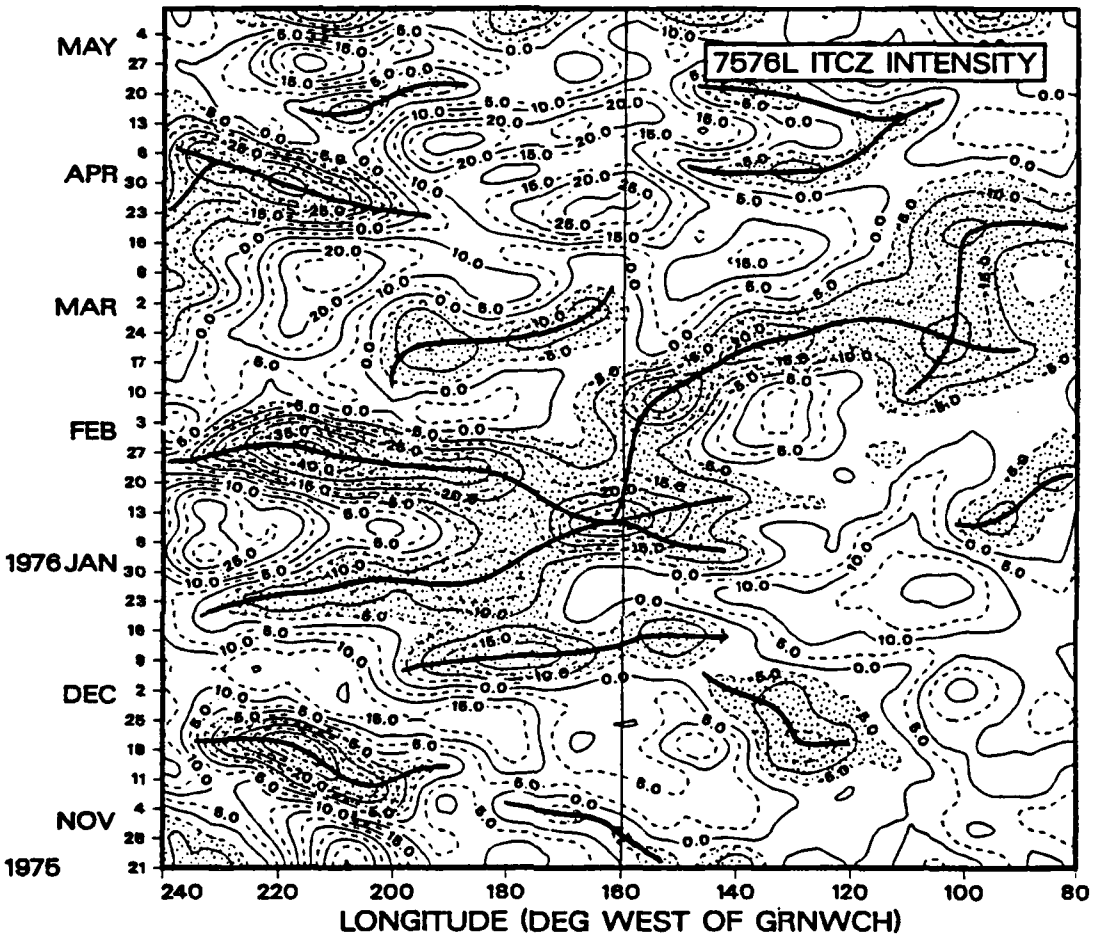


Fig. 15b. Same as Fig. 15a, except 75–76 cool season.

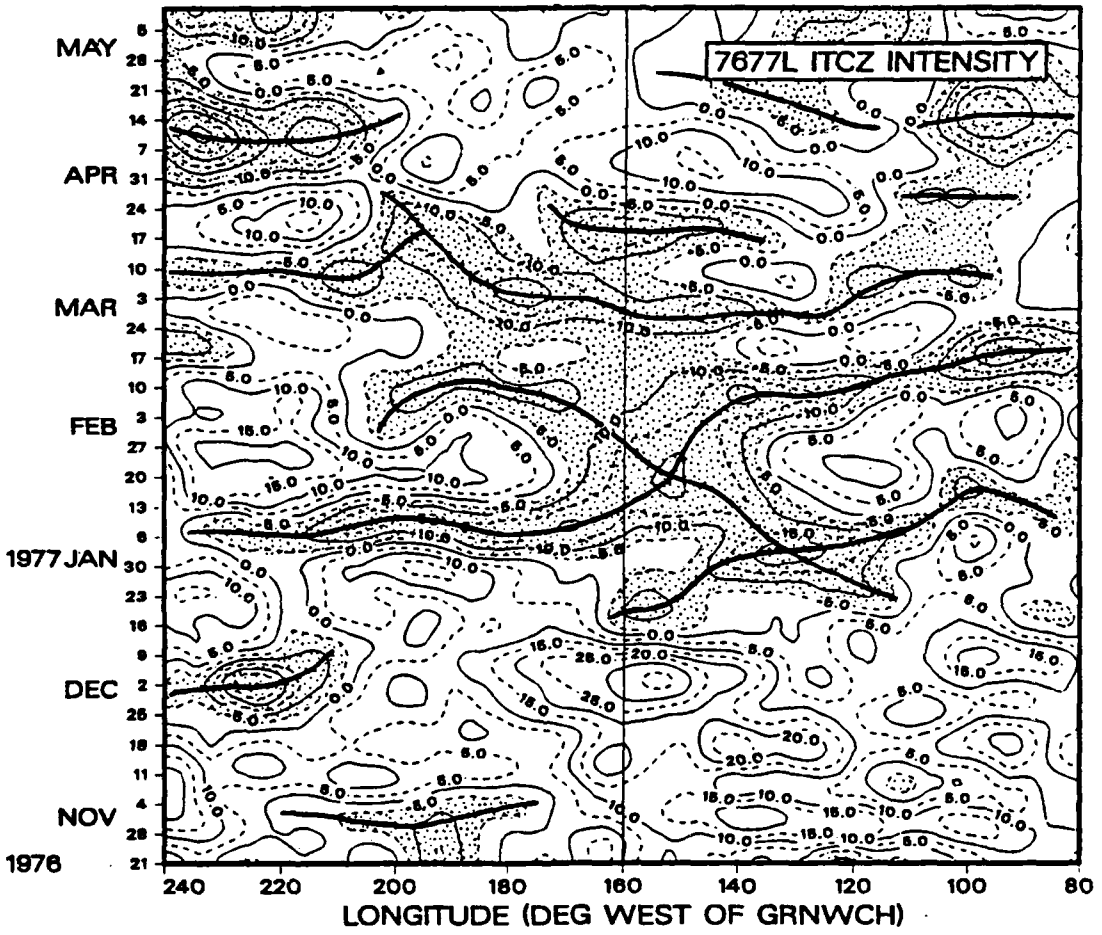


Fig. 15c. Same as Fig. 15a, except 76–77 cool season.

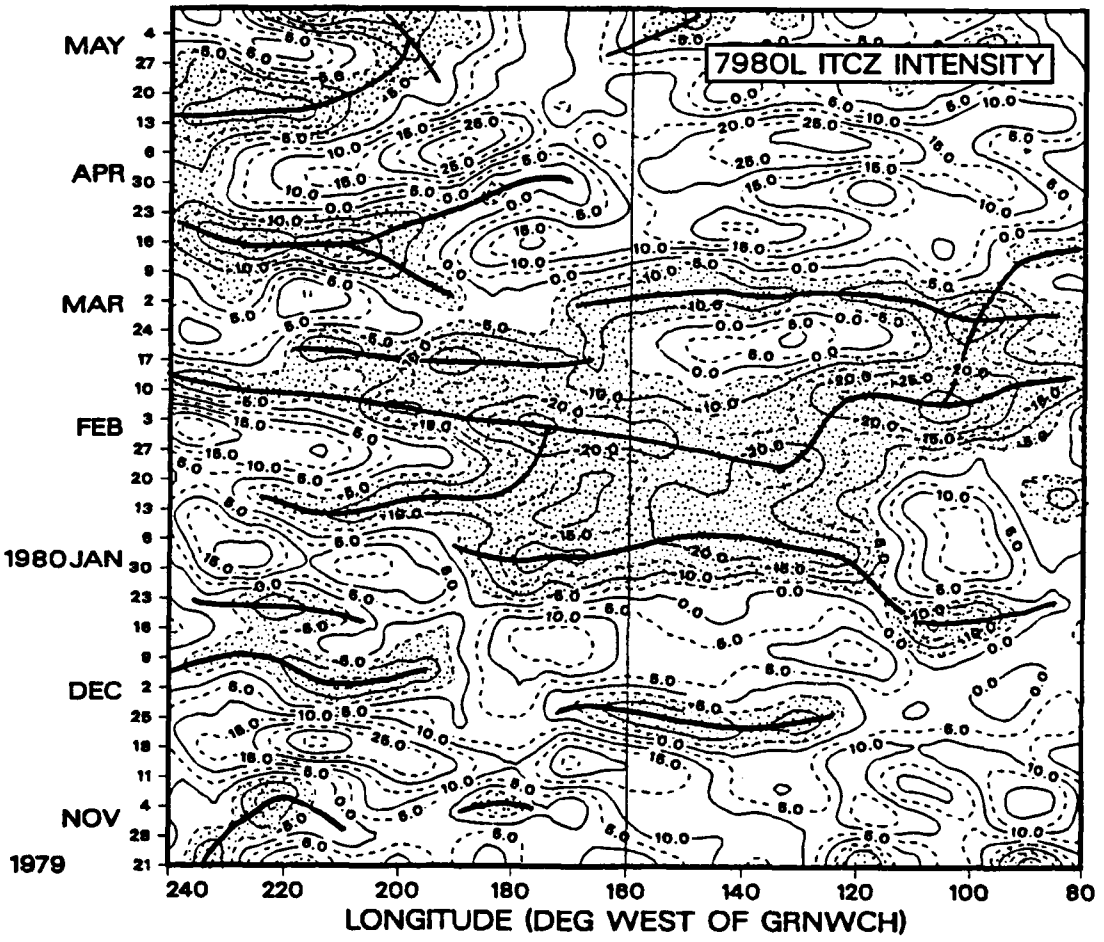


Fig. 15d. Same as Fig. 15a, except 79–80 cool season.

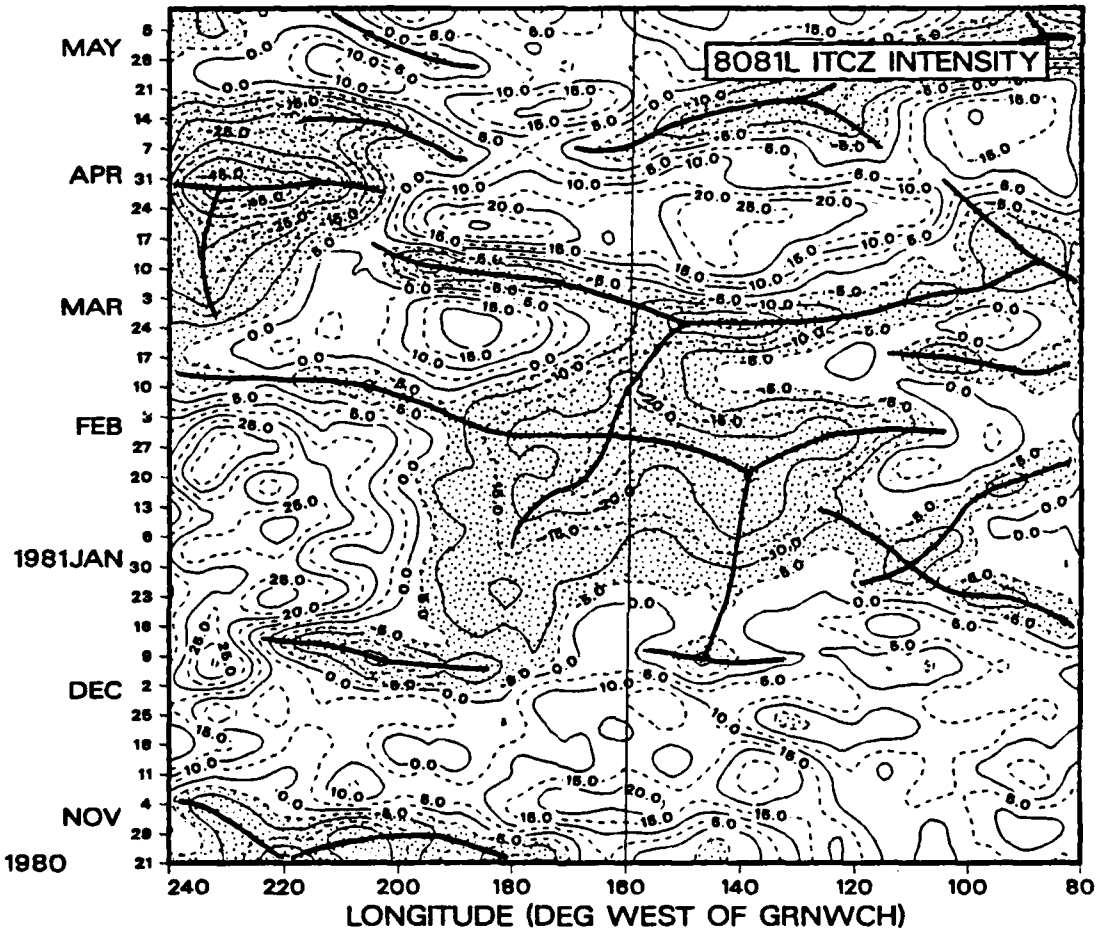


Fig. 15e. Same as Fig. 15a, except 80–81 cool season.

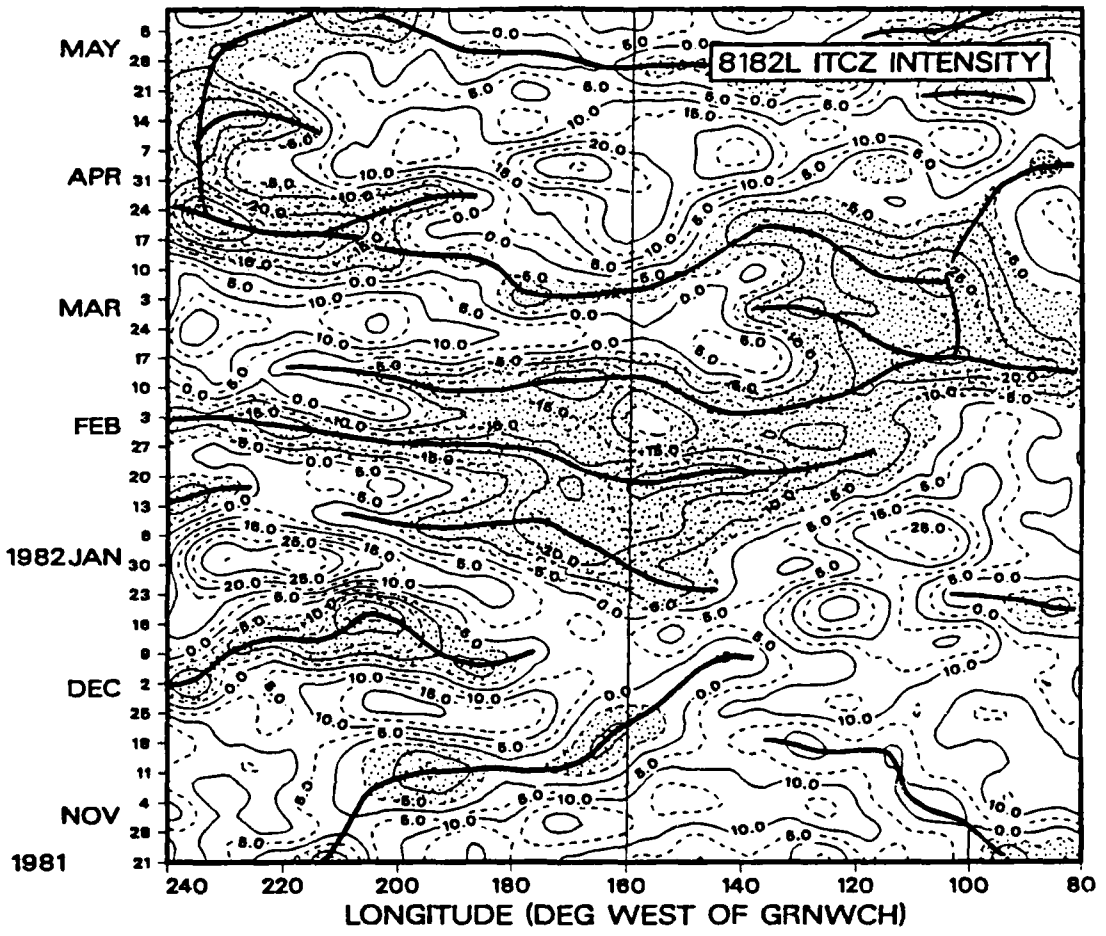


Fig. 15f. Same as Fig. 15a, except 81–82 cool season.

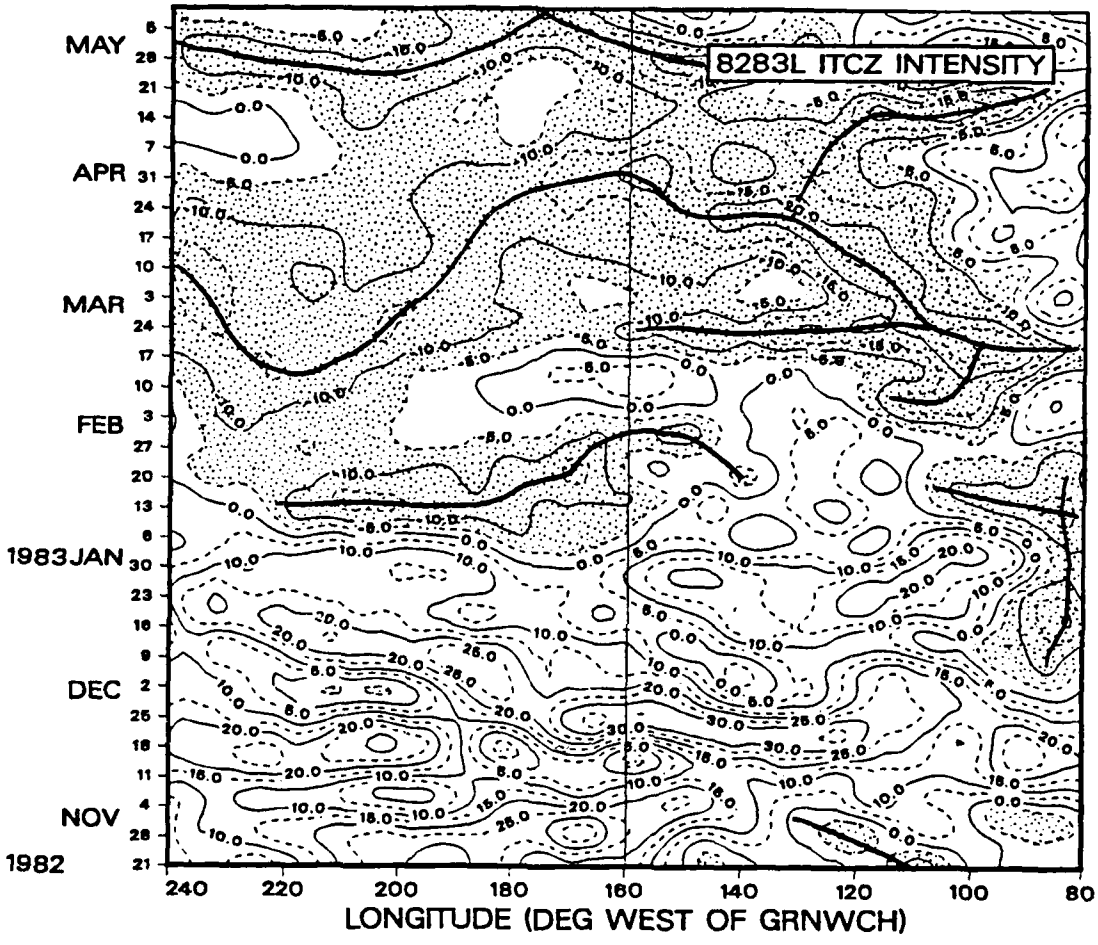


Fig. 15g. Same as Fig. 15a, except 82–83 cold season.

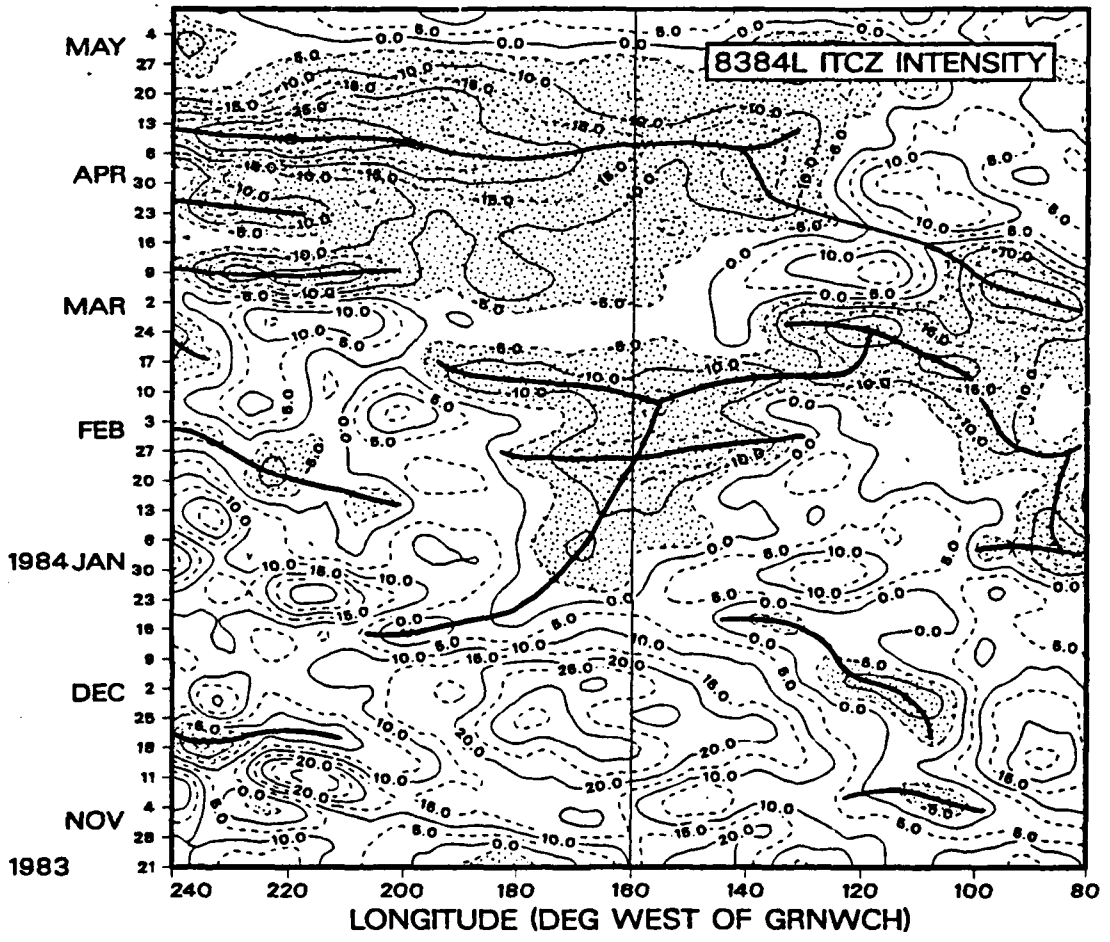


Fig. 15h. Same as Fig. 15a, except 83–84 cool season.

appear to originate near the center of the domain, and then spread longitudinally.

The spatial and temporal scales of the active modes (shaded areas in Fig. 15) vary considerably both between seasons, and within seasons across the domain and throughout the season. Heavy lines in Fig. 15 are attempts to classify active mode variability into three types. The first type occurs with small spatial scales (less than 4000 km), short temporal scales (lasting 10–20 days) and is observed most frequently in the eastern Pacific. Examples of the first type of active mode variability appear in the early and eastern portions of the time–longitude diagram of the 74–75 season (Fig. 15a).

The second type of variability has longer spatial scales (5000–10,000 km), short temporal scales (10–25 days), and is found throughout the domain. Two examples of this type of variability occurred between 9 Dec 74/140°E and 1 Jan 75/140°W, and between 6 Jan 77/120°E and 20 Jan 77/150°W. This feature often propagates, and may exhibit several cycles of development/decay during its lifespan.

There is a third type of variability that may be unique or a juxtaposition of two or more of the first two types of features. These active modes have intermediate spatial scales (2000–6000 km), persist over a long period (greater than 30 days), and occur throughout the domain. They develop and decay within a localized region of the ITCZ. An examples of this third type of variability appears between 10 Feb 75/120°E to 180° and 31 Mar 75/same locations (Fig. 15a).

The time–longitude sections show how the 160°W and zonal–average intensity series (in Fig. 14) are related. Fine structure in Fig. 14 will not appear in Fig. 15, as the estimates in the time–longitude sections were computed using the 20–day filtered OLR. There does *not* appear to be a compelling correlation between days having active zonal–average intensity (shaded across most of the domain) and days having

shaded areas at 160°W. For this reason, the first two methods of finding active modes do not capture convection that is, simultaneously, intense in the eastern Pacific, as well as all across the domain.

It is not clear how the analysis should proceed to resolve this complex behavior quantitatively. This is left as an unsolved problem for future investigation.

**ITCZ Position Index**

The ITCZ intensity index was modified to provide estimates of the latitudinal position of the ITCZ at longitude meridians across the Pacific. The same basic assumption used in the intensity index holds here; that relatively low area-averaged OLR in the ITCZ indicates deep convection. Time series of the position estimates show how the latitude of maximum convection, at a single longitude or in the zonal mean, varies through the season.

Figure 16 shows the ITCZ region used by the position index. This domain is larger than that used by the intensity index, extending from 5°N to 20°N latitude. The "wider" domain was selected in an attempt to capture local excursions of intense convective activity extending northward out of the ITCZ into the subtropics. These excursions of cool-season ITCZ convection normally are synoptic scale ITCZ disturbances called tropical plumes (previously cited) and are thought to be an important part of the active-mode variability of the cool-season ITCZ.

At intervals of 2.5° longitude across the domain, area-averaged OLR was calculated at seven latitude parallels (5°N, 7.5°N, 10°N, 12.5°N, 15°N, 17.5°N, and 20°N) using an area-averaging template identical to that of the intensity index. The latitude with the *lowest* area-averaged OLR was selected as the local position (for that day and meridian) of the ITCZ. Position estimates were computed at every 2.5° longitude across the Pacific and on every day of each 185-day season. As with the intensity

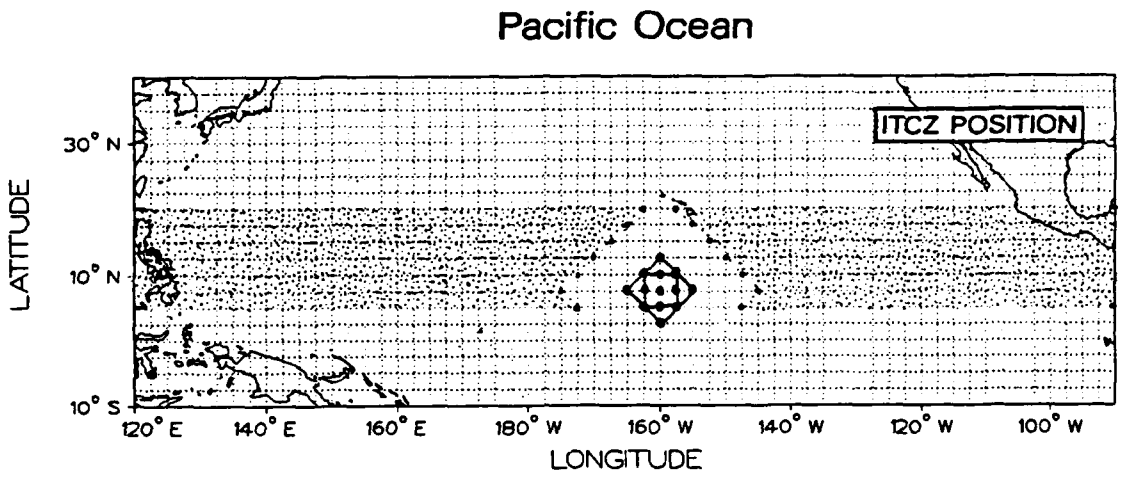


Fig. 16. ITCZ region used by the position index. Area-averaging template is identical to that used in the intensity index. Template shown applied at 160°W/7.5°N.

with the *lowest* area-averaged OLR was selected as the local position (for that day and meridian) of the ITCZ. Position estimates were computed at every 2.5° longitude across the Pacific and on every day of each 185-day season. As with the intensity index, daily zonally-averaged position estimates were also calculated. The values of the index are degrees North latitude, not departures from a mean value.

*Behavior of ITCZ Position*

Figure 17 shows time series of the ITCZ position estimates at 160°W during the 81-82 cool season. Estimates calculated using the 10-day filtered OLR are shown at the top, and the 20-day estimates, on the bottom. The horizontal lines represent the seasonal means. The daily zonal-average position estimates using both 10- and 20-day data are shown in Fig. 18. Notice that, even with the "smoother" 20-day filtered OLR, the 160°W position estimates frequently shift rapidly over 10° of latitude over just a few days. The zonal-average estimates behave in a smoother manner. Figure 19 is similar to Fig. 14, showing the position estimates (solid lines) at

160°W longitude and the zonal–average estimates (dashed lines) for the eight cool seasons using the 20–day filtered OLR.

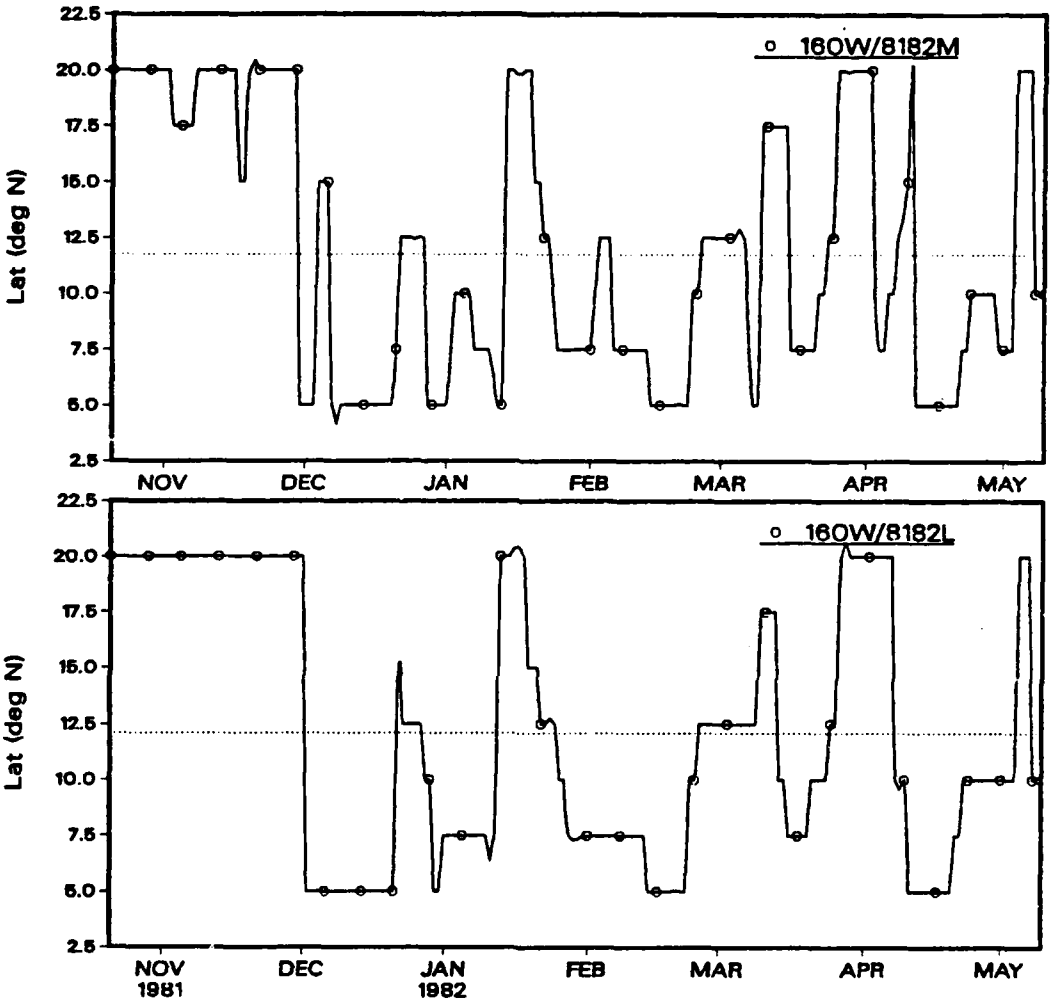


Fig. 17. ITCZ position estimates sampled at 160°W during 81–82 cool season. Ordinate units are °N latitude; 10–day (top) and 20–day (bottom).

The 160°W position estimates in Figs. 17 and 19 appear to have a bimodal distribution of position. For much of the time, the location of maximum convective intensity is either at, or north of, the northern limit (20°N); or at, or south of, the southern limit (5°N). This may be due to convection not normally associated with the

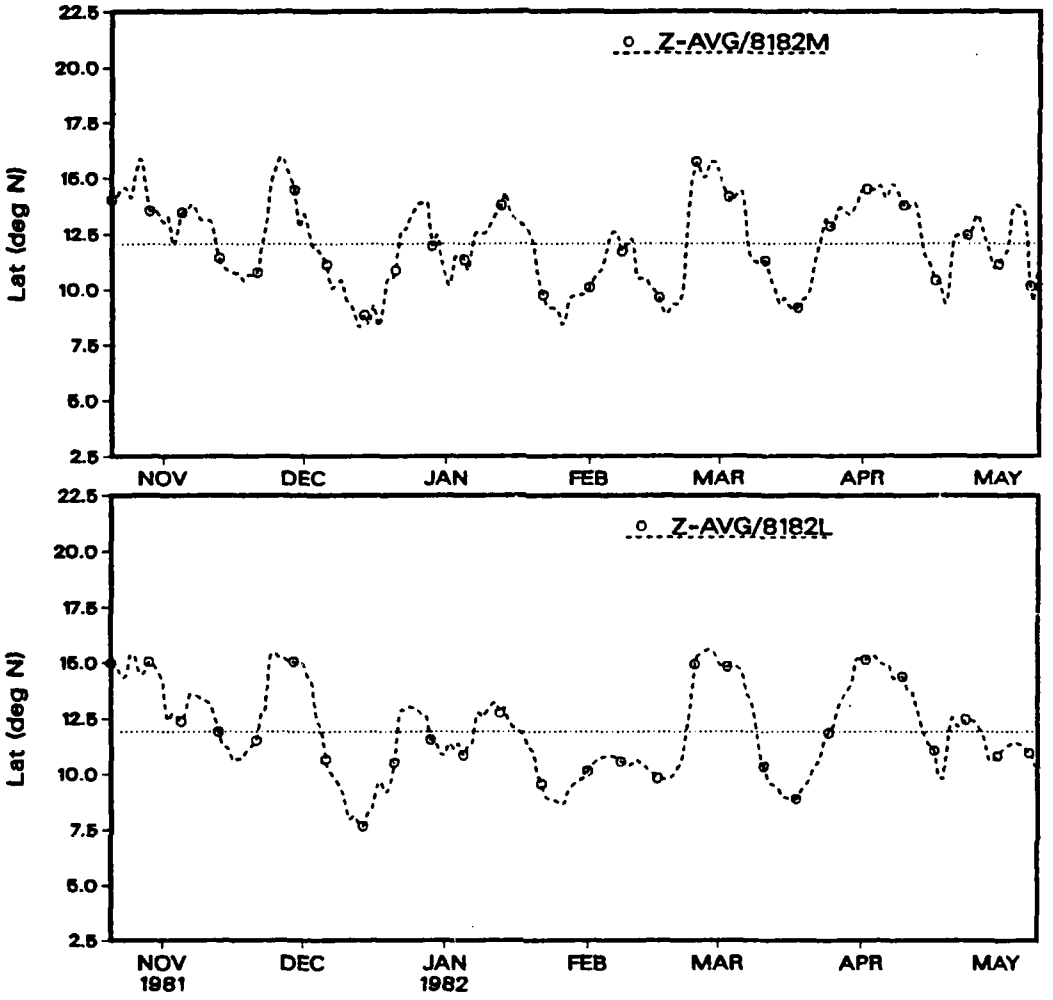


Fig. 18. Same as Fig. 17, except for zonal-average position estimates.

Pacific ITCZ. For example, cloudiness associated with mid-latitude cold fronts that extend equatorward to 20°N at 160°W may appear in Figs. 17 and 19 as a 20°N position of maximum intensity of ITCZ convection. A less-probable occurrence of Southern Hemisphere convection extending northward to 5°N at 160°W may account for some of the position estimates at the southern limit.

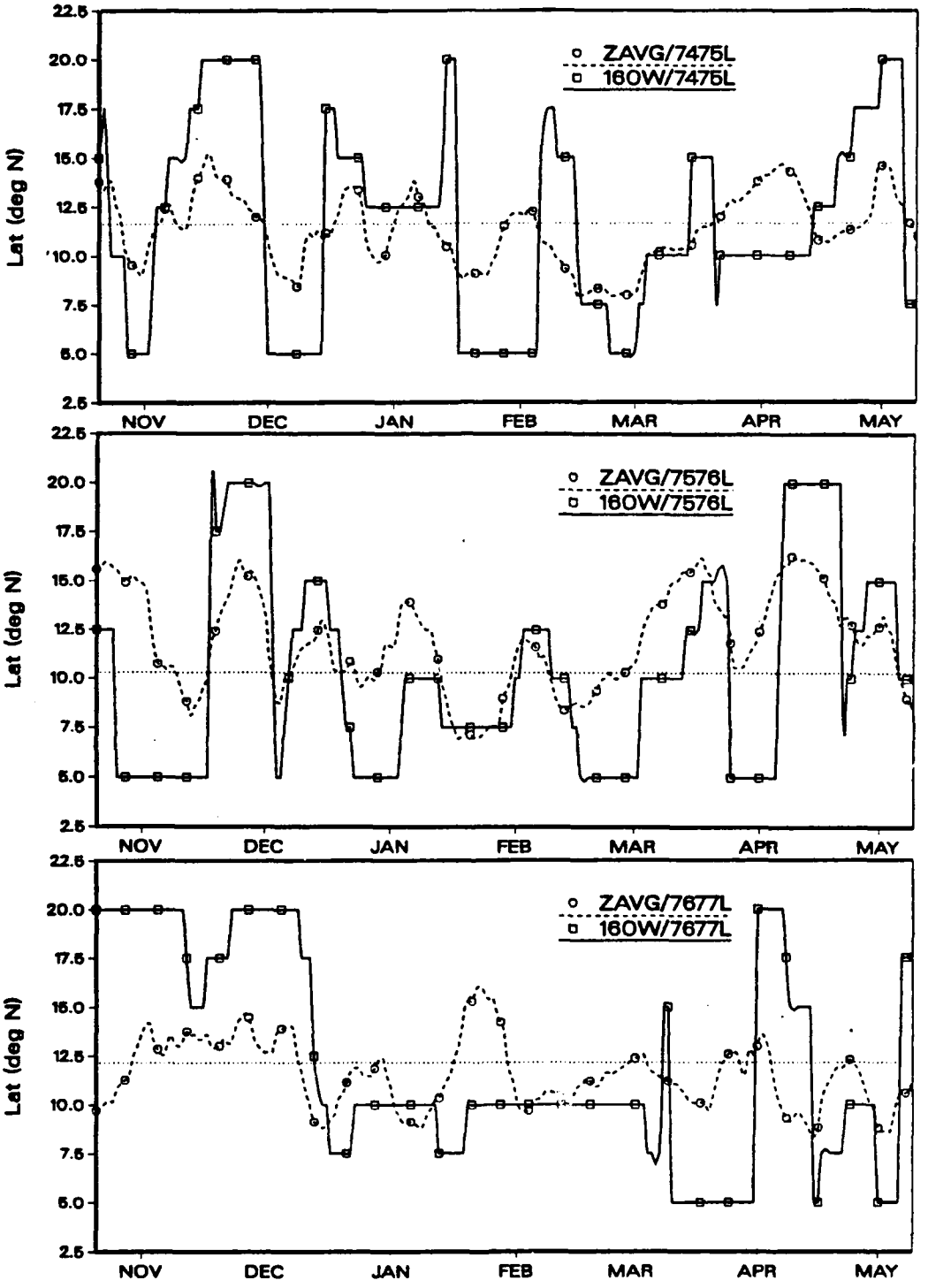


Fig. 19a. Combination of Figs. 17 and 18; gridpoint (solid) and zonally-averaged (dashed) estimates. Nov 74–May 75 (top), 75/76 (middle), and 76/77 (bottom).

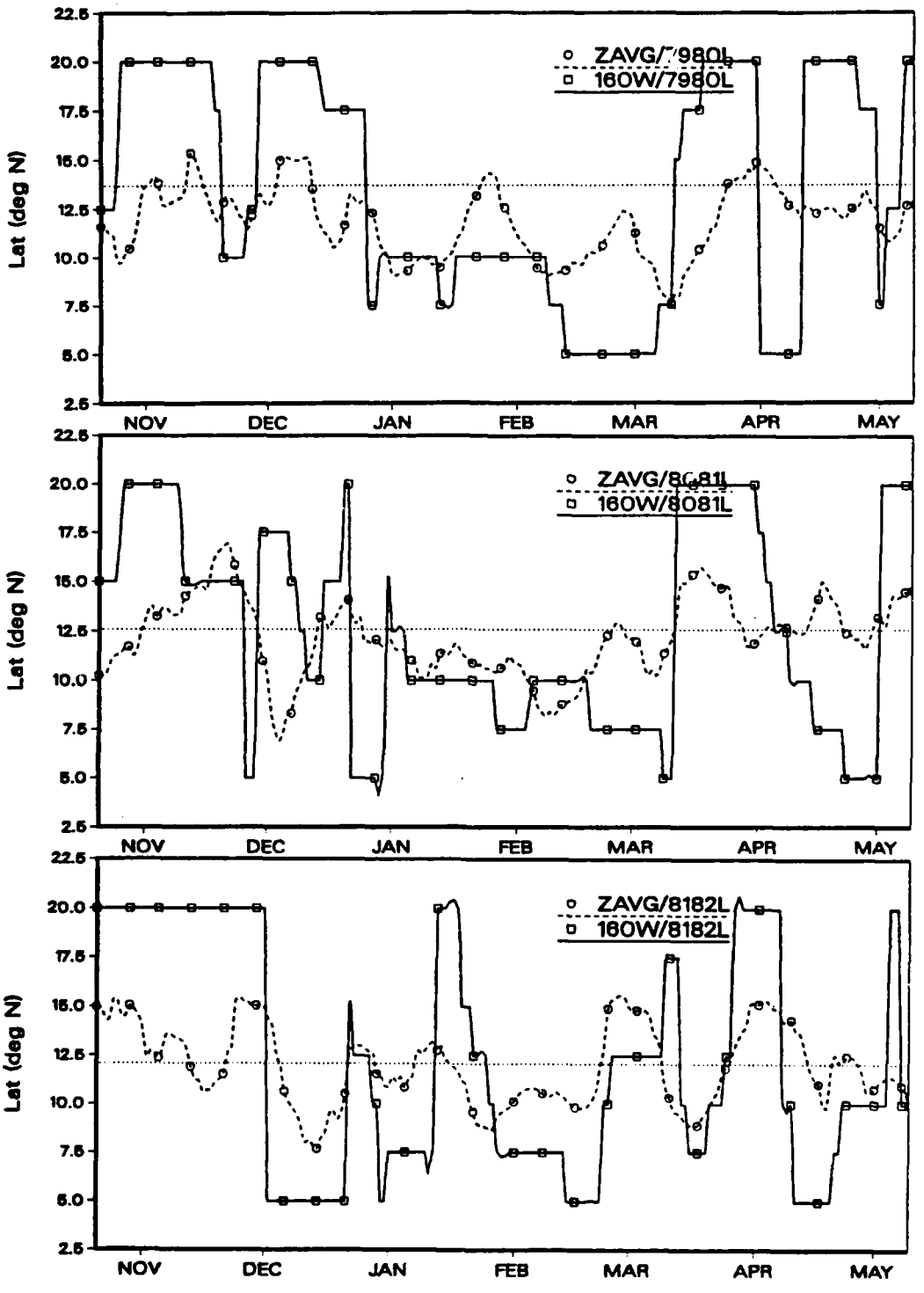


Fig. 19b. Same as Fig. 19a, except 79/80 (top), 80/81 (middle), and 81/82 (bottom).

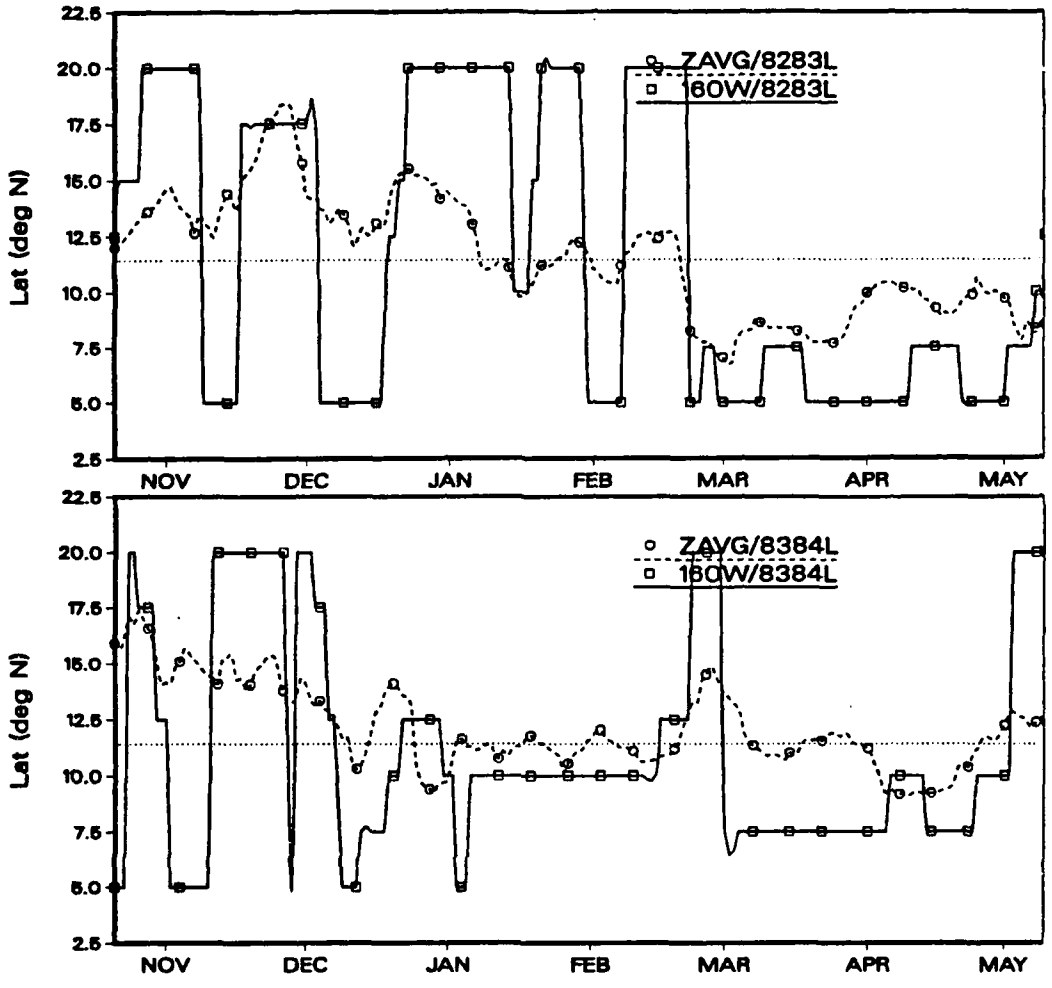


Fig. 19c. Same as Fig. 19a, except 82/83 (top) and 83/84 (bottom).

*Frequency Distributions*

The frequency distributions of position estimates sampled each season at 160°W are shown in Fig. 20, primarily to quantify the apparent bimodality in the time series of position estimates. The 160°W distributions clearly fall into two classes: a strongly bimodal distribution during the ENSO seasons of 76–77 and 82–83; and a trimodal distribution, with a central peak at 12.5°N, for the non–ENSO seasons. The central

convection, while the peaks at 20°N in both classes are due to intrusions of mid-latitude convection which are stronger than any convection occurring at normal ITCZ latitudes. (Recall that during the northern *winter*, the seasonal mean ITCZ is relatively weak and shifts *southward* toward the equator.) The peak at 5°N may be due mostly to southward-displaced ITCZ convection, but may also be affected by Southern hemisphere convective systems. A curious feature is that the latitudes of 7.5°N and 10°N (the expected ITCZ locations) have such low frequencies.

This may be a question valid only at this location (160°W), because examination of the frequency distributions of the zonal-average position estimates (Fig. 21) reveals quite different results. These distributions are uniformly single-peaked, with modes located between 10°N and 12.5°N. Only the strong ENSO season of 82-83 had a mode (near 7°N) outside this range. The remainder of locations across the tropical Pacific must have time series of position estimates different from that at 160°W for the zonal-average distribution to be so different from the 160°W distribution.

*Intensity/Position Comparison*

As a final subjective comparison, the intensity estimates and the position estimates were compared. The zonal-average intensity estimates (solid lines) and the zonal-average position estimates (dashed lines) are shown in Fig. 22 for all eight seasons. Similarly, the gridpoint estimates, intensity (solid) and position (dashed), are shown in Fig. 23. The different time series are all aligned about their seasonal mean values. The striking feature here is that the zonal-average estimates often are in phase, while the more-chaotic gridpoint series are difficult to interpret.

The time series shown in Fig. 22 are remarkably coherent, such that when the mean ITCZ is in an *active* mode (minima in the [solid] intensity curves), the

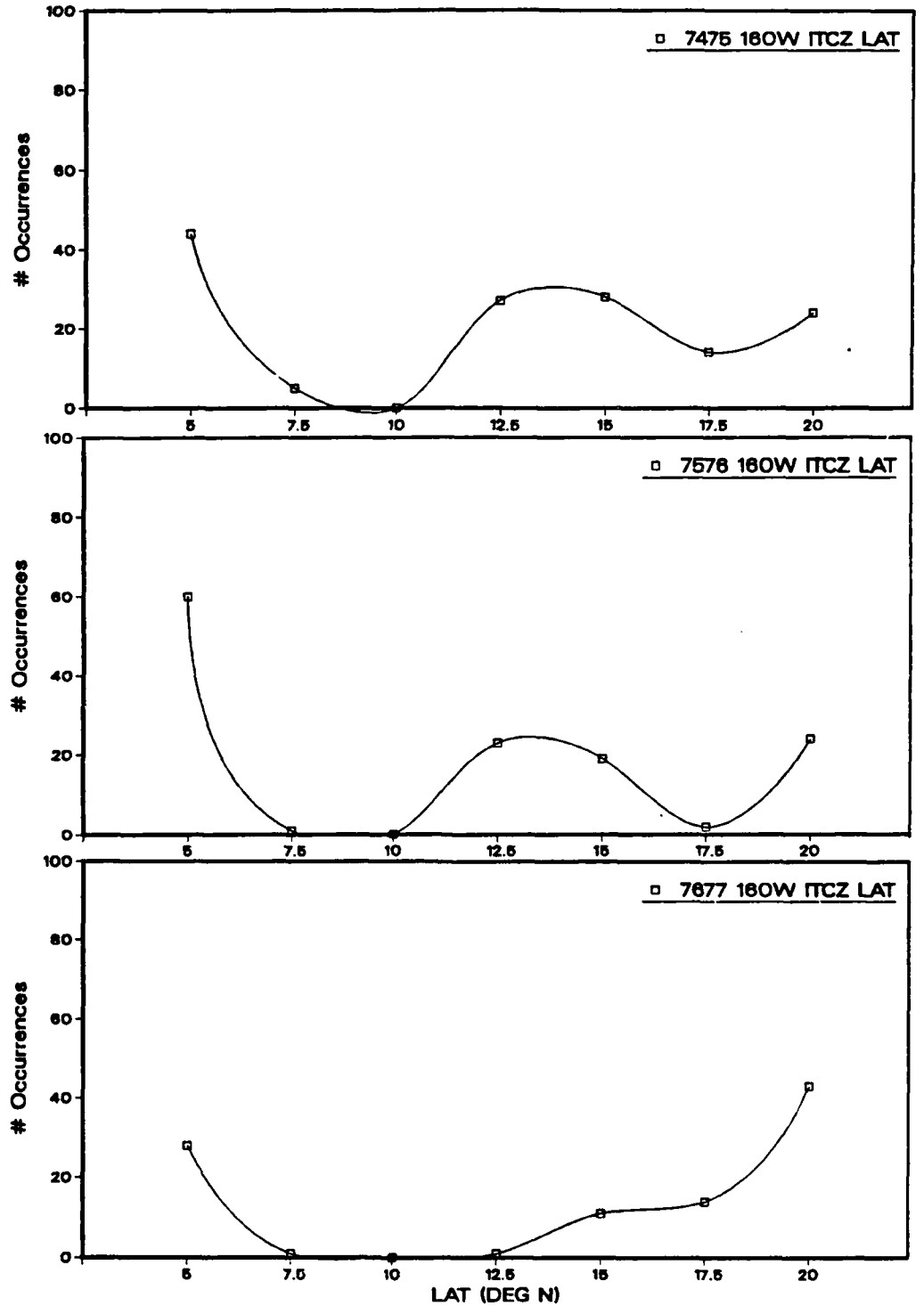


Fig. 20a. Distribution of position estimates of OLR minima sampled at 160°W. Abscissa is intervals of position; Nov 74–May 75 (top), 75/76 (middle), and 76/77 (bottom).

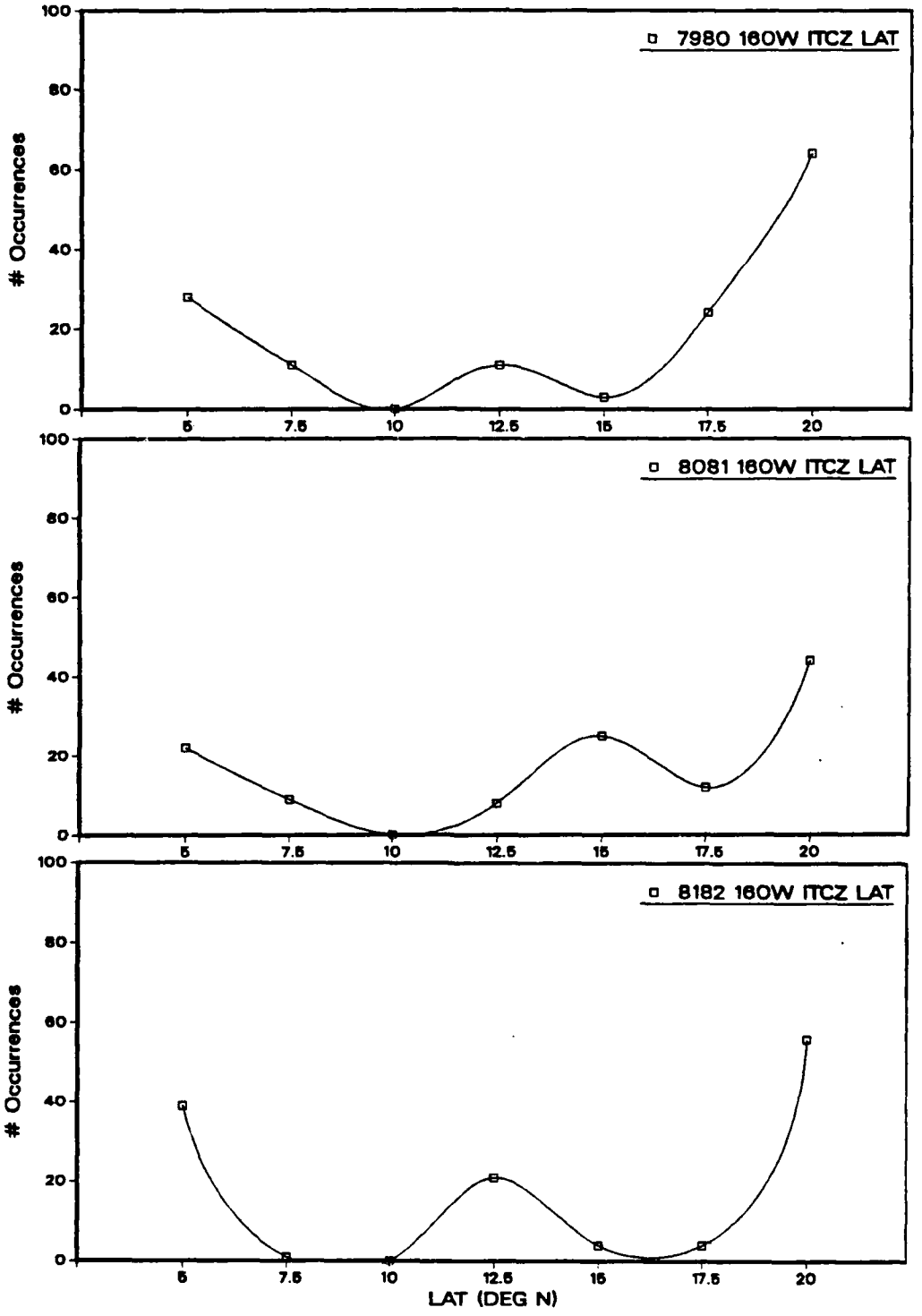


Fig. 20b. Same as Fig. 20a, except 79/80 (top), 80/81 (middle), and 81/82 (bottom).

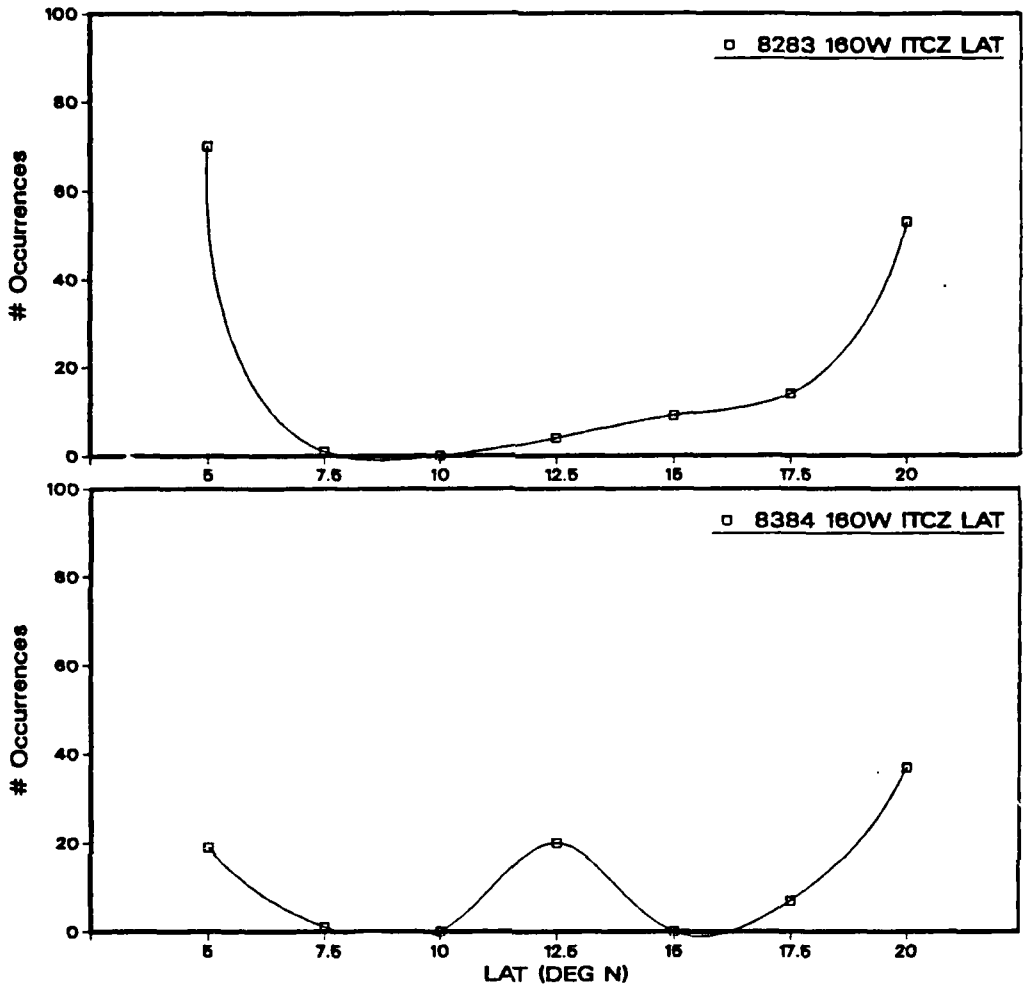


Fig. 20c. Same as Fig. 20a, except 82/83 (top) and 83/84 (bottom).

the mean ITCZ is in an *active* mode (minima in the [solid] intensity curves), the mean position normally moves *south* (minima in the [dashed] position curves). The converse is also suggested by Fig. 22: when shifting to an inactive mode (warmer area–averaged OLR), the mean position moves north. The 160°W time series in Fig. 23 show a similar active/south–inactive/north behavior at the given location, but the correlation is not as compelling as for the zonal–mean results.

The first objective of this study was to find periods of locally–intense convective

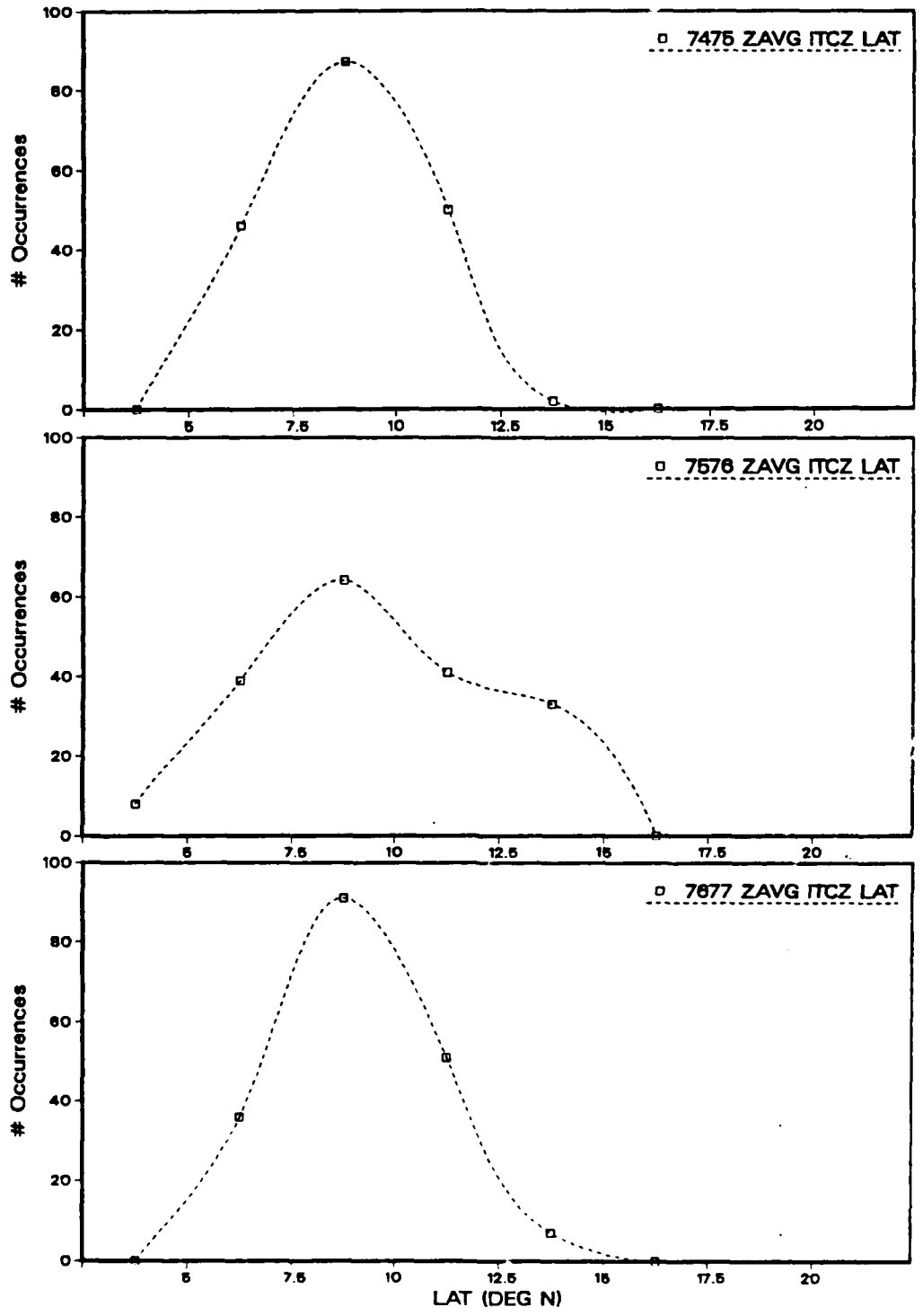


Fig. 21a. Same as Fig. 20a, except for zonal-average position estimates. Nov 74–May 75 (top), 75/76 (middle), and 76/77 (bottom).

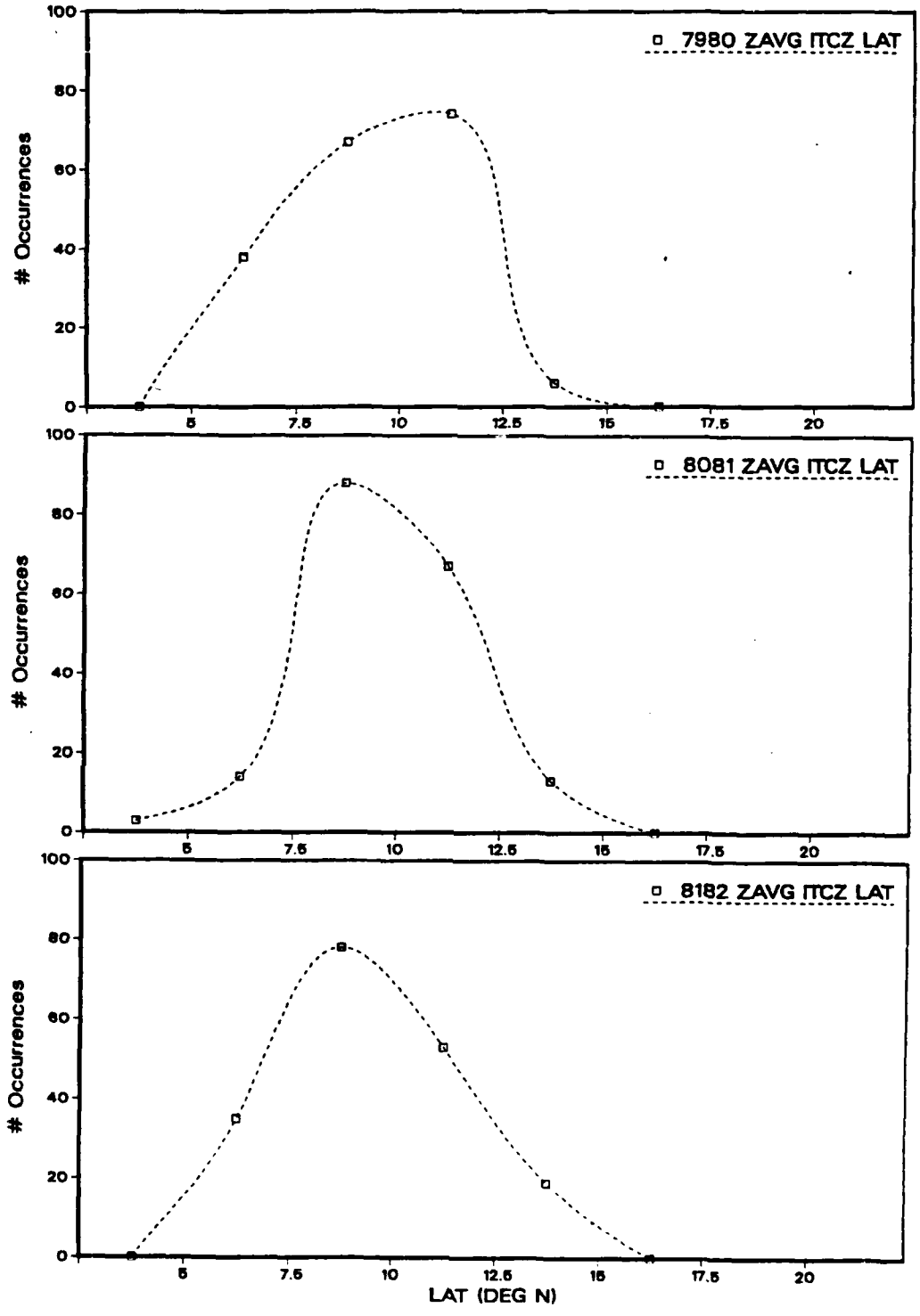


Fig. 21b. Same as Fig. 21a, except 79/80 (top), 80/81 (middle), and 81/82 (bottom).

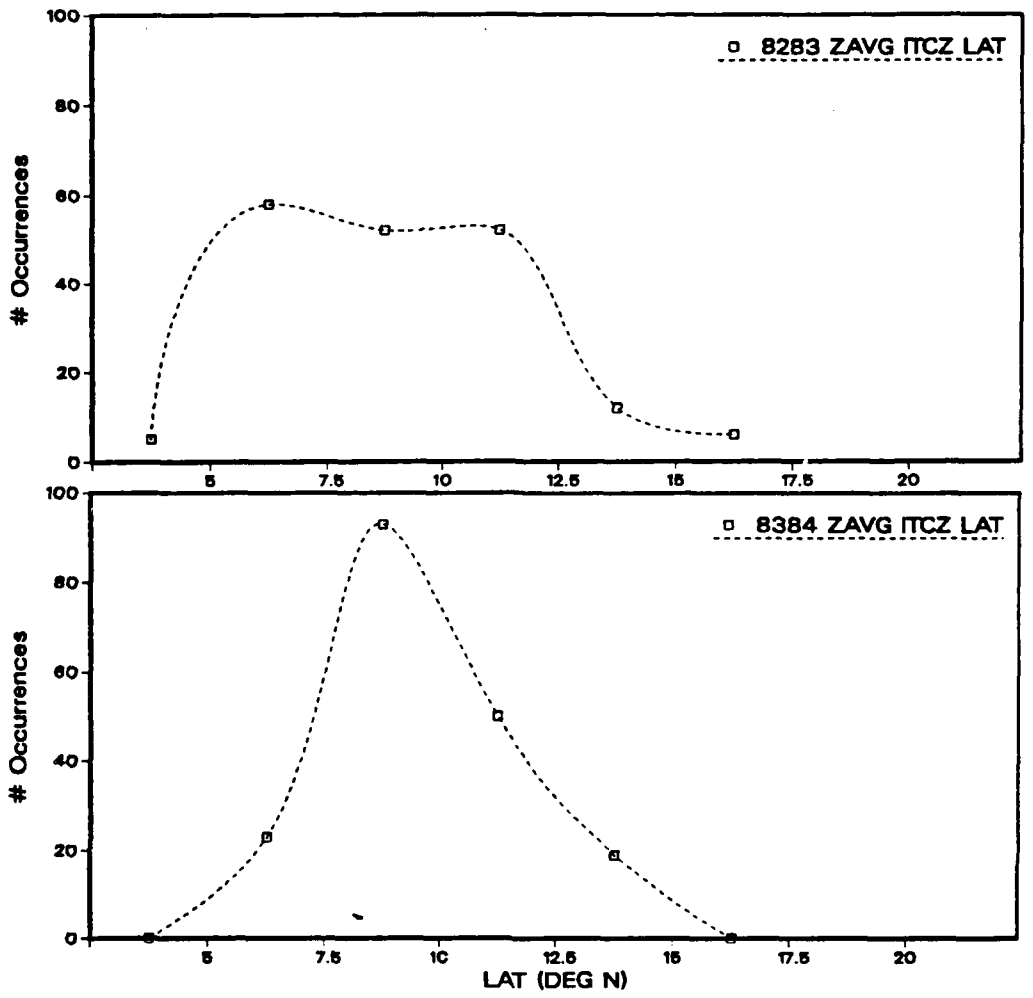


Fig. 21c. Same as Fig. 21a, except 82/83 (top) and 83/84 (bottom).

activity in the Pacific ITCZ during cool seasons. This was accomplished by analyzing time series of estimates of convective intensity. Results show that some cool seasons have strong episodes of alternating active and inactive convection at given locations. Other seasons have relatively few and/or weak active episodes, at least in the areas investigated here. A possible link between ITCZ convective intensity and ITCZ position was also identified, where above-average convective intensity is related, at least subjectively, to southward excursions of ITCZ position.

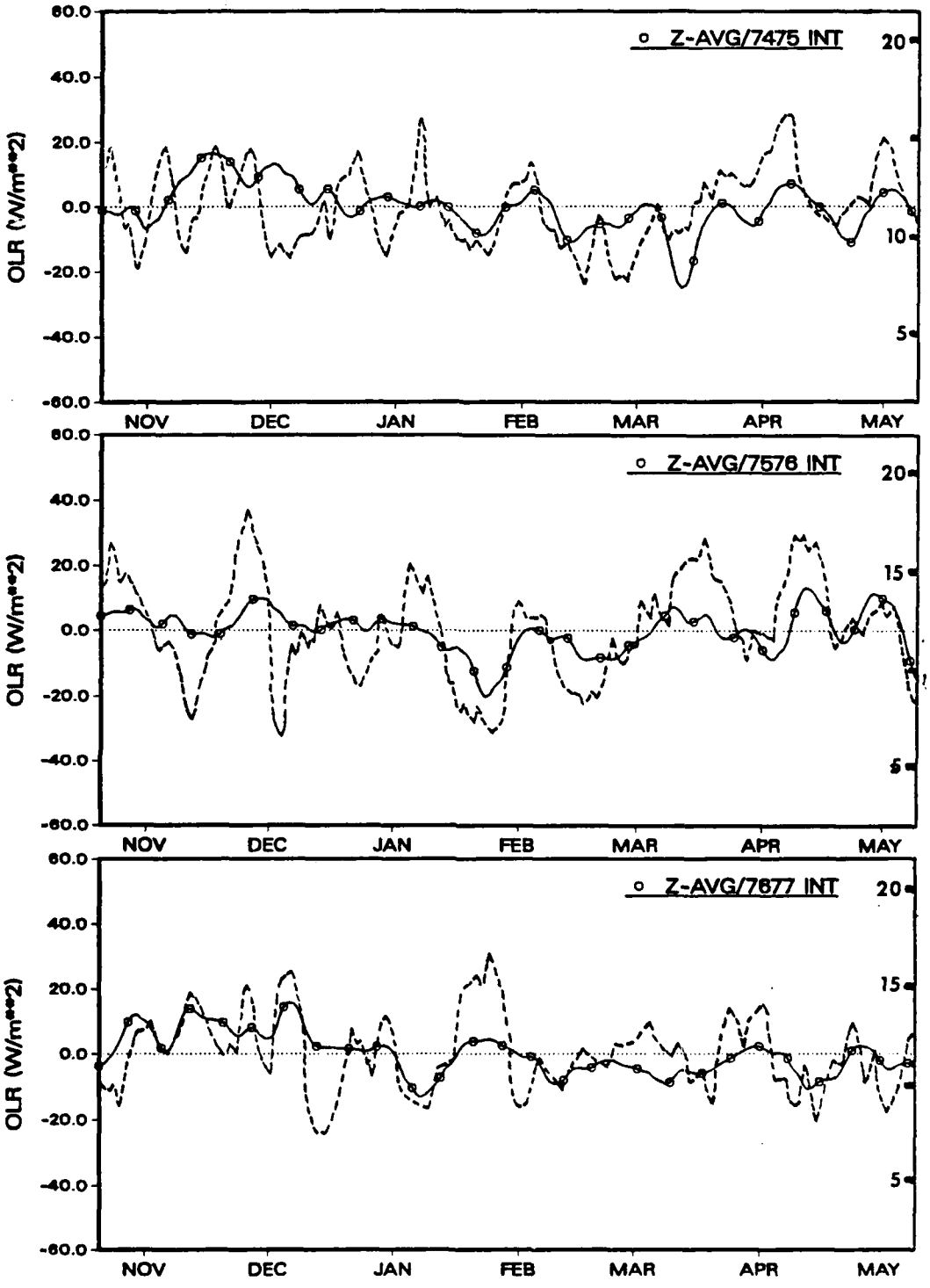


Fig. 22a. Zonal-average estimates of intensity (solid) and position (dashed). Units are (left) $W/m^2$, and (right) °N lat. Nov 74–May 75 (top), 75/76 (middle), and 76/77 (bottom).

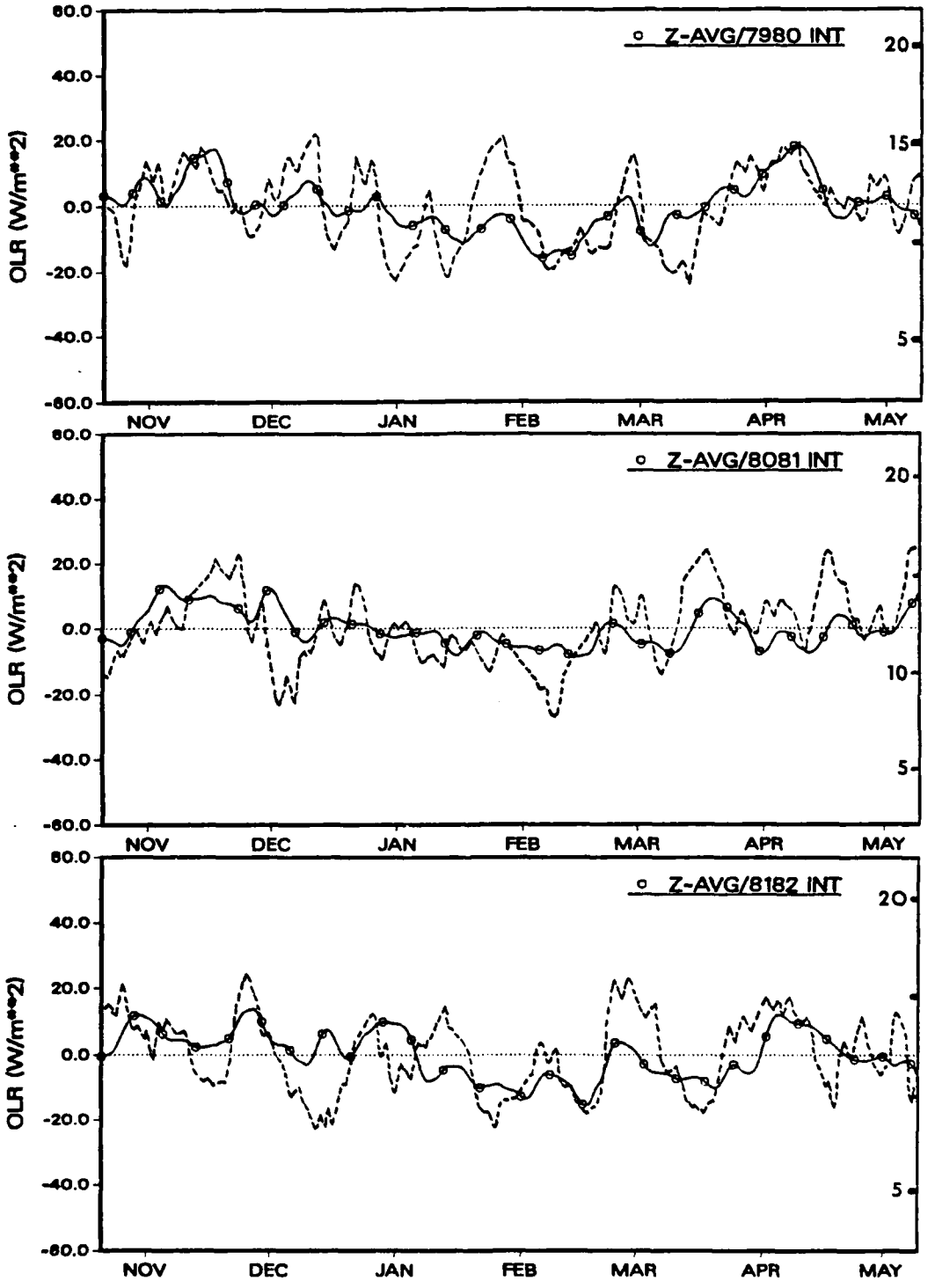


Fig. 22b. Same as Fig. 22a, except 79/80 (top), 80/81 (middle), and 81/82 (bottom).

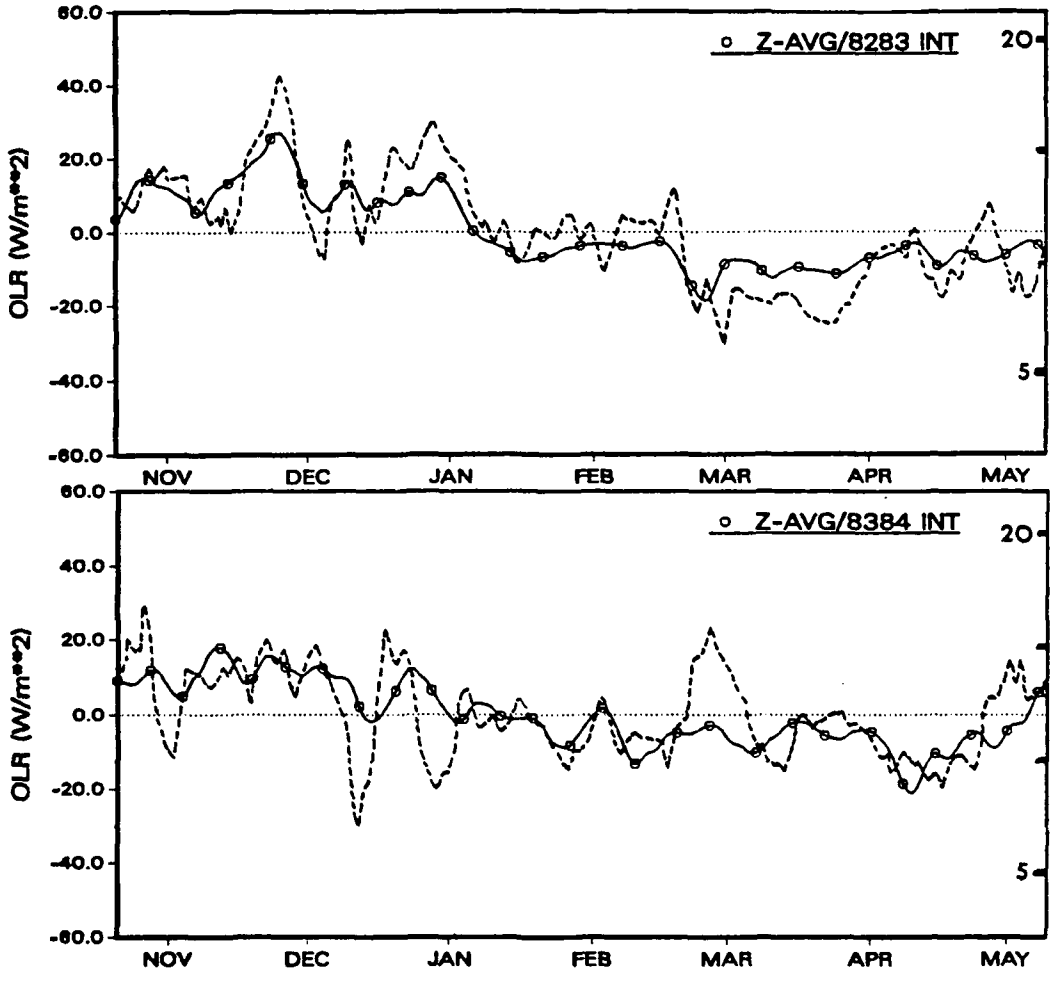


Fig. 22c. Same as Fig. 22a, except 82/83 (top) and 83/84 (bottom).

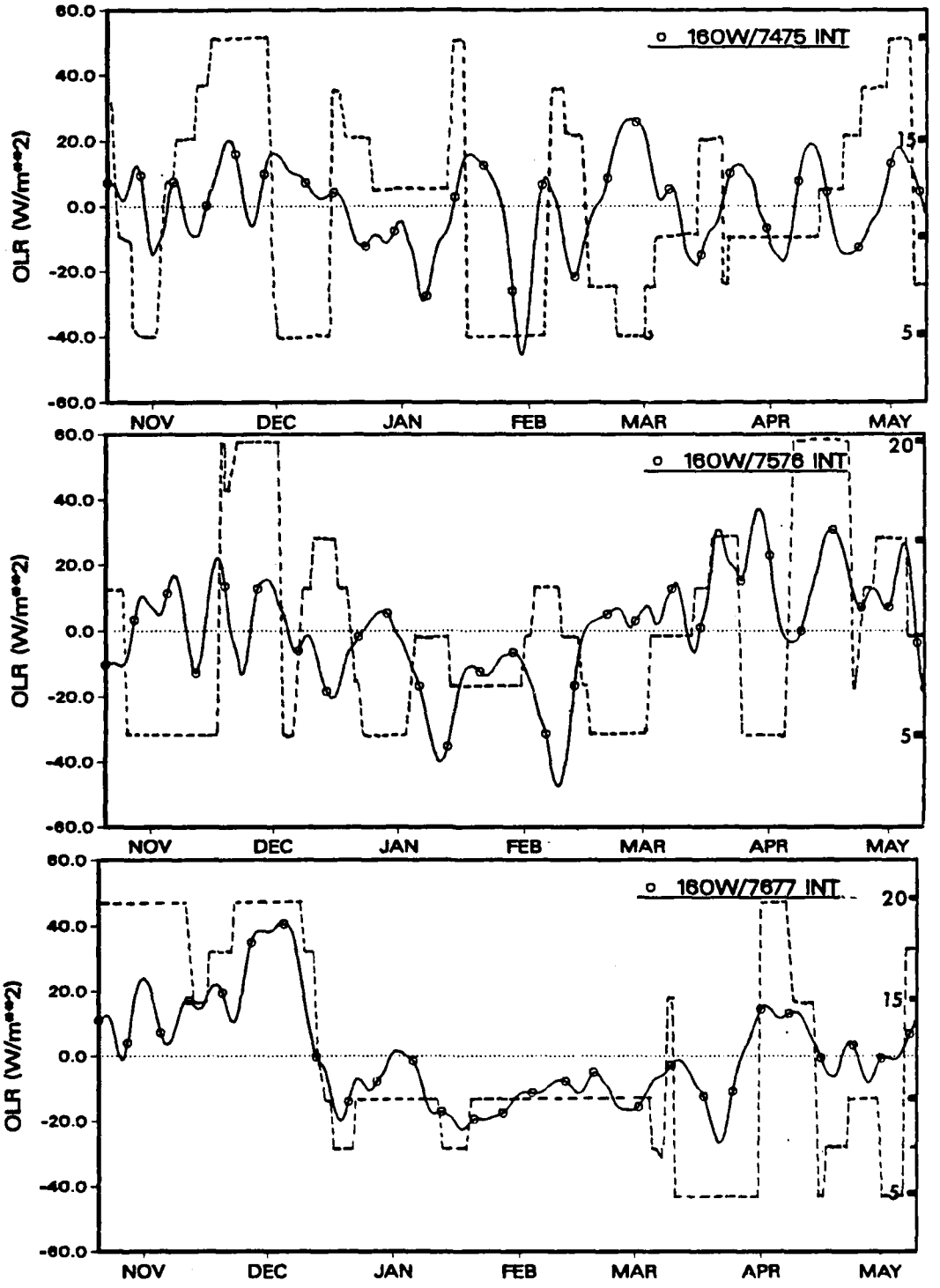


Fig. 23a. Same as Fig. 22a, except gridpoint estimates at 160°W. Nov 74–May 75 (top), 75/76 (middle), and 76/77 (bottom).

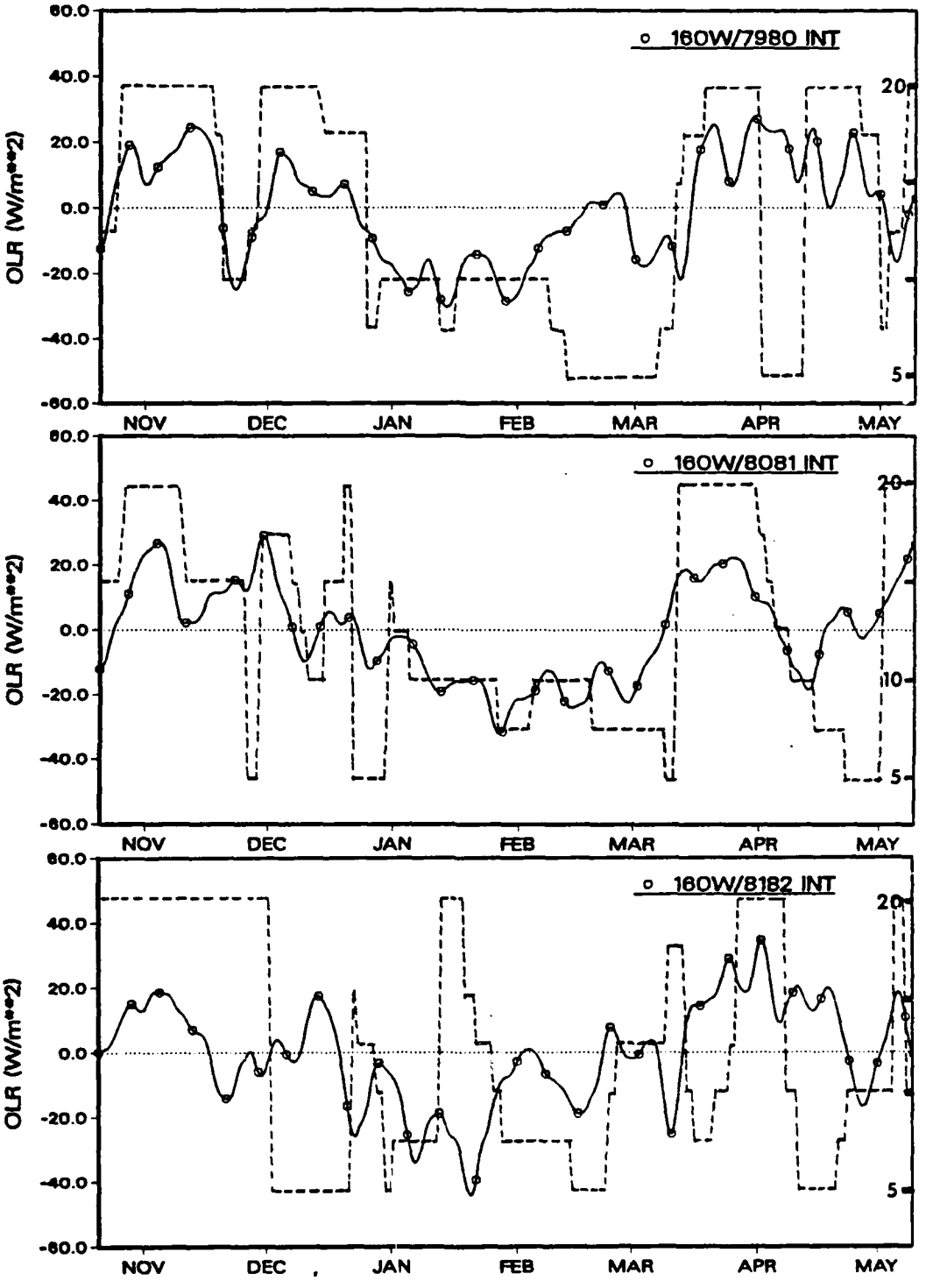


Fig. 23b. Same as Fig. 23a, except 79/80 (top), 80/81 (middle), and 81/82 (bottom).

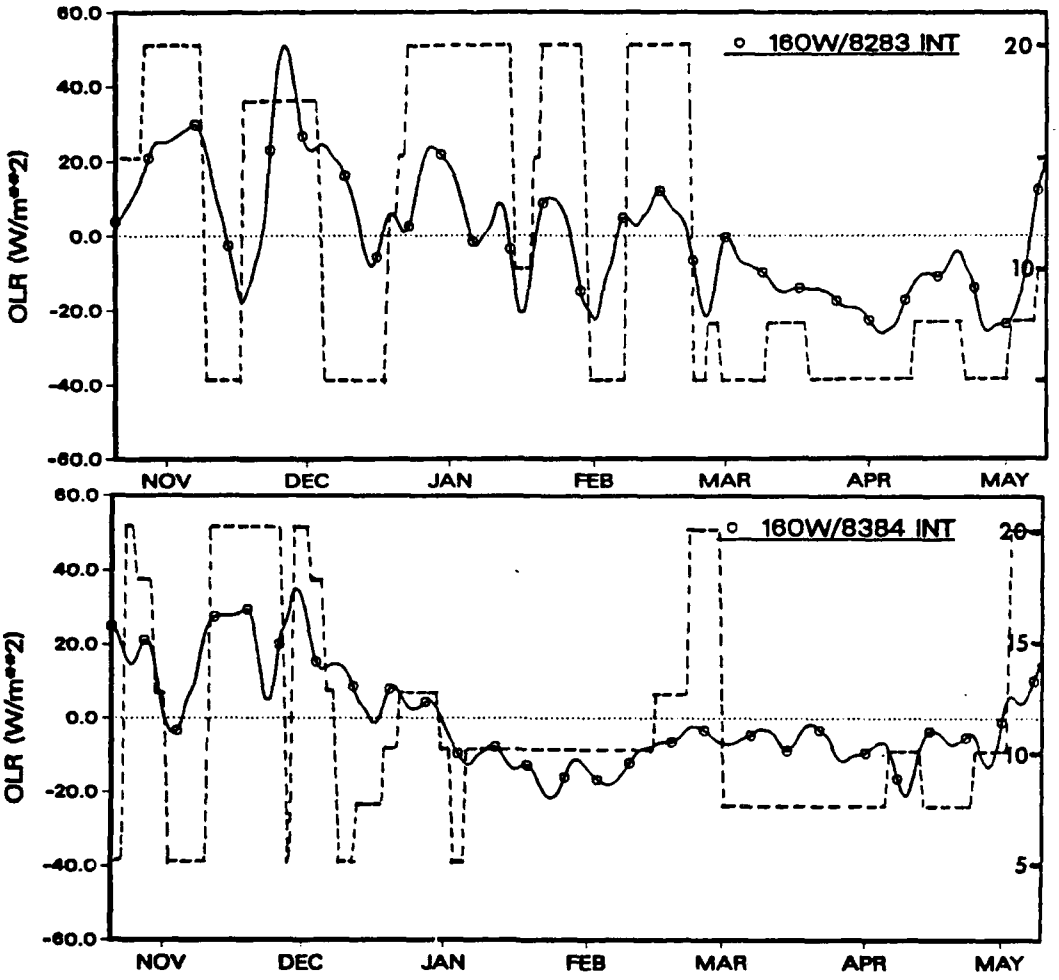


Fig. 23c. Same as Fig. 23a, except 82/83 season (top) and 83/84 (bottom).

# VI. CONVECTIVE ORGANIZATION DURING ACTIVE MODES

The second objective of this study was to describe convective organization during periods of active convection in the Pacific ITCZ. Periods of active convection were previously identified using time series of an index estimating convective intensity in the ITCZ region. Three methods of selecting "active" days were used. Daily OLR from the active days was temporally averaged over a number of events to form composites of typical convection patterns. Composites from days selected by each of the three methods were compared.

Convective organization across the domain on active days was examined in composites of daily OLR. "Active" days were chosen based on three conditions: days with large negative values of area–averaged OLR in the ITCZ intensity estimate at a single gridpoint (160°W); days with low values in the zonal–average intensity; and, days with low intensity estimates in *both* the 160°W and zonal–average series. It was hypothesized that if convection was organized in a particular fashion during the active modes, the composite technique would identify statistically significant convective spatial features in a time–averaged OLR map.

### Time–Averaged OLR Fields

A composite OLR map was constructed using days with active convection at 160°W during three seasons. Maps of unfiltered daily OLR from 22 days in the 74–75, 75–76, and 81–82 seasons were composited to form a single average OLR field (caption in Fig. 24 is "GRID" for the gridpoint method of selection). The "bullseye" pattern obtained in the composite was expected, due to the method of selection of active days. There is little intense convection, throughout the domain as a whole, that is correlated to active modes occurring at 160°W (see Fig. 15). Likewise, in

Fig. 24, there is no significant convection organization (shaded regions) at distances away from the reference point of 160°W/7.5°N.

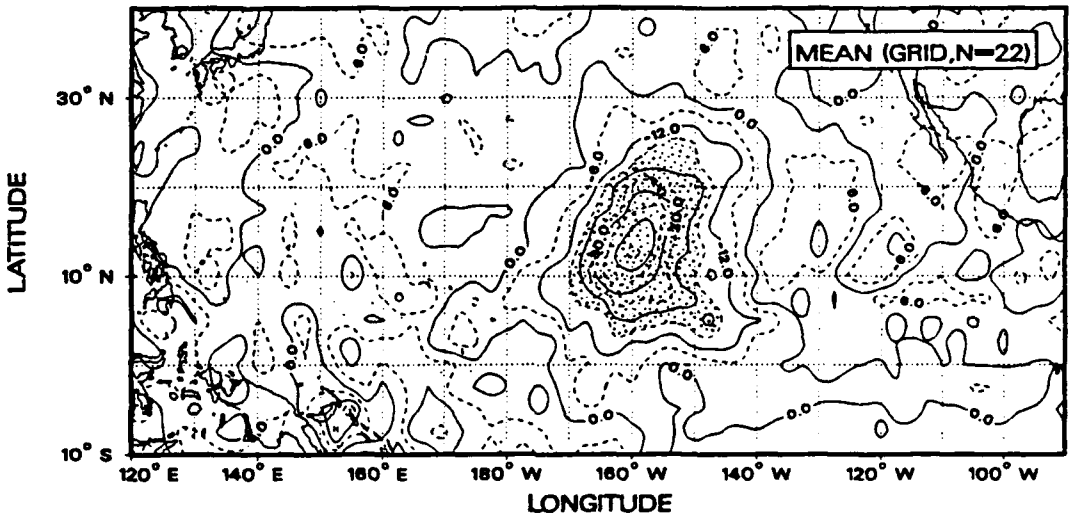


Fig. 24. OLR composite map constructed from 22 days in the 74–75, 75–76, and 81–82 seasons. Intervals are 5 $W/m^2$, with values < -18 $W/m^2$ shaded.

Two other composite maps were constructed. Figure 25 is the composite OLR from days selected using the zonal–average method (caption is "ZAVG" ). Figure 26 is the composite made from days selected using the combination 160°W/zonal–average method ("ZGRD" ). Daily OLR from four seasons (74–75, 79–80, 81–82, and 83–84) was used for these composites. The ZAVG composite consisted of 26 days, while the ZGRD used 16 days.

The convection pattern obtained in the composite of ZAVG active days contains some similarities to the pattern from the ZGRD days. In both, there appears to be three areas of intense ITCZ convection, located near 140°E, 160°W, and 110°W. Both maps show a warm anomaly extending northward out of the Southern hemisphere near the dateline.

An expected difference between the two patterns is the larger amplitude of

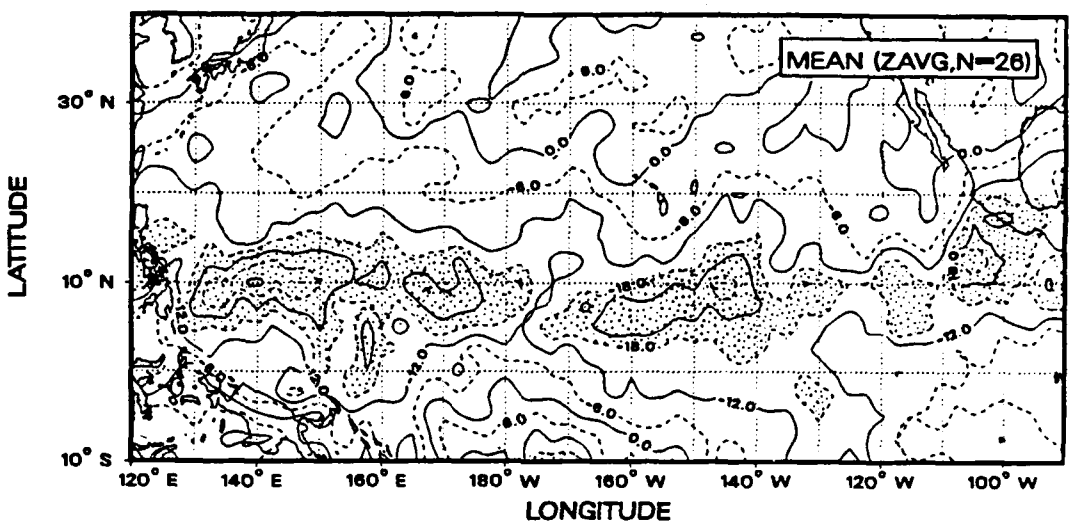


Fig. 25. OLR composite map constructed from 26 days in four seasons. Intervals are 5 W/m$^2$, with values < −18 W/m$^2$ shaded.

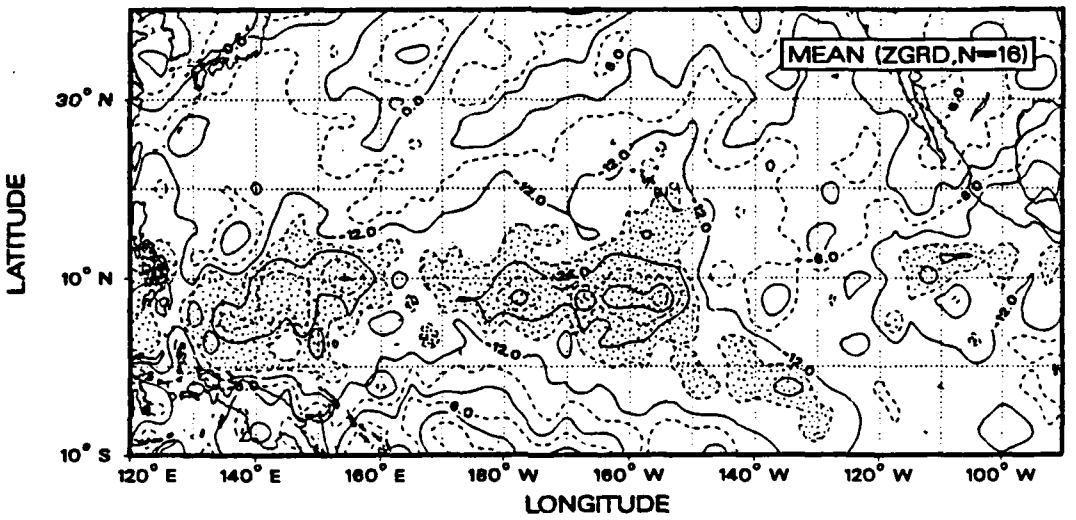


Fig. 26. Same as Fig. 25, except using 16 active days.

the cool anomaly located at 160°W in the ZGRD composite; this is one of the criteria for selecting active days in this method. The extension of cool OLR extending southeastward from near 160°W is also more intense in the ZGRD composite.

**Normalized Anomaly Fields**

To estimate the level of significance of these composite patterns, the OLR in the composites (denoted $\widehat{\mathbf{OLR}}_{(i,j)}$) were normalized by the three– and four–season–means and the associated standard deviation at each gridpoint. The results yielded t–statistics:

$$\mathbf{t}_{(i,j)} = \frac{(\widehat{\mathbf{OLR}}_{(i,j)} - \mu_{(i,j)}) \cdot \sqrt{N - 1}}{\mathbf{s}_{(i,j)}}, \tag{11}$$

where $\mu_{(i,j)}$ are the season–average OLR (averaged over the appropriate number of seasons; three for the "GRID" case, and four for the "ZAVG" and "ZGRD" cases). $\mathbf{s}_{(i,j)}$ are the associated sample standard deviations. The degrees of freedom was $N - 1$, or 21 for the GRID, 25 for the ZAVG, and 15 for the ZGRD composites.

Maps of these t–values are shown in Figs. 27, 28, and 29 for the GRID, ZAVG, and ZGRD composites respectively.

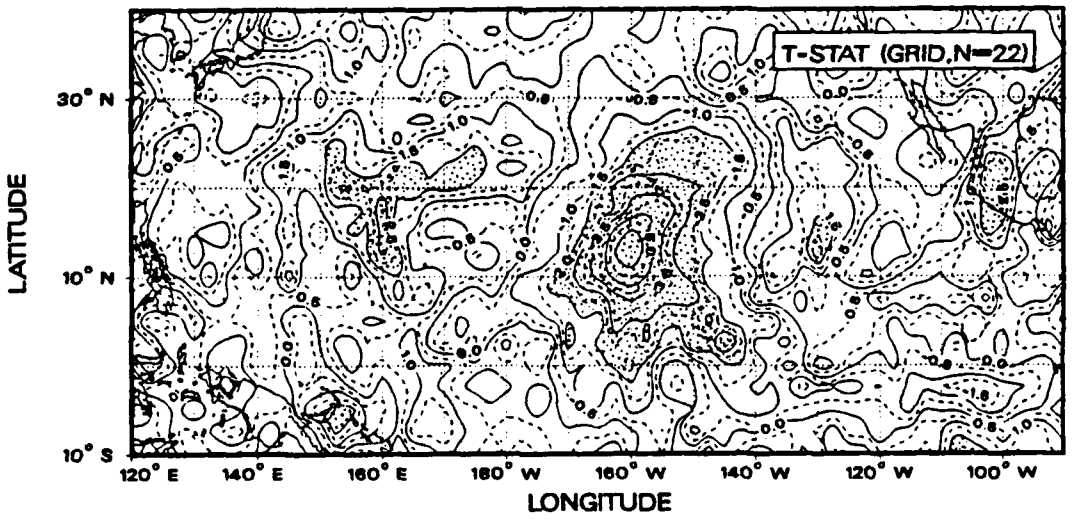


Fig. 27. t–statistics obtained from the GRID composite. Intervals are 0.4 (no units), and values exceeding ± 2.0 are shaded.

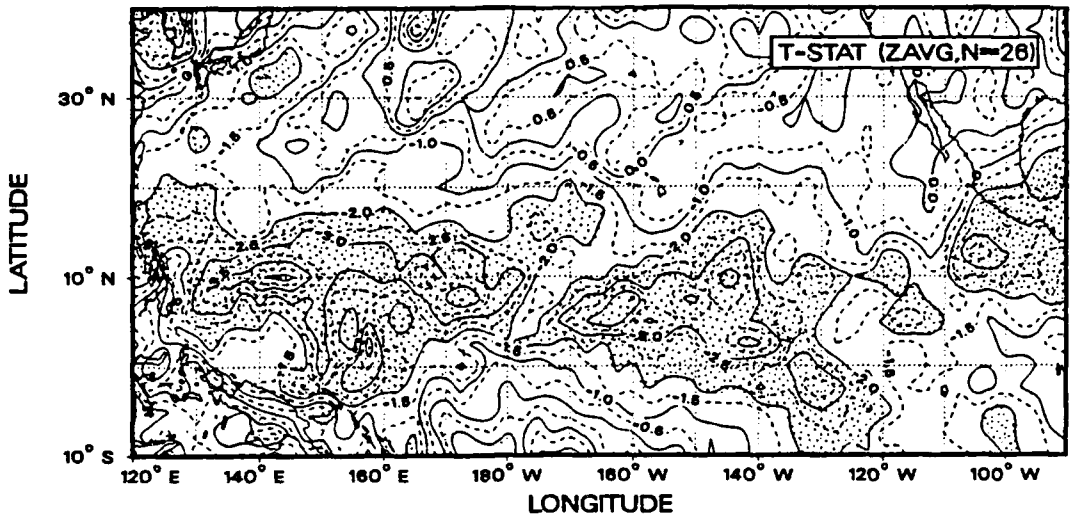


Fig. 28. Same as Fig. 27, except from the ZAVG composite.

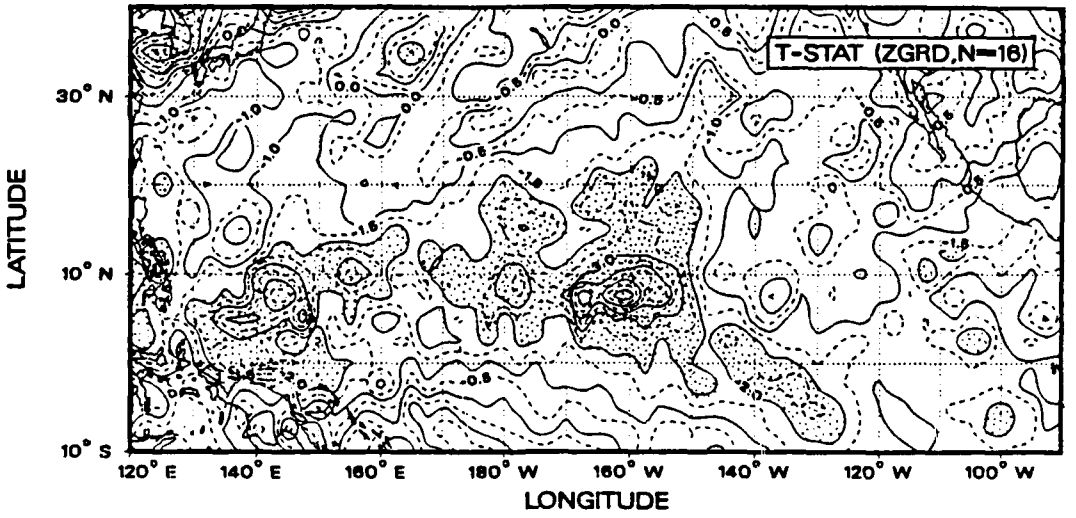


Fig. 29. Same as Fig. 27, except from the ZGRD composite.

In Figs. 27, 28, and 29, values exceeding $\pm$ 2.0 are significant at the 5% level. That is to say, in the fields of normalized OLR anomalies, one would expect to find a value of $t_{(i,j)}$ exceeding $\pm$ 2.0 over less than 5% of the domain. The shaded regions

AD-A196 406 ACTIVE MODES OF THE PACIFIC INTERTROPICAL CONVERGENCE ZONE (ITCZ)(U) AIR FORCE INST OF TECH WRIGHT-PATTERSON AFB OH P M HAYES MAY 88 AFIT/CI/NR-88-29 2/2

UNCLASSIFIED F/G 4/1 NL

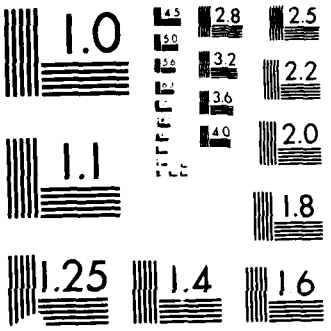


UTION TEST CHART

to 5% of the area in the domain is roughly the area covered by three 10° by 10° boxes (3 out of 60 total = 5%). The shaded area in the GRID composite (Fig. 27) is approximately 6 boxes, or about 6/60 = 10% of the domain. In the ZAVG composite (Fig. 28), there are 18 shaded boxes or about 18/60 = 30% of the domain. A smaller proportion is shaded in the ZGRD composite (Fig. 29), 12/60 or 20%.

The features of spatial organization of intense convection are subtle, but discernable. In the GRID composite, the pattern is not strictly a bullseye, but contains a south–north oriented axis of maximum intensity. Given the *zonal* nature of the mean ITCZ, this is an unexpected result. As noted in Section IV, circulation cannot be inferred using OLR data alone. However, there may be a meridional component of circulation associated with the meridional cloudiness feature in the eastern Pacific during GRID active modes.

The other composites show a similar meridional axis of peak intensity, located near 145°W in the ZAVG composite, and near 160°W in the ZGRD composite. In the ZGRD composite, the eastern Pacific is inactive east of 150°W, while in the ZAVG composite, the intense ITCZ convection is essentially continuous across the domain. This study examined a small sample of the available record. To draw more–specific conclusions about spatial organization and circulation during active modes of the Pacific ITCZ requires further investigation.

# VII. SUMMARY AND DISCUSSION

Satellite–observed OLR data from eight cool seasons were examined to find periods of active convection within the Pacific ITCZ. Data were averaged and interpolated to 24 h/2.5° latitude/longitude resolution. The annual and semiannual signals were removed, and a low–pass time filter was used to remove high–frequency variability. The filtered data sets contained variations on temporal scales from 10–150 days, approximately.

An index was designed to provide estimates of intensity of convection in the ITCZ region. Intensity was represented by area–averaged OLR in the region between 12.5°N and 5.0°N at every 2.5° of longitude across the domain between 120°E and 90°W. Time series of the intensity estimates were analyzed to find days having low area–averaged OLR, or active convection. Time–longitude diagrams of the intensity estimates were constructed to show relationships between active modes in various parts of the domain. The intensity index was modified to provide estimates of the latitudinal position (between 5°N and 20°N) of maximum convection, again, at 2.5° longitude intervals, every day. Time series of the intensity and position estimates were compared to find relationships between active modes and ITCZ position.

The main results from the first portion of the study may be summarized as follows:

- Interannual variability of seasonal mean convection is considerable. The ENSO signal is most obvious in the 82–83 season, and, to a lesser degree, in the 76–77 season. Fields of parameters computed during the 74–75, 75–76, 79–80, and 80–81 seasons show small interannual variations.

- Characteristics of the zonal–average ITCZ are strongly influenced by activity in the western and central Pacific. The frequency distribution of position estimates

averaged across the domain is exactly opposed the the distibution obtained from a point in the eastern Pacific. Also, the time–longitude diagrams of intensity estimates show little correlation between days having active convection in the zonal mean and days with active convection in the east.

- Active modes appear to originate near the dateline and spread longitudinally with time. During some seasons, active modes appear to propagate westward in the central and western Pacific.

- The daily position of maximum convection changes quickly, shifting up to 15° latitude over a few days. Position estimates sampled at 160°W show a bimodal distribution, with peaks at 5°N and 20°N, the limits of the index. Zonal–average position estimates have a mound–shaped distribution, with a mode near 10°N.

- There is a close correlation between the series of zonal mean intensity and position. When the mean ITCZ became active, it normally shifted southward. Conversely, it shifted north when inactive.

The second objective was to describe convective organization during the active modes. Composites were constructed using daily OLR from days selected by each of three methods. The convection pattern obtained from the composite of gridpoint method–selected days was an uninteresting "bullseye" .

The convection pattern obtained from active days selected using the zonal–average method showed an east–west oriented region of convection stretching across the entire domain. The pattern consisted of three major cells, ranging in width from 3000 km in the eastern (100°W) and central (160°W) Pacific, to nearly 5000 km in the western Pacific (140°E).

The pattern of convection obtained using active days selected by the combination gridpoint/zonal–average method was different in several respects. The eastern

Pacific cell was absent, and the amplitude of the central Pacific cell was greatly enhanced. The central cell also extended southeastward into the Southern hemishpere, perhaps indicating cross-equatorial influences during active modes.

## REFERENCES

Bettge, T.W., and D.P. Baumhefner, 1980: A method to decompose the spatial characteristics of meteorological variables within a limited domain. *Mon. Wea. Rev.*, **108**, 843–854.

Cahalan, R.F., D.A. Short, and G.R. North, 1982: Cloud fluctuation statistics. *Mon. Wea. Rev.*, **110**, 26–43.

Frank, W.M., 1983: The structure and energetics of the East Atlantic Intertropical Convergence Zone. *J. Atmos. Sci.*, **40**, 1916–1929.

Gruber, A., 1972: Fluctuations in the position of the ITCZ in the Atlantic and Pacific Oceans. *J. Atmos. Sci.*, **29**, 193–197.

—— , and J.S. Winston, 1978: Earth–atmosphere radiative heating based on NOAA scanning radiometer measurements. *Bull. Amer. Meteor. Soc.*, **59**, 1570–1573.

—— , and A.F. Krueger, 1984: The status of the NOAA outgoing longwave radiation data set. *Bull. Amer. Meteor. Soc.*, **65**, 958–962.

—— , M. Varnadore, P.A. Arkin, and J.S. Winston, 1986: Monthly and seasonal mean outgoing longwave radiation and anomalies. *NOAA Tech Report NESDIS 26*, 352pp.

Hartmann, D.L., and E.E. Recker, 1986: Diurnal variation of outgoing longwave radiation in the tropics. *J. Climate Appl. Meteor.*, **25**, 800–812.

Hastenrath, S., 1985: *Climate and Circulation of the Tropics*. D. Reidel, Boston, 445pp. (see Ch. 6).

Heddinghaus, T.R., and A.F. Krueger, 1981: Annual and interannual variations in outgoing longwave radiation over the tropics. *Mon. Wea. Rev.*, **109**, 1208–1218.

## REFERENCES (Continued)

Krishnamurti, T.N., and D. Subrahmanyan, 1982: The 30–50 day mode at 850 mb during MONEX. *J. Atmos. Sci.*, **39**, 2088–2095.

Lau, K.–M., and P.H. Chan, 1983: Short–term climate variability and atmospheric teleconnection as inferred from satellite–derived outgoing longwave radiation I: Simultaneous relationships. *J. Atmos. Sci.*, **40**, 2735–2750.

—— , and —— , 1985: Aspects of the 40–50 day oscillation during the northern winter as inferred from outgoing longwave radiation. *Mon. Wea. Rev.*, **113**, 1889–1909.

—— , and —— , 1986: Aspects of the 40–50 day oscillation during the northern summer as inferred from outgoing longwave radiation. *Mon. Wea. Rev.*, **114**, 1354–1367.

Liebmann, B., and D.L. Hartmann, 1982: Interannual variations of outgoing longwave IR associated with tropical circulation changes during 1974–1978. *J. Atmos. Sci.*, **39**, 1153–1162.

Lin, R.–Q., and D.R. Mock, 1986: A test of the ECMWF model in tropical synoptic–scale diagnosis. *Mon. Wea. Rev.*, **114**, 1519–1538.

Madden, R.A., and P.R. Julian, 1971: Detection of a 40–50 day oscillation in the zonal wind in the tropical Pacific. *J. Atmos. Sci.*, **28**, 702–708.

—— , and —— , 1972: Description of global-scale circulation cells in the tropics with a 40–50 day period. *J. Atmos. Sci.*, **29**, 1109–1123.

McGuirk, J.P., and A.H. Thompson, 1984: Transient tropical disturbances within the Pacific Hadley cell. *Proc. 15th Tech. Conf. on Hurricanes and Tropical Meteorology*, Miami, Amer. Meteor. Soc., 249–255.

## REFERENCES (Continued)

—— , —— , and L.L. Anderson, Jr., 1986: Wintertime disturbances in the tropical Pacific: FGGE IIIb and satellite comparisons. *Preprints Nat. Conf. on Scientific Results of FGGE*, Miami, Amer. Meteor. Soc., 4pp.

—— , 1987: Climatology of various synoptic systems over the tropical North Pacific. *Proc. Twelfth Annual Climate Diagnostics Workshop*, Champaign, IL, NOAA, U.S. Dept. Commerce, Washington. D.C., (in press).

Meehl, G.A., 1987: The annual cycle and interannual variability in the tropical Pacific and Indian Ocean regions. *Mon. Wea. Rev.*, **115**, 27–50.

Murakami, M., 1979: Large–scale aspects of deep convective activity over the GATE area. *Mon. Wea. Rev.*, **107**, 994–1013.

Murakami, T., 1980: Empirical orthogonal function analysis of satellite–observed outgoing longwave radiation during summer. *Mon. Wea. Rev.*, **108**, 205–222.

—— , L.–X. Chen, and A. Xie, 1986: Relationship among seasonal cycles, low frequency oscillations, and transient disturbances as revealed from outgoing longwave radiation data. *Mon. Wea. Rev.*, **114**, 1456–1465.

Nakazawa, T., 1986: Intraseasonal variations of OLR in the tropics during the FGGE year. *J. Meteor. Soc. Japan*, **64**, 17–34.

Ohring, G., A. Gruber, and R.G. Ellington, 1984: Satellite determinations of the relationship between total longwave radiation flux and infrared window radiance. *J. Climate Appl. Meteor.*, **23**, 416–425.

Ramage, C.S., S.J.S. Khalsa, and B.N. Meisner, 1981: The Central Pacific near–equatorial convergence zone. *J. Geophys. Res.*, **86**, 6580–6598.

## REFERENCES (Continued)

Short, D.A., and R.F. Cahalan, 1983: Interannual variability and climatic noise in satellite–observed outgoing longwave radiation. *Mon. Wea. Rev.*, **111**, 572–577.

Smith, N.R., J.P. McGuirk, and A.H. Thompson, 1985: The synoptic structure of tropical Pacific moisture bursts. *Proc. 16th Conf. on Hurricanes and Tropical Meteorology*, Houston, Amer. Meteor. Soc., 192–193.

—— , 1986: A climatology of tropical moisture bursts in the eastern North Pacific Ocean. M.S. thesis, Dept. of Meteorology, Texas A&M University, College Station, 77843, 76 pp.

Thompson, A.H., J.P. McGuirk, L.L. Anderson, and N.R. Smith, 1984: Analysis of tropical synoptic disturbances using satellite–derived soundings and radiance data from selected channels. *Preprints Conf. on Satellite/Remote Sensing and Applications*, Clearwater Beach, FL, Amer. Meteor. Soc., 135–142.

Weickmann, K.M., G.R. Lussky, and J.E. Kutzbach, 1985: Intraseasonal (30–60 day) fluctuations of outgoing longwave radiation and 250 mb streamfunction during northern winter. *Mon. Wea. Rev.*, **113**, 941–961.

# VITA

Patrick Michael Hayes [redacted]. He was the first of ten children born to John David and Millie Hayes. Patrick attended elementary school in Baraboo, La Crosse, and Germantown, Wisconsin. After completing high school at Washington High in Germantown in 1974, he studied at the University of Wisconsin at Green Bay (UWGB).

Patrick held many jobs while attending UWGB, including sail and ski instructor at the university's bayside recreation center. It was while sailing that he became interested in serious study of meteorology. He eventually graduated *cum laude* with a Bachelor of Science degree in Science and Environmental Change, Earth Science major, in 1982.

After entering the U.S. Air Force and completing Officer Training School, Patrick attended Texas A&M University (TAMU) in the Air Force Institute of Technology (AFIT) Basic Meteorology Program during 1983. He was then assigned to Fort Bragg, North Carolina where he was the Staff Weather Officer for the U.S. Army's XVIII Airborne Corps. Included in his regular weather support duties were frequent exercise deployments, usually by paradrop, to locations such as Puerto Rico, Honduras, Hawaii, and the Republic of South Korea. He was selected for an AFIT advanced degree assignment at TAMU and left Fort Bragg in August, 1986.

He is married to the former Dawn-Marie Zak, and they have two daughters, Megan and Brynn, and a son, Michael, who all want to grow up to be meteorologists like their mother.

[redacted]